Wave damping by large-scale offshore kelp farms

A numerical modelling framework using a porous medium approach

J. J. Ruesen

Master of Science Thesis
Offshore & Dredging Engineering

TU Delft

Wave damping by large-scale offshore kelp farms

A numerical modelling framework using a porous medium approach

by

J. J. Ruesen

to obtain the degree of Master of Science
at the Delft University of Technology.
to be defended publicly on Thursay January 20, 2022 at 16:00.

Student number:	4284208	
Project duration:	April 15, 2021 – January 20, 2022	
Thesis committee:	Prof. dr. ir. A. V. Metrikine,	TU Delft
	Dr. O. J. Colomés Gené,	TU Delft
	Ir. R. van Driel,	Mocean Offshore
	Ir. M. Hoogeveen,	Mocean Offshore

mocean
ADVANCED OFFSHORE TECHNOLOGY

TU Delft

Abstract

Large-scale cultivation of seaweed presents opportunities for multiple global challenges currently at play. Cultivated seaweed can provide a sustainable source of protein for humans and cattle without competing for land, fresh water supply or the use of fertilisers. Kelp forests are known to be a solid basis for an elaborate biome that supports biodiversity in areas that have been damaged by over-fishing or rising sea temperatures. Additionally, kelp forests can lock-in large amounts of Blue Carbon, expanding the oceans' buffering capacity to mitigate anthropogenic emissions. Furthermore, with their densely seeded lines, offshore kelp farms are found to attenuate wave amplitude, thus providing coastal protection, and benefits like increased workability for offshore operations. Both academic publications and industry review underline the potential of this sector and significant growth in cultivation is expected in the near future.

Methods currently used for quantification of the damping effects of large-scale offshore kelp farms are diverse, and entail varying degrees of accuracy and computational cost. Experimental observations that support the outcomes of these methods are limited to scaled experiments in wave flumes, with various methods used to mimic vegetation. No convergence is found in most suitable methods for application to large-scale offshore kelp farms.

This research presents a novel modelling framework based upon the Finite Element method, implemented using Julia Programming Language. The effects of the vegetation on the wave climate are represented with a Darcy-Forchheimer term borrowed from porous medium flow theory, including a linear and a quadratic resistance term. The framework comprises a numerical wave tank, using the incompressible Navier Stokes equations. The single-phase model captures the free surface using the coupling of dynamic pressure with a virtual elevation variable through a linearized transpiration boundary condition.

Wave energy dissipation is shown to increase significantly by moving the farm structure close to the water surface. Similarly, decrease in relative water depth - compared to the vegetated height - increases damping potential. Wave period is found to be of strong influence on dissipation, where short waves are attenuated more. Scaling vegetation length with wave length, however, diminishes the reduction in damping of longer waves. Conversely, wave amplitude is shown to be of less influence on the transmission of amplitude through a vegetated patch.

The framework presents a method that is easily scalable, flexible in application on a wide range of flows and vegetation characteristics, and at reasonable computational cost. Introduction of both the linear and quadratic terms extends applicability compared to traditional methods. The approach is verified using convergence studies, application of the model is validated by comparison to existing experimental data. It is shown that experimental set-ups can be reproduced effectively, and simulation results coincide with experimental findings. Validation of outcomes on scales larger than common wave tanks was found unfeasible due to lack of measurement data. A theoretical case study was performed to predict wave damping of a full-scale kelp farm, demonstrating promising potential with up to 40% wave energy reduction at the local peak wave period.

Further research into establishment of the Darcy- and Forchheimer-coefficients is recommended. A preliminary range of values has been found, based upon calibration on existing experiments that represent realistic ranges of vegetation characteristics. Furthermore, the main conditions of the flow and vegetation that dictate damping potential are identified. On this basis, research into a physics-based determination of the coefficients is recommended. Additionally, full-scale measurements are advised to validate application on future kelp farm designs.

Through this novel approach, the range of application is increased compared to existing methods, while straightforward set-up and usage is governed, and limited computational costs allows for simulation without the need for a dedicated computer setup. The framework is shown to be robust by generating consistent simulation results. In summary, the established framework shows to be a good alternative to existing approaches to investigate wave damping potential of large-scale offshore kelp farms.

Preface

The past nine months mark the final stretch of my road to becoming an engineer, the last part in fulfillment of my master's degree in Offshore Engineering at the Delft University of Technology. It started with an open-ended question of what the kelp cultivation sector might have in store in the near future, which Mocean Offshore allowed me to dive into. This broad direction evolved into the development of a numerical model, enabling analysis of the influence of vegetation on propagating waves offshore.

Halfway through April 2021 I knew I was getting myself into a challenging project. I hoped that consciously aiming for a scope outside of my comfort-zone would allow me to gain experience that would not only be beneficial to my work as an offshore engineer, but be valuable overall. I am amazed at the satisfaction I encountered in gaining some insight in the mathematics behind numerical set-ups. While far from an expert, I have learned valuable lessons on numerical computation and developing code. Performing the industry review allowed me to meet some inspiring professionals in the sector. In addition, I've gained new experience in research and in individual project work, which isn't entirely individual in the end.

My gratitude goes out to Robert, for the numerous spars on the content of my research and the moments of reflection on the process. Experience as project manager shined through in sensing where I could use some extra guidance along a generally solitary road. And to Maas, who managed to pick out key choices at any point along the way, impressing me with the ability to not only identify core issues quickly, but consistently convey profound understanding of modelling and engineering clearly as well. Additionally, the others at Mocean who got dragged into my fascination for kelp and proved great sparring partners throughout the project. Specifically Sander, who helped me set-up the project and Sjoerd, who held my hand the first steps into the wondrous world of Julia programming. My initial enthusiasm for Mocean's work and people have proven durable, I couldn't have wished for a better climate to perform this project in.

Next, I'd like to thank Oriol Colomés Gené, my supervisor at the university. I'm perplexed with how it proved possible to combine an, undoubtedly overfull, academic schedule with instantaneous reaction to my requests for feedback and consistently very timely meetings. I am humbled that, despite the obviously immense gap in in-depth knowledge, I felt welcome to ask support at every step along the way. From guiding me to the first Julia-install to the elaborate model now present. And lastly Andrei Metrikine who, as chair of the committee, kept me sharp with critical questions along the moments where the committee was present entirely. It has kept me on my toes in a very constructive sense.

Lastly, I'm in debt to the people close to me. In nine months of work both ups and downs are inevitable - graduating during a global pandemic might further contribute to this as well - and I've felt supported throughout. Also, they have endured my enthusiasm for everything kelp, an achievement in itself.

I hope this report will provide you with new insights, and might even awaken some interest in the developments in kelp cultivation. I know that I'm not done yet, with this fascinating sector!

Joël Ruesen
Rotterdam, January 2022

Contents

List of Figures

List of Tables

Nomenclature

Acronyms

BC	Boundary Condition
EDR	Energy Dissipation Rate
FEM	Finite Element Method
FLS	Fatigue Limit State
FSI	Fluid Structure Interaction
GMRes	Generalized minimal residual method
HTR	Wave Height Transmission Ratio
ILU	Incomplete Lower-Upper factorization
ISS	*inf-sup* stable
ODE	Ordinary Differential Equations
OSS	Orthogonal Subscales
PIV	Particle Image Velocimetry
RANS	Reynolds-Averaged Navier-Stokes
SDG	Sustainable Development Goal
SFM	*Standard Flume Model*
ULS	Ultimate Limit State
VOF	Volume Of Fluid

Greek Symbols

α	Darcy coefficient
β	Forchheimer coefficient
Δ	Laplace operator
η	Free surface elevation
Γ	Denotes boundary
λ	Wave length
μ	Dynamic viscosity
$\nabla\cdot$	Divergence operator
∇	Gradient operator
ν	Kinematic viscosity
Ω	Denotes domain

ω	Wave frequency
ρ	Density
σ	Stress
τ	Traction
τ_{ILU}	ILU preconditioning tolerance
θ	Wave phase
ε	Test function for the stabilization parameter variable
$\varepsilon(x)$	Symmetric gradient operator of variable x
ε_v	Energy dissipation by vegetation drag

Roman Symbols

f	Body force vector
s	Arbitrary source function
u	Velocity field
a	Wave amplitude
E_{total}	Total wave energy
I	Identity tensor
k	Wave number
k_h	Hydraulic permeability tensor
p	Pressure field
T	Wave period
g	Gravitational constant
p	Pressure variable
q	Test function for the pressure variable
s	Stabilization parameter variable
v	Test function for the velocity variable
w	Test function for the surface elevation variable

Subscripts

atm	Atmospheric (pressure)
eq	Equivalent
hor	Horizontal component
in, inc	Incident
kin	Kinetic energy
out	Outflow
pot	Potential energy
veg	Vegetation
ver	Vertical component

1 Introduction

With a growing global population and its density concentrating in coastal areas, the need for expansion towards the ocean arises. The Blue Economy comprises all possibilities that the ocean offers for economic activities that are traditionally land-based. It introduces solutions to a variety of problems that arise in areas where land-scarcity is (becoming) an issue.

One of the topics that increasingly raises interest in context of this Blue Economy is the production of biomass for food, feedstock (e.g. for cattle) and biochemicals. Through cultivation of algae, ocean-based production can aid in the land-scarcity problem that obstructs traditional agriculture in its fulfilment of growing demand for biomass.

This introductory chapter provides background that illustrates the relevance of the research conducted. After setting the backdrop of kelp cultivation offshore, section 1.3 presents the research objectives. Lastly, section 1.4 provides an overview of the structure of this report.

1.1 Background of kelp cultivation

As frequently underlined, the emergence of the Blue Economy must be accompanied by the constant assurance that the biome itself is protected. Moreover, positive externalities of increased ocean-bound activities should be strived for. Instead of approaching the expanding Blue Economy as an option for colonization of undisturbed territory, the possibilities for protection and synergistic value should be exploited.

Cultivation of seaweed is one area where such synergies are expected to be found on a large scale. With a proper eye for side-effects, the expansion of this sector is expected to contribute to many of the UN's Sustainable Development Goals (SDGs). Besides the primary goal of sustainable production of resources (SDG 12), growth of the seaweed cultivation sector is identified to contribute to ending poverty and hunger (SDG 1 and 2) as well as multiple others Hossain et al. [26].

Figure 1.1: Sugar kelp cultivated on a longline.

Figure 1.2: Naturally occurring sugar kelp in tidal zone.

Seaweeds have long been an accepted part of diets in Asia, and seaweed-extracts make up part of everyday lives in Europe through additives to foods for gelling and emulsifying. Other uses besides food are, amongst others, in toothpaste, fertiliser, livestock feed and cosmetics.

Additionally, seaweeds have a potential role in battling both the drivers, as well as the effects of climate change. As a sustainable source of proteins for animals and humans they decrease strain on natural resources by traditional methods. In their rapid growth they take up carbon dioxide from the ocean - the largest natural carbon sink. Lastly, cultivation sites can provide shelter for many animal and plant species, expanding biomes locally. In terms of environmental services kelp forests may aid in flood-defenses by damping waves, or could be used to damp waves around offshore structures to increase workability during O&M activities.

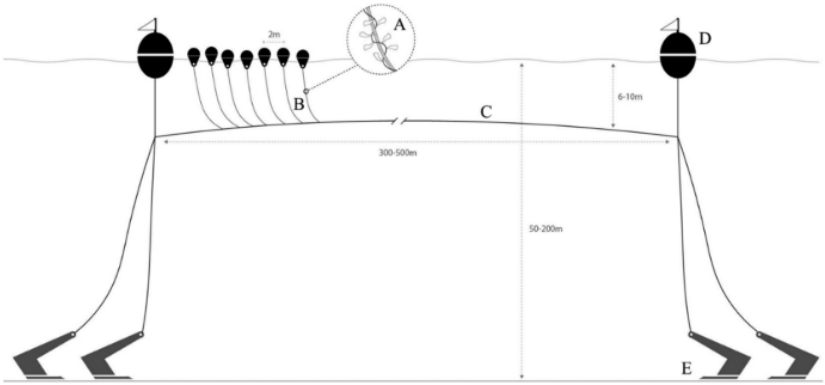

Figure 1.3: Macro-Algae cultivation rig as used by the Ocean Rainforest organisation. From Bak et al. [5].

1.1.1 Expansion of kelp cultivation sector

Currently, kelp production efforts outside of Asia experiences a set of challenges in scaling up to significant size. Lack of experience and especially high labour costs introduce difficulties in reaching scales that provide the benefits discussed. In order to aid the sector in its growth it would be beneficial to quantify the positive side-effects. For this thesis focus is laid on the wave damping characteristics of large scale offshore kelp farms. The accompanying literature review identifies a knowledge gap in robustly modelling the influence of kelp forests on the wave-climate. The present thesis aims to further insights in regards to this.

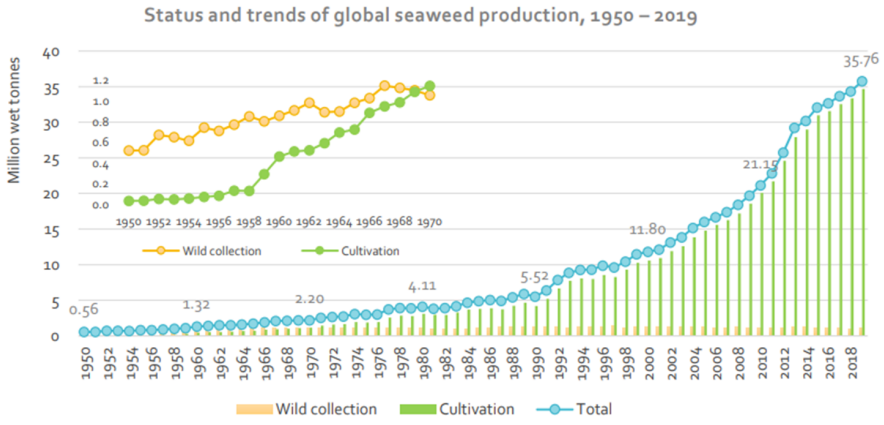

Figure 1.4: Global rise in seaweed production, as presented by FAO, 2021.

1.1.2 Wave damping by kelp

Research indicates large scale forests can modulate waves and influence currents. The wave damping potential of kelp fields could be exploited for coastal protection, for increase of workability in offshore operations (such as windfarm maintenance) and for decreasing loads on structures like wind turbines, allowing for less stringent design requirements for safe design.

In the last case, it should always be noted that varying biomass density influences the amount of wave damping with a variable magnitude over time. It is expected that if any significant wave damping can be

determined for the conditions applicable to wind farms, it would be likely to influence the Fatigue Limit State (FLS) only, by decreasing incident wave energy over certain wave frequencies. With respect to the Ultimate Limit State (ULS), the situation should still be based upon representative waves without any damping. For both limit states it would be essential to include any adverse effects vegetation would have on wave heights in the windpark.

The potential benefits of using (cultivated) kelp forests for wave damping are currently subject of research. Application of this potential has not yet been conducted by installation of kelp forests, but Reshore's living breakwater [72] is one example of the numerous project on the verge of commercial implementation.

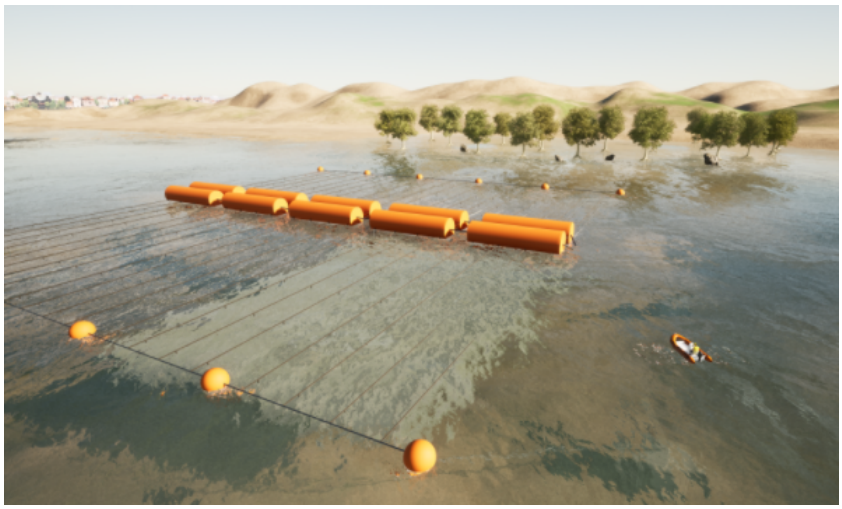

Figure 1.5: Graphical representation of the living breakwater concept by Reshore.

1.1.3 Modeling difficulties

Literature describes a diverse landscape when it comes to models that capture the behaviour of kelp and the influence of seaweed patches on the fluid dynamics around it. The models vary immensely in what physical effects are captured, and what characteristics of the plants, patches and flows are included. This leads to a wide spectrum of complexity, applicability and universality.

Overall, it can be expected that models with different objectives focus on different aspects of the problem. However, for models with wave-damping focus specifically, no convergence is found in what methods to use. The difficulties in establishing a fit-for-purpose modelling technique with balanced accuracy and computational cost are seen to create an obstacle in expansion of the sector. Much is still unknown regarding the damping potential of large-scale offshore kelp farms, modelling their influence on the wave climate is one step towards further understanding it.

1.2 Research gaps

An elaborate literature review was performed to identify the main gaps regarding the modelling of large-scale offshore kelp farms. In short, current research does not seem to focus on the scale of the near-future farms. Furthermore, current models focus on investigation of a specific phenomena instead of a more general overview of the processes of flow through a vegetated patch. The literature review is referred to for a full overview.

To advance the modelling capabilities for fluid-vegetation interaction, a method that combines the strengths of the three identified classes of modelling approaches is deemed beneficial. A set-up that allows for modelling beyond the standard quadratic drag law, allows for straightforward application and adjustments in design, but does not require excessive computational power could aid in wave damping quantification. A more generalized approach to modelling vegetation flow would aid insights and added value to developing future farms.

The majority of research - both experiments and numerical models - have focused on bottom-founded vegetation. Mangroves and seagrasses are the most referenced vegetation types in the processed publications. For both types, evidently, no flexibility exists in varying the vertical location within the water column.

There are indications that location within the water column has significant influence on the ability to attenuate waves. Further research into this effect is proposed in different studies.

In general no specific research has been done in the direction of large-scale kelp forest with the majority of the vegetation in the upper part of the water column. Various wave flume experiments are available, however no specific focus has been found on application of insights from these experiments on the expected lay-out of an offshore kelp farming structure.

To comment on the expected wave damping potential of future seaweed farms two ingredients are essential. A proposed layout is needed, which should be based on a best estimate of what such farms would look like. This includes where they are installed, the possible types of vegetation and a general overview of likely dimensions. Secondly, a model should be present to accommodate the modelling of the vegetation-flow interactions that result in wave dissipation.

1.3 Research objectives and methodology

The objectives of this research are to develop a numerical model to quantify wave damping by offshore kelp farms. A novel approach is investigated using the Darcy-Forchheimer equation for porous media. The backbone of implementation of this model are the language Julia and the FE package Gridap. The main objectives of the model presented in this report are described in detail in the literature review. Reference is made to this report for an elaboration of the analysis of existing literature that lead up to the objectives. For clarity, this section shortly restates the research proposal's main take-aways.

The main research objective of this thesis is summarized to the following:

A numerical model to simulate the influence of large-scale offshore kelp farms on the wave climate, using a porous medium approach.

1.3.1 Research questions

In order to structure research, and coherently order the questions needed to arrive at the main objectives of this MSc thesis, a set of sub-questions is established. This includes some background on the current state of the sector and prospects for the near future to indicate what farm layouts and conditions would be relevant to model.

1. What could a future offshore kelp farm look like?
2. Could large-scale offshore wave farms be effectively used for wave damping?
3. How does wave damping by kelp relate to incoming wave conditions?
4. How does vertical position within the water column influence attenuation?

As stated, focus of further research will be laid on modelling the process of wave damping. Therefore, the following questions are formulated to contribute towards structuring that part of the scope:

5. How are kelp forests currently being modelled?
6. How do these modelling techniques compare to each other?
7. Can a numerical model using a Darcy-Forchheimer porous zone reproduce existing experiments?
8. How can resistance parameters be determined to accurately describe fluid-vegetation interaction?

Note that a significant part of the background research is presented in the literature review. This report focuses on the technical implementation of the proposed model, while reference is made to the literature review for the majority of the insights regarding the kelp sector, background theory and state of the art in modelling.

1.3.2 Scientific approach

The main focus of the research presented in this report lies with development of a numerical model that quantifies wave damping. The model is supported with background from the literature review. Overall the build- up of all items used in answering the research questions are shown in Figure 1.6.

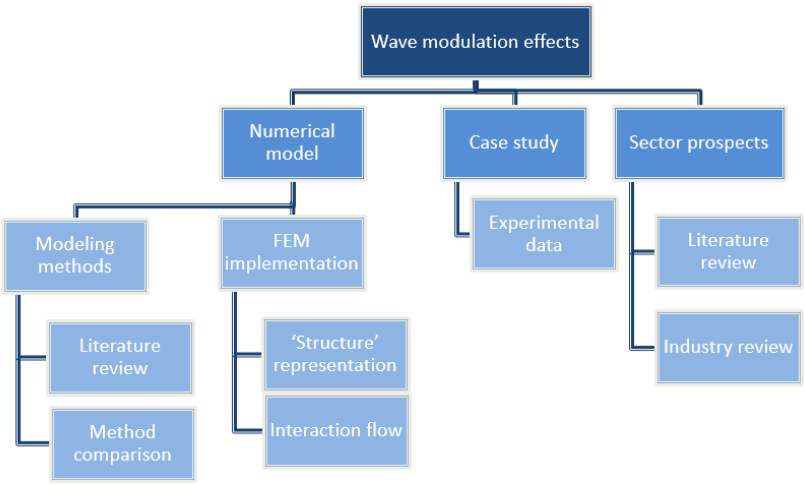

Figure 1.6: Schematic overview of all components in the proposed scope.

In terms of modelling, the activities done to achieve a successful numerical wave tank are presented in a task-list which entails:

- ☐ Mathematical formulation of flow through a porous domain
- ☐ Numerical methods for solving the problem
- ☐ Implementation of the numerical methods in FEM using *Gridap*
- ☐ Verification and validation of the numerical model
- ☐ Reproduction of existing experiments in the numerical wave tank
- ☐ Execution of a hypothetical farm case study
- ☐ Analysis and interpretation of simulation results

As with any numerical model, its credibility is dependent on the degree to which its structure itself, and the application thereof on the area of interest, is validated and verified. An extensive effort is made to test credibility of the results that the numerical model produces. To this end, a validation and verification strategy has been set up, which is graphically represented in Figure 1.7.

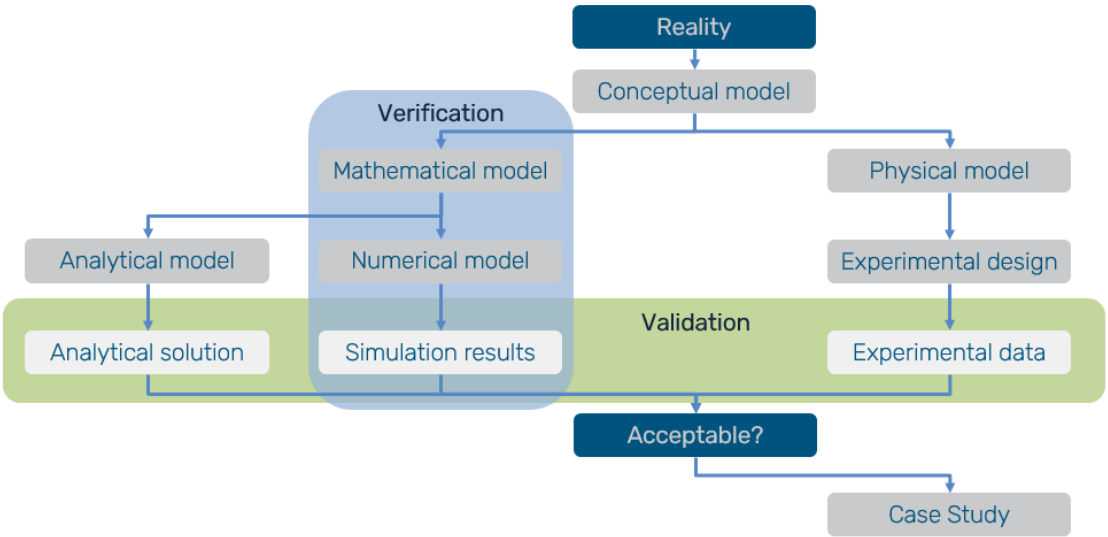

Figure 1.7: Validation and verification procedure used to test credibility of model results.

1.4 Thesis outline

After introduction of the main focus, and expression of the relevance of this research in the current chapter, the report goes on to present the main findings of the anterior literature review in chapter 2. The theoretical basis for the model is laid in chapter 3. This includes derivation of the main mathematical expressions used and justification of the route chosen and components that make up the numerical model.

In chapter 4, the basic properties of the model are presented. The same chapter goes on to expand on the validation and verification methods used to substantiate the credibility of the model. In the results in chapter 5, a sensitivity analysis is done to illustrate behaviour and runs are presented that display the phenomena in the numerical wave tank. This chapter also includes comparison to the existing experiments to judge the ability of the model to reproduce reality. In chapter 6, a case study that provides insights into how the proposed modelling method could be used is presented. This includes elaborate assumptions on the layout of the farm, based upon available data and information provided through the industry interviews that have been performed beforehand.

Finally, in chapter 7 the results are discussed, interpretation of whether these results make sense with the chosen assumptions and modelling approaches is included. Furthermore, conclusions are drawn that work towards answering the research questions. Recommendations on further research are included to provide a basis of expansion of the model to further improve accuracy, applicability and overall added value.

The entirety of the content discussed up to now is supplemented by background in the appendices. This includes information provided by industry partners, which will be omitted in the public version of this document. Additionally, a step-by-step setup of the model itself is appended for follow-up research.

2

Literature Review

The main findings from the literature review conducted prior to the modelling in this report are presented in this chapter. This includes the theoretical basis for creating the model in section 2.1, as well as the fundamentals on fluid-vegetation interaction and the main findings on current modelling methods, in section 2.2.

Part of the research questions that work towards the numerical model are derived from existing literature. They form ingredients to the model that are essential in the understanding of the problem, and therefore do not belong to the insights gained from the model. These key insights from the industry review and literature that aid in answering the research questions but aren't directly related to the numerical model itself are summarized in this chapter.

2.1 Theoretical background

Every attempt to capture fluid flow in a model is subject to the conservation of mass, momentum and energy. These balances can be used to derive nonlinear partial differential equations that describe the behaviour of fluids. This forms the backbone of any numerical method and for a large part determine the setup up a numerical wave tank. As these PDEs are the core of the method, they are derived elaborately in chapter 3, the other key elements that make up the modelling of fluid are touched upon more briefly in the following sections.

In this section the basic principles of linear wave theory are described. A short summary of the theory of vegetation interacting with fluid flow is considered as well. Additionally, the fundamentals of porous medium theory are stated, where the vegetation-representation in the numerical wave tank is built upon. All subjects in this chapter are documented more thoroughly in the elaborate literature review predating this report, for further background the reader is referred to this report.

2.1.1 Water waves

Different models exist to describe free surface water waves, for a comprehensive and very thorough overview reference is made to Holthuijsen [25]. One notable approach is often used for describing ocean waves, because of its simplicity but accurate description for mild conditions in deep water, this is linear wave theory. The region of application for linear wave theory is presented in the well known graphic of Figure 2.1.

Following this theory, the superposition principle holds, wavefields can be described with a combination of sinusoidals with varying amplitudes, wavefrequencies and phase shifts. This stems from the solution to the free surface that describes a progressive monochromatic wave, the pure sinusoidal; $\eta(x,t) = a\sin(\omega t - kx)$.

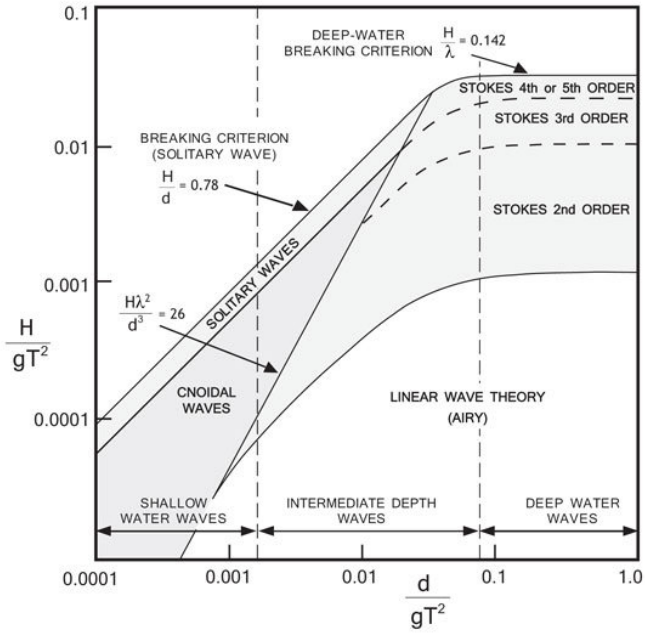

Figure 2.1: Overview of the ranges where different wave theories hold.

In linear wave theory, inviscid, irrotational and incompressible fluid is assumed, this allows for straightforward description of free surface waves and velocity profiles, derived from the velocity potential $\Phi(x, y, z, t)$. For deep water ($kd \longrightarrow \infty$), the assumption is made that the surface waves do not experience any effects of the bottom, i.e. the velocity profile tends to zero towards the seabed, and with relatively small-amplitude waves, linear wave theory can be applied in models that do not strictly follow its assumptions.

The implication of using linear wave theory is that higher order contributions to the surface elevation are neglected. Figure 2.2 visualized what this means for the generated waves and displays the purely sinusoidal wave $\eta(x, t) = a\sin(\omega t - kx)$ in the top pane.

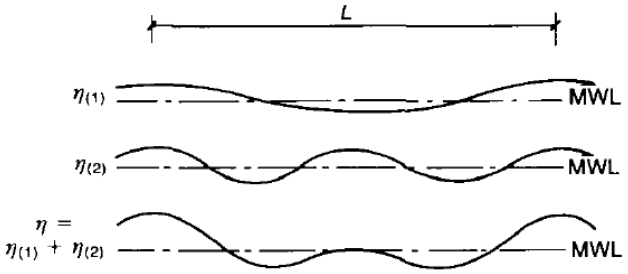

Figure 2.2: First and second order contributions to surface elevation.

Dispersion relation

The key relation that links the wavelength or wave frequency to its frequency is the dispersion relation. This formulation describes how waves of different frequencies travel at different velocities, it forms an integral relation that is used throughout fluid dynamics to relate the properties of surface gravity waves.

$$\omega^2 = gk\tanh kd \tag{2.1}$$

And for deep water, where $\tanh(kd) \longrightarrow 1$ since $kd \longrightarrow \infty$ this reduces to:

$$L = \frac{gT^2}{2\pi} \tag{2.2}$$

These expressions form a useful tool during the analysis of simulation results later on.

Wave energy

The energy present in waves per unit wave front can be expressed in terms of the kinetic energy and potential energy that travel with the wave. Equation 2.3 derives the total wave energy on the basis of the time-averaged kinetic energy in the entire column, and the potential energy that is present in the wave minus what is present without the wave:

$$\begin{aligned} E_{\text{pot}} &= \overline{\int_{-\text{d}}^{\eta} \rho g z \, \text{d}z} - \overline{\int_{-d}^{0} \rho g z \, \text{d}z} = \overline{\int_{0}^{\eta} \rho g z \, \text{d}z} = \frac{1}{4}\rho g a^2 \\ E_{\text{kin}} &= \overline{\int_{-\text{d}}^{\eta} \frac{1}{2}\rho u^2 \, \text{d}z} = \frac{1}{4}\rho g a^2 \\ E_{\text{total}} &= E_{\text{pot}} + E_{\text{kin}} = \frac{1}{2}\rho g a^2 \end{aligned} \tag{2.3}$$

This is a second-order property of the wave and it is estimated using linear wave theory, thus is bound by the same restrictive assumptions.

2.1.2 Drag

Structures induce resistance when placed in a fluid flow through drag. At low Reynolds numbers, the amount of drag has a linear dependence on the flow velocity. This regime is described as Stokes flow, where flow separation plays no role. It is governed by viscous drag, caused by the shear layers due to the difference of velocity around the structure's boundary. As Re rises above 10, this laminar flow starts to be disturbed, as inertial effects start to play a role. Eventually, when velocities rise high enough, the flow becomes fully turbulent.

This results in a non-linear progression of the added resistance to flow. Usually, drag force is approximated using a quadratic velocity-relation. Combination of these two givens results in the use of drag factor that is depended on Re, the ratio between inertial and viscous forces. In Figure 2.3, the progression of C_d is illustrated as a function of the flow regime for a cylinder and a sphere for illustration.

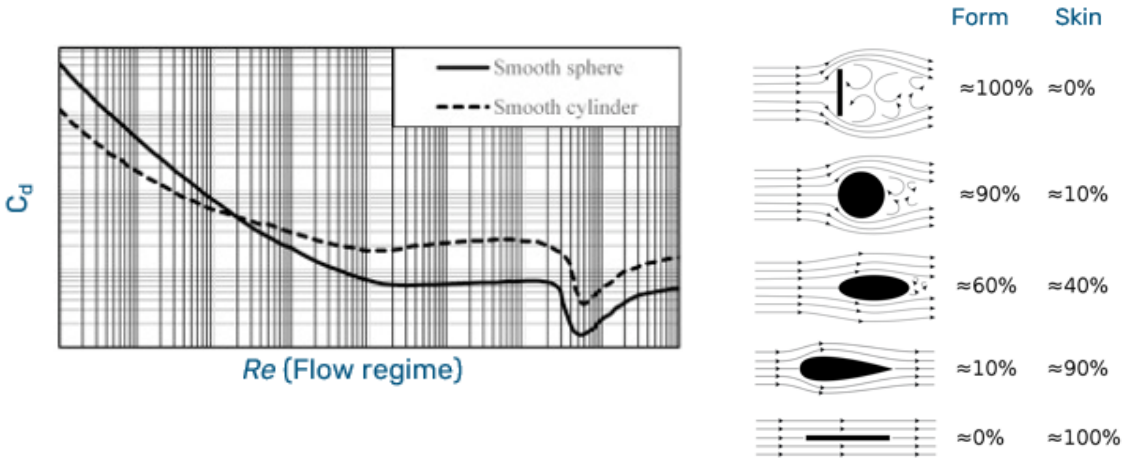

Figure 2.3: Illustration of 1) the unordered trend of C_d, and 2) Contribution of skin drag and form drag.

The graphics in Figure 2.3 aim to illustrate that drag force is not a phenomenon easily captured within a certain trend. Determination of drag force is usually done on the basis of calibration, but some idealized situations have been well well-researched like cylinders. For those, the trend in drag is studied extensively and formulations of the drag factor are available. With increasing complexity of the structure, the contribution of different phenomena do the total drag term become less obvious and structured.

2.1.3 Fluid-vegetation interaction

The presence of vegetation in a flow introduces resistance to the original flow. Meadows are known to induce shear layers, changing velocity structures and promoting mixing behaviour. Energy is dissipated due through vegetation drag forces mostly, which are greatly dependent on flow behaviour and plant characteristics.

As waves travel over, or through, vegetation patches, energy is dissipated due to the work of the wave forces done on the plant elements, reducing the left-over energy content behind the meadow. Drag contributions are usually assumed to be the main phenomena that dissipates energy. For the often-made assumption of rigid cylinder-like vegetation, the well-known Morison equation [52] can directly be used to derive the dissipated energy. Neglecting the out-of-phase inertial contribution, this reduces the energy dissipation by a single vegetation stem to only reflect the drag force (Equation 2.4).

$$\varepsilon_v = \int_{s=0}^{h_v} \overline{F_d u} ds \tag{2.4}$$

Where the integral represents the work done over the length of the vegetation from its root at $s = 0$ to the total vegetation height h_v. The overbar denotes phase-averaging over a wave cycle. The velocity u should be chosen as the velocity at the vertical center of the vegetation segment to best represent the physical situation.

Note that this approach neglects the influence of any force other than the drag. The added mass force, is an inertial force that stems from the acceleration of a body of fluid with the acceleration of the obstacle itself. The Froude-Krylov force is a non-viscous force from the unsteady pressure field induced by waves. The contribution of both F_A and F_{FK} are out of phase with the water motion, making their phase-averaged work done negligible, as presented in van Veelen et al. [71].

2.1.4 Porous media

Porous medium theory was initially developed to describe laminar flow through densely porous media, like packed beds. Originally, the relation was upon experimental results, in the meanwhile it has been mathematically derived via homogenization methods as well. The key philosophy behind porous medium approaches are representing the characteristics of a medium with a highly complex micro-scale geometry in a more generalized way.

The Darcy equations describes single-phase flow of a fluid through a porous medium, through the following balance:

$$-\frac{\partial p}{\partial x} = -\frac{\mu}{k_h}\mathbf{u}_D \tag{2.5}$$

Here k_h denotes the hydraulic permeability, μ is the viscosity and u_D represents the Darcy-velocity, the velocity at the pore-sale. Darcy describes laminar flow before nonlinear effects are introduced by inertial effects, and then turbulent effects at higher velocities.

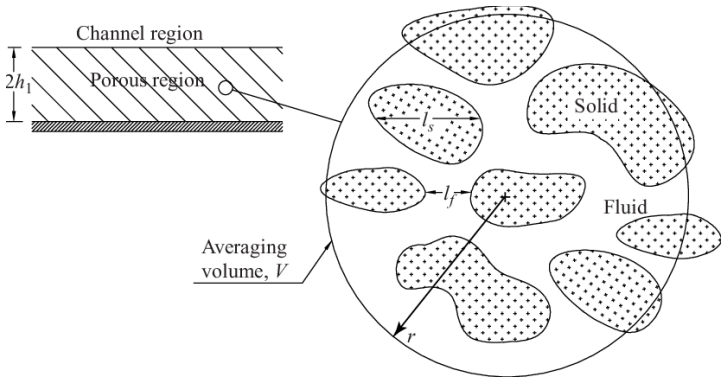

Figure 2.4: Spatial averaging of geometrical properties in a porous medium [66].

Darcy-Forchheimer formulation

However, the Darcy Law does not hold for all flows. Numerous additions have been proposed to describe flow rates in porous media, where the majority consist of additional terms to account for inertial, oscillatory and added mass effects. The coefficients of additional terms are often represented as a function of Re, KC, geometric parameters alone or solely best-fits to experimental data with very limited applicability. The latter can be seen as the origin of the expansion on Darcy's law, where the quadratic term was heuristically introduced to account for experimental outcomes [78].

To account for higher velocities, the Darcy formulation is usually expanded with a term that is quadratic with flow velocity. The Forchheimer equation (Eq. 2.6) is derived numerous times e.g. by means of the averaging theory for idealized periodic porous media, through Navier-Stokes for equal diameter spheres and through the fundamentals of continuum mechanics [64] . Zimmerman et al. [83] states that the Forchheimer equation can probably be used for the entire range of Reynolds numbers, as it effectively reduces to the Darcy equation for low Re.

$$-\frac{\partial p}{\partial x} = \alpha\mu\mathbf{u}_D + \beta\rho|\mathbf{u}_D|\mathbf{u}_D \tag{2.6}$$

Generally, non-Darcy flow can be presented by the three classes according to Jensen et al. [32]. The dominant phenomena in the classes start from purely laminar flow below Re < 1 and increase to the fully turbulent regime.

1. Forchheimer flow regime, $10 < Re_p < 150$
2. Transitional flow regime, $150 < Re_p < 300$
3. Fully turbulent regime, $Re_p > 300$

The introduction of higher order terms, and the derivative of the local velocity has been coined as well. Overall, most research agrees that the physical effects pertaining to these terms would be negligible compared to the linear and quadratic drag terms that dominate the problem under investigation.

Porous representation of vegetation

The suggestion that a Darcy-Forchheimer equation could be applicable to the wave-vegetation interaction problem has been coined before [84], [85]. Ghisalberti and Nepf [21] suggests that the lower part of dense, bottom founded vegetation can be described by the balance of drag and hydraulic gradient, much like Darcy flow. In Tsakiri and Prinos [67], porous representations with porosities between 0.55 for mangroves, and 0.99 for waterlillies were suggested.

In Brito et al. [7], porous coefficients are used to represent bottom-founded grass-like vegetation in a channel flow model. To the knowledge of the author this is one of the few, if not the only, study where this specific approach has been used and documented in detail. The study defines the coefficients using the assumption that parallels can be made between the geometries of dense vegetation and packed beds of grains. The coefficients that follow the Darcy-Forchheimer formulation are proposed to be established as follows:

$$\begin{aligned} K &= \frac{d_{eq}^2\psi^3}{150(1-\phi)^2} \\ T &= \frac{1.75(1-\phi)}{d_{eq}\phi^3} \end{aligned} \tag{2.7}$$

In the above, the viscous and inertial parameters K and T, which can be tensors for anisotropic systems, are dependent on the equivalent diameter d_{eq}, the porosity ϕ and ψ, the ratio between surface of an equal-volume sphere to the surface of the particle itself.

2.2 State-of-the-art

The novel approach used in this research exercise was inspired by the limitations of existing models. Thorough analysis of current modelling methods was performed to identify the state-of-the-art. This section describes the most important findings.

2.2.1 Modelling methods

Existing modelling methods can roughly be divided into three groups, based on the complexity of the approach. Yang and Chan [76] proposed to distinguish the following classes:

1. A (quadratic) drag force term applied to the governing equations on the existing non-dissipative wavelength scale. For instance using the Boussinesq equations, or shallow water formulation;
2. A higher resolution model using RANS or LES to capture wave-vegetation interaction with considerable detail;

3. A mathematical approach to multi-scale modelling through the homogenization technique.

In this classification, complexity intuitively increases with the classes. As the first class makes use of elaborately developed and well-documented base equations, and straightforward implementation of the vegetation effects, it is computationally relatively inexpensive. More emphasis is on computational resources for the second class. The third class is fully dependent on the mathematical approach taken.

Depending on the objective, the different classes might be more or less suitable for hydrodynamic analysis. However, in literature a clear preference lies with the straightforward formulations using a classical quadratic drag law, despite its limited flexibility in application and range of accuracy. Overall, research currently mainly relies on calibration of a (bulk) drag coefficient to quantify the influence for the specific conditions under observation. Efforts to apply C_d-based formulations to a somewhat wider range of conditions usually rely on Re- and KC-dependence. No complex models are found that have been validated over multiple species with different vegetation and flow characteristics.

Table 2.1: Comparison of strength and weaknesses of different modelling approaches.

	Computational cost	Resolution	Accuracy	Application flexibility
Class 1	++ Well-known existing frameworks	- - Only bulk quantities known	0 Potentially okay, but dependent on calibration range	0 Calibration-specific
Class 2	- - Resolving small scale immensely expensive	++ Ability to resolve up to smallest scale	++ Costly but high	+ Technically all situations feasible
Class 3	0 Separately solving micro- and macro scale offers optimization	++ Technically all scales possible	+ Dependent on coupling method	- Coupling method complexity is variable

Performance is indicated from very favorable (++) to very unfavorable (- -).

The overview of modelling techniques and their comparison is covered in depth in the literature review and provides insights into two of the more introductory research questions:

5. How are kelp forests currently begin modelled?
6. How do these modelling techniques compare to each other?

A wide variety of approaches are used to represent the interaction problem between current and waves through vegetation. As with any computational exercise of a physical problem, performance of the model representation relies entirely on the assumptions and simplifications made. The accuracy increase by including additional mechanisms must be carefully weighed against the computational costs for this specific area of interest [71]. Application of a porous medium formulation is considered to have a high potential in balancing the computational cost of the model to the adequacy of the simulation outcomes.

2.2.2 Analytical formulations

Only semi-empirical solutions exist to the vegetation-induced wave modulation problem. Reason for this is that the effects are generally described through the application of a drag coefficient C_d. This is inherently an empirical coefficient, which is determined through either calibration or direct measurements, as illustrated by the numerous formulations presented in Table C.

For validation purposes, the reproduction of a situation with a known analytical solution would be of value to strengthen the credibility of the numerical method. Since no purely analytical formulations exist, a closer look is taken at the semi-analytical solution that describes the influence of vegetation height in the water column. This problem has been derived by Zhu and Zou [80], and provides the opportunity to judge model behaviour regarding a known drag coefficient for different vegetation lay-outs. See subsection 5.2.5 for more details and the comparison with simulation results.

2.2.3 Experimental insights

The majority of academic publications regarding experiments on wave damping by vegetation consider bottom-founded vegetation in a wave tank under the influence of harmonic wave components. The main outline is usually comparable and features a setup similar to the one found in Figure 2.5.

Flume tank experiments using kelp mimics are the main source of experimental data. Apart from a sporadic study using real kelp, or very closely resembling mimics, the largest body of work centers around approximation of plants as rigid cylinders. Scaled experiments are the main - if not only - source of validation data for any large-scale offshore kelp field. Partly since only very rarely publications contain real-life measurements, and the few that do are not representative for the objective of studying forests at the intended large scale.

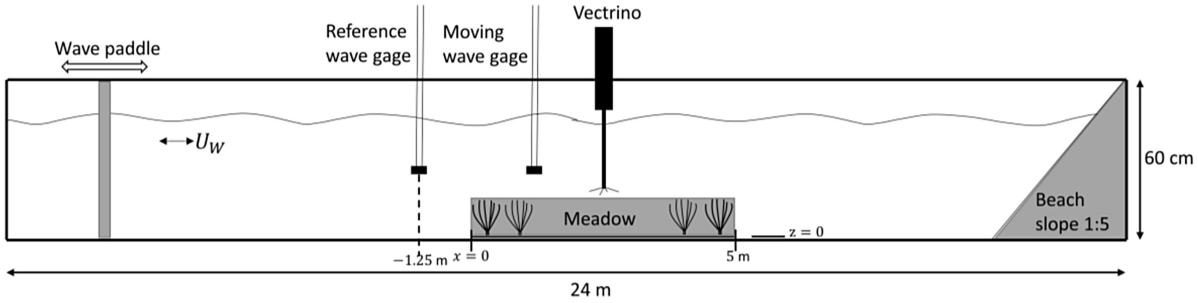

Figure 2.5: Example of exemplary experimental setup. Image taken from Lei and Nepf [39]

Overall, the available experimental data is broadly variable in chosen conditions, justification for and description of the conditions and characteristics is often lacking. It is difficult to establish a damping factor or range of percentages, but generally studies agree that wave energy can be significantly reduced for some combination of vegetation layouts and incoming wave conditions. A set of experiments is highlighted in Table C.3 as particularly well-documented for reproduction in a numerical wave flume.

There are various reasons why comparing results from different publications on scaled experiments can be a tedious job. Any analysis of available data should consider the absence of e.g. comments on flow development, missing parameters required to reproduce the experiments, inherent errors in using complex materials like plants or flexible plant mimics. Furthermore, as with any scientific experiment, systematic and random errors can be introduced by measuring equipment.

Taking lacking data and probable errors in account, the collection of experiments presented in the literature review can be used to form a qualitative image of expected results. In addition, the listing provides the opportunity to focus on similar experiments when comparing to a new experiment or model.

Three studies have been highlighted that are expected to provide sufficient background information to adequately remodel the physical situation in a numerical model. This implies that, despite the issues with contradictory sources as stated in this chapter, these three publications should be suitable sources to validate a model with.

3

Numerical framework

This chapter aims to provide a clear overview of the main components of the model. For an introduction to the software used, Julia language, and the main package Gridap [3] within this environment, reference is made to Appendix D. The contents of this chapter are focused on a conceptual description of the method and its implementation. The chapter begins by introducing the method applied, Finite Element Method, and continues to expand on the components that make up the model using this method. The chapter ends with a discussion on some of the implications of the chosen modelling assumptions.

3.1 Finite Element modelling

The Finite Element Method (FEM) is a numerical method that can be used to solve partial differential equations. The original, continuous, problem is discretized into smaller subproblems, dividing the original domain into elements with a finite number of nodes on the mesh. Furthermore, the original strong form of the governing equations is integrated by parts to reach the weak form, which is equivalent to the strong form but relaxes the requirements of the possible solutions and satisfies the problem in integral sense. Through integration by parts, the higher order derivatives are removed and smoothness (i.e. continuity) is ensured.

The solutions at the nodes are approximated using pre-defined types of functions. In predefining the functions, an assumption is made on their type, and boundary conditions can be considered. For simple problems, piece-wise linear functions might be sufficient, often piece-wise polynomial basis functions are used, as is the case for the present model.

Eventually, combining these solutions over the entire mesh provides an approximation to the solution of the original problem statement. In Figure 3.1, the building blocks of the numerical method, needed to reach a solution for the variables under investigation, are gathered in a flow diagram.

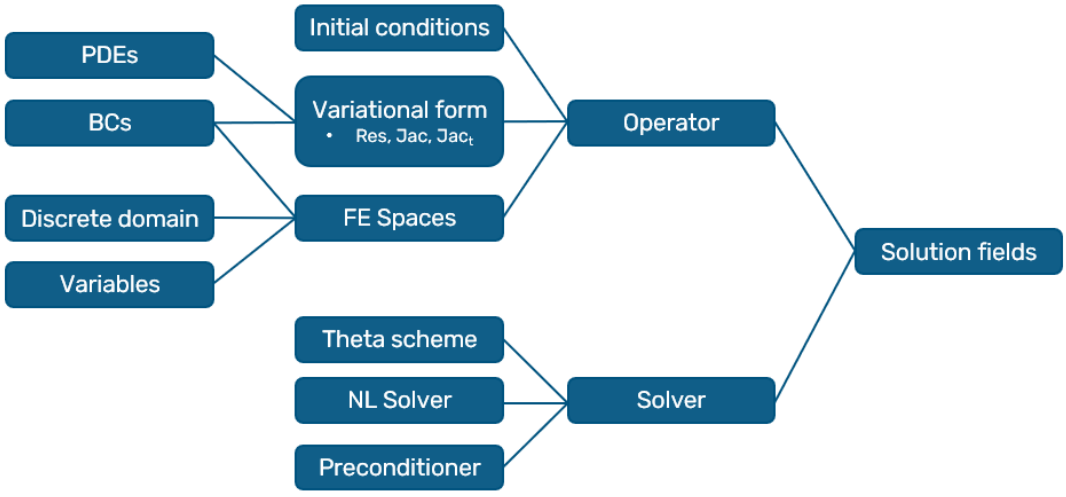

Figure 3.1: Schematic overview of the components that make up the numerical method.

3.2 Governing equations

As with any physics-based model, the backbone is formed by the governing equations in the strong form. The basis is formed by the universally known Navier-Stokes equations, derived from momentum conservation and mass conservation, this derivation is presented in subsection 3.2.1. The partial differential equations (PDEs) these derive towards represent the physics in the building blocks of Figure 3.1. How these are implemented into Julia Language through the Gridap package is presented in section 3.4.

3.2.1 Momentum and Continuity equations

The goal of the model is to describe the processes and changes in the fluid under influence of the conditions that are used as input for a certain simulation. This requires description of the fluid and its properties throughout the domain and throughout time. Changes in the properties of a fluid can be described using the derivative following a moving particle; the Lagrangian derivative, or material derivative, which consists of the Eulerian derivative and the advective term:

$$\frac{D}{Dt} = \frac{\partial}{\partial t} + \mathbf{u}\cdot\nabla \tag{3.1}$$

This conservation relation can be applied to the mass flux $\rho\mathbf{u}$ to obtain the momentum equation. In the following expression, s represents an arbitrary source term and $\rho\mathbf{u}\otimes\mathbf{u}$ can be simplified out using the identity of the divergence of the tensor product.

$$\begin{aligned} \frac{\partial}{\partial t}(\rho\mathbf{u}) + \nabla\cdot(\rho\mathbf{u}\otimes\mathbf{u}) &= \mathbf{s} \\ \mathbf{u}\frac{\partial\rho}{\partial t} + \rho\frac{\partial\mathbf{u}}{\partial t} + \mathbf{u}\mathbf{u}\cdot\nabla\rho \dashv\cdot\rho\mathbf{u}\cdot\nabla\mathbf{u} + \rho\mathbf{u}\nabla\cdot\mathbf{u} &= \mathbf{s} \end{aligned} \tag{3.2}$$

Further simplification using $\mathbf{u}\cdot\nabla\rho+\rho\nabla\cdot u = \nabla\cdot(\rho\mathbf{u})$, and applying mass conservation this further simplifies towards the following:

$$\mathbf{u}\underbrace{\left(\frac{\partial\rho}{\partial t}+\nabla\cdot(\rho\mathbf{u})\right)}_{\text{mass cons.}} + \rho\left(\frac{\partial\mathbf{u}}{\partial t}+\mathbf{u}\cdot\nabla\mathbf{u}\right) = \mathbf{s} \tag{3.3}$$

This leaves us with the basis for the Navier Stokes expression to be used in the model. However, further derivations can be made regarding the, currently still general, source term. We know this to be the part where any body forces and internal forces should come in. This allows for distinction between body forces and the Cauchy stress tensor to contribute to the source term, $\mathbf{s} = \mathbf{f}+\sigma$. Dividing σ into the pressure-induced stresses and the deviatoric stress tensor τ we get an expression that allows for isolation of the pressure.

$$\sigma_{ij} = \begin{pmatrix} \sigma_{xx} & \tau_{xy} & \tau_{xz} \\ \tau_{yx} & \sigma_{yy} & \tau_{yz} \\ \tau_{zx} & \tau_{zy} & \sigma_{zz} \end{pmatrix} = -\begin{pmatrix} p & 0 & 0 \\ 0 & p & 0 \\ 0 & 0 & p \end{pmatrix} + \begin{pmatrix} \sigma_{xx}+p & \tau_{xy} & \tau_{xz} \\ \tau_{yx} & \sigma_{yy}+p & \tau_{yz} \\ \tau_{zx} & \tau_{zy} & \sigma_{zz}+p \end{pmatrix} = -p\mathbf{I}+\boldsymbol{\tau} \tag{3.4}$$

Now $\mathbf{s} = -\nabla p + \nabla\cdot\tau + \mathbf{f}$, and the pressure gradient is isolated which enables easier setup of the numerical model later on. We can further simplify the stress tensor to include the assumption that the stress is proportional to the velocity gradient in the fluid, one of the well-known assumptions made by Stokes. Under assumption that viscosity is constant (and diminishing any effects of volume change by viscosity, meaning $\lambda = 0$), the deviatoric stress tensor simplifies to:

$$\begin{aligned} \tau &= \mu\left(\nabla\mathbf{u} + (\nabla\mathbf{u})^\top\right) + \underbrace{\lambda(\nabla\cdot\mathbf{u})\mathbf{I}}_{0} \\ \tau &= \mu\nabla^2\mathbf{u} \end{aligned} \tag{3.5}$$

3.2.2 Case specific formulation

For this model the Navier-Stokes equations are simplified for a non-compressible fluid of constant viscosity, resulting in a constant density. Taking into account mass conservation, momentum conservation, the assumption of incompressibility and a Newtonian fluid, the Navier-Stokes equations were derived in the previous section, this section provides the case-specific formulation. The assumptions posed result in a strong form that finds the velocity field $\mathbf{u}$ and the pressure field p as follows:

$$\begin{aligned} \rho\left(\frac{\partial \mathbf{u}}{\partial t} + \mathbf{u}\cdot\nabla\mathbf{u}\right) - \mu\Delta\mathbf{u} + \nabla p = \mathbf{f} \quad &\text{on } \Omega \\ \nabla\cdot\mathbf{u} = 0 \quad &\text{on } \Omega \end{aligned} \tag{3.6}$$

As by convention, ρ and ν are the density and kinematic viscosity of the fluid. The gradient and divergence of properties are denoted by ∇ and $\nabla\cdot$, respectively. The Laplace operator with respect to the spatial coordinates is denoted by Δ, equaling ∇^2.

In this equation, the f terms represents any external forcing. For the case of fluid-vegetation interaction, and considering the influence of gravity, this contains both phenomena.
The basic statement of the continuity and momentum equation are adapted to the specific needs of the model. This includes processing the assumption of constant density, the addition of gravitational force and the application of the external forcing as stated in the Darcy-Forchheimer porous medium equations. This results in the following expression, where p^* denotes the pressure, factored for the density ρ:

$$\begin{aligned} \underbrace{\frac{\partial \mathbf{u}}{\partial t}}_{\text{Velocity change}} + \underbrace{\mathbf{u}\cdot\nabla\mathbf{u}}_{\text{Convection}} - \underbrace{\nu\Delta\mathbf{u}}_{\text{Diffusion}} + \underbrace{\nabla p^*}_{\text{Pressure gradient}} = \underbrace{\alpha\mathbf{u} + \beta\mathbf{u}^2}_{\text{Darcy-Forchheimer resistance}} + \underbrace{\mathbf{g}}_{\text{Gravity}} \quad &\text{on } \Omega \\ \nabla\cdot\mathbf{u} = 0 \quad &\text{on } \Omega \end{aligned} \tag{3.7}$$

Furthermore, it should be noted that generally this formulation is well-suited to numerically solve laminar flows, with relatively low Reynolds numbers. As Re increases, turbulent effects introduce the need for turbulence model to model flows successfully, for instance through Reynolds-Averaging and the implementation of some closure method. As this research does not require detailed modelling on the micro-scale, reference is made to subsection 2.1.4, and the literature review, for more details.

3.3 Boundary Conditions

Within the model, two domains are defined to distinguish between 'free-flowing' water and the vegetated porous medium zone. Furthermore, model boundaries are defined to be able to apply boundary conditions. In Figure 3.2 a schematic representation is given of the components in within the stationary domain. The following subsection proceed to state a description of these boundaries and sub-domains, and present how they are captured in the numerical wave flume.

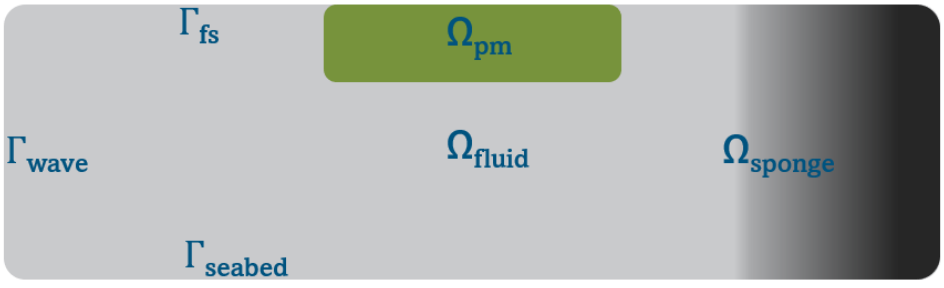

Figure 3.2: Schematic overview of the model domains and boundaries.

3.3.1 Wave generating boundary condition

For definition of the inflow condition, water particle velocities are implemented using a deep water wave formulation. As the model is based on a 2D approach, where only the vertical dimension y and wave propagation

direction x are considered, the classical description is reduced with one dimension. This entails horizontal and vertical water velocities that are defined using Equation 3.8, based upon linear wave theory Dalrymple et al. [17], see also subsection 2.1.1:

$$\begin{aligned} u_{\text{hor}}(x,y,t) &= a_i \omega_i \frac{\cosh(k_i y)}{\sinh(k_i d_{\text{water}})} \sin(k_i x - \omega_i t - \theta_i) \\ u_{\text{ver}}(x,y,t) &= a_i \omega_i \frac{\sinh(k_i y)}{\sinh(k_i d_{\text{water}})} \cos(k_i x - \omega_i t - \theta_i) \end{aligned} \tag{3.8}$$

The method used makes it static boundary wave generation, where only velocities are prescribed. This allows pressures to be calculated and prevents over-specification of the problem.

The model setup is versatile in the possibilities of wave generation. In the current research, use has mainly been made of regular waves using single frequency harmonic surface elevations. However, wave generation of many kinds of waves would be possible. To illustrate versatility of modelling setup, the option to combine multiple harmonic waves to represent an irregular sea-state was implemented. Referring to Figure 2.1, non-linear theories can be used to generate the inflow boundary. In Table 3.1 sources regarding numerical wave generations for different types of waves have been included for further developments.

Table 3.1: References on wave generation of different wave theories, from Higuera et al. [24].

Theory	Reference	Comments
Stokes I and II	Dean and Dalrymple (1991)	
Stokes V	Skjelbreia and Hendrickson (1960)	
Cnoidal	Svendsen (2006)	Best fit solver. Makes use of ALGLIB open source libraries'.
Streamfunction	Fenton (1988)	No solver programmed. Its input is the output coefficients from Fenton (1988) programme.
Solitary wave	Lee et al. (1982)	Boussinesq theory.

Even though the current model representation theoretically allows for generation of any of these waves through application of their velocity profile, it is important to note that the linearised boundary condition strongly limits the range of waves that can be realistically modelled to propagate through the domain. Special attention is paid to this limitation in interpretation and discussion of the simulation results. Already, it should be noted that, since the objective of this thesis is modelling the offshore environment, deep water, small-amplitude waves are assumed thus limiting the immediate effect of the linearisation.

3.3.2 Numerical damping beach

The rightmost boundary condition is of the Dirichlet-type where zero velocity is forced, meaning a reflective boundary is put in place. This boundary ensures that no leakage occurs at the rightmost boundary, ensuring conservation of mass over the domain.

In order to counter the occurrence of reflections within the domain, which obscure the analysis of the vegetation's influence, a damping zone is implemented in front of the reflective boundary. See the element indicated by Ω_{sponge} in Figure 3.2. This method is often found in literature [11], as it provides a numerically robust method to counter reflections and ensure conservation of mass, even though calibration of the damping coefficient is needed.

A sponge layer that linearly increases in damping resistance is modelled, that acts like a wave absorber. The characteristics needed to absorb wave energy is dependent on the incident wave. Deriving the sponge's damping factor μ_d is a lively field of research, for this model calibration was used. See subsection 4.1.2 for details on the calibration procedure that was used to ensure minimal reflections.

3.3.3 Free surface boundary condition

For free surface definition, the choice made to implement a method similar to the linearized free surface boundary conditions as used in Airy wave theory. Two boundary conditions are implemented, a static and

a dynamic formulation. The static boundary condition dictates that displacements and velocities must be equal for the fluid and the adjacent air.

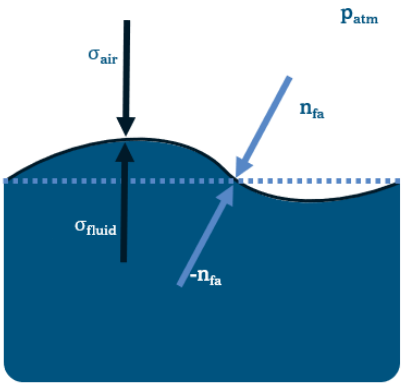

Figure 3.3: Schematic overview the traction balance used in free surface definition.

The dynamic boundary condition relates the stresses in the air and fluid, respectively σ_{air} and σ_{fluid} in Figure 3.3 and Equation 3.11, to satisfy continuity of traction over the interface. This entails a linearized transpiration BC, where the a new variable η is used to signify deviation from the at-rest-surface. This could be seen as the *virtual* surface elevation, denoted with the dark solid line in Figure 3.3, since in the stationary grid does not extend beyond the light dotted line, representing at-rest-surface. Two additional balances are introduced to calculate where the free surface is to be modelled. Representation of the interface is shown in Figure 3.3.

The additional balances are based upon the traction continuity and the displacement/velocity, and are formulated by plugging the stresses in the fluid and air into the traction equilibrium at the interface.

$$\begin{aligned} \sigma_{\text{fluid}} &= \tau_{\text{s,v}} - pI \\ &= 2\mu\varepsilon(\mathbf{u}) - pI \end{aligned} \tag{3.9}$$

$$\sigma_{\text{air}} = p_{\text{atm}} + \rho_{\text{fluid}} g\eta \tag{3.10}$$

These expressions for the stresses are then plugged into the traction equilibrium on the free surface, providing:

$$\begin{aligned} \tau_{\text{fluid}} &= \tau_{\text{air}} \\ -(\sigma_{\text{fluid}})n_{\text{fa}} &= \sigma_{\text{air}} n_{\text{fa}} \\ -(2\mu\varepsilon(\mathbf{u}) - pI)n_{\text{fa}} &= (p_{\text{atm}} + \rho_{\text{fluid}} g\eta)n_{\text{fa}} \end{aligned} \tag{3.11}$$

where n_{fa} represent the outward normal vector to the free surface (light blue arrows in Figure 3.3), from fluid to air and $\varepsilon(\mathbf{u})$ is the symmetric gradient of the velocity. Additionally, we have the identity matrix I, gravitational constant g and the constant atmospheric pressure p_{atm}.

The method used allows for modelling the free surface without the need to introduce a secondary fluid domain. Instead, a virtual interface is determined along the boundary of the original domain. In the modelling domain this elevation corresponds to increased pressure that represents additional pressure due to the water extending past the at-res-surface. In short this means that the pressure field in the solution space contain a dynamic term that is dependent upon the virtual elevation η.

3.3.4 Seabed boundary condition

For the stationary lid (confined flow) and the seabed (all set-ups), a classical no-slip condition is applied. The no-slip boundary condition is mathematically represented by the following statement:

$$\mathbf{u}|_{z=0} = 0 \tag{3.12}$$

This condition forces fluid velocity at the location of the boundary to remain zero and produces a gradient towards the free-flow velocity.

3.4 Weak form

The governing equations, including the boundary conditions, make up the *strong form* of the problem. In the Finite Element Method, this strong form is transformed to its equivalent (variational) *weak form*. This is done by multiplying with an arbitrary weight function, or test function, and integrating over the applicable domain. Through integration by parts, the higher order derivatives are removed and smoothness (i.e. continuity) is ensured. When the solution is found for the weak form of the problem, this directly implies the solution to its strong counterpart as well, thus solving the modelled system.

In the Galerkin method of weighted residuals, the integral of the inner product of the residual with the test functions is set to zero. This minimizes the approximation error of the trial solutions and finds the solution to the original PDEs of the problem statement. For reference, the weak form as used in the numerical model is presented in Equation 3.13, this contains all terms that follow from the previous sections.

$$\begin{aligned}
&\int \underbrace{\left(\mathrm{v}\cdot\frac{\partial u}{\partial t}+\mathrm{v}\cdot\left(\left(\nabla(\mathrm{u})'\right)\cdot\mathrm{u}\right)+2\nu(\varepsilon(\mathrm{v})\odot\varepsilon(\mathrm{u}))-(\nabla\cdot v)*\mathrm{p}+q*(\nabla\cdot u)\right)}_{\text{Incompressible NS}}\mathrm{d}\Omega+\int\underbrace{\left(v\odot(\alpha u)+v\odot\left(\beta|u|u\right)\right)}_{\text{Darcy-Forchheimer terms}}\mathrm{d}\Omega+\ldots\\
&\int\underbrace{\left(v\cdot f_g\right)}_{\text{Gravity}}\mathrm{d}\Omega+\int\underbrace{\left(\tau_m*\left(\left(\nabla(u)'\right)\cdot u-s\right)\cdot\left(\left(\nabla(v)'\right)\cdot u-\epsilon\right)\right)}_{\text{Stabilization term}}\mathrm{d}\Omega+\ldots\\
&\int\underbrace{\left(\left(\mathrm{p_{atm}}-\mathrm{g}\eta\right)*\mathrm{n_{fa}}\cdot w\right)\mathrm{d}\Gamma_{\mathrm{fa}}+\int\left(\left((u\cdot n_z)-\frac{\partial\eta}{\partial t}\right)*w\right)}_{\text{Free surface equilibrium terms}}\mathrm{d}\Gamma_{\mathrm{fa}}
\end{aligned}\tag{3.13}$$

3.4.1 Convection stabilization

As stated, stability of the model is largely ensured by the dissipation terms in the vegetation patch(es) and the sponge layer. However, for empty domain runs without activated sponge, stability can be enhanced to ensure convergence to a solution for a larger set of input parameters. In this formulation, *inf-sup* stability is ensured by choosing 2^{nd} order interpolation for the velocity field, with a 1st order pressure interpolation. Still, convection could theoretically dominate the flow, therefore a convection-stabilization term is considered.

A stabilization term was added to the incompressible Navier-Stokes problem described in section 3.2, to avoid convective instabilities and enhance convergence to a solution. In Colomés et al. [13], a term-by-term OSS method is proposed to stabilize the convective term, pressure stabilization is neglected as this is guaranteed for the ISS FE Space used. A projection is introduced through an additional variable s, which represents the orthogonal FE projection. The existing bilinear weak form is supplemented with two terms, found in Equation 3.14.

$$B_{\text{tbt-oss-iss}}\left(\mathbf{u},\left(\mathbf{u},p\right),\left(\mathbf{v},q\right)\right)=B_{\text{original}}\left(\mathbf{u},\left(\mathbf{u},p\right),\left(\mathbf{v},q\right)\right)+\left(\tau_m\mathbf{u}\cdot\nabla\mathbf{u},\mathbf{u}\cdot\nabla\mathbf{v}\right)-\left(\tau_m\boldsymbol{\eta},\mathbf{u}\cdot\nabla\mathbf{v}\right)\tag{3.14}$$

In this equation, the stabilization parameter τ_m is based upon the mesh size h and the algorithmic constants c_1 and c_2 as further elaborated in Colomés et al. [12].

$$\begin{aligned}
\tau_m&=\left(\frac{c_1\nu}{h^2}+\frac{c_2\left|\mathbf{u}_h\right|}{h}\right)^{-1}\\
c_1&=12\\
c_2&=2
\end{aligned}\tag{3.15}$$

3.5 Solver

The setup of the PDEs for the problem is a nonlinear system of equations, this requires a nonlinear solver to be implemented in the numerical scheme. In this case, a Newton-Raphson method is chosen with back-tracking line-search, it relies on preconditioned GMRes.

3.5.1 Newton-Raphson method

The Newton-Raphson method can iteratively find better approximations of the solution of all unknown variables, it makes use of a linearization of the weak form through the Jacobian. This is a result of the Newton-method's main approach, where it finds successively better approximations using the function and its derivative as follows:

$$x_{n+1} = x_n - \frac{f(x_n)}{f'(x_n)} \tag{3.16}$$

Discretization is thus required for both the residual and the Jacobian. The Jacobian itself is found through differentiation by parts of the residual as presented in Equation 3.13, the option for auto-differentiation using Gridap is in the pipeline at time of writing, this would allow for definition of only the residual.

3.5.2 Generalized minimal residual method

The Newton method described above and used for the nonlinear PDEs in turn relies on solving sets of linear equations. In this model, the generalized minimal residual method (GMRes) is used. As the name implies, this method approximates the solution by minimizing the residual stated in Equation 3.13.

3.5.3 Preconditioning

In order to decrease computation time, the system is preconditioned before the GMRes iterative solver is applied. Incomplete Lower-Upper factorization (ILU) is used to rearrange the matrices beforehand.

Solving the system $Ax = y$ can be optimized for quicker convergence using $A = LU$ to $Ly = b$ and $Ux = y$. This proves a more efficient method if L and U can be reduced to a lower unitriangular and upper triangular matrix, respectively, resulting in $A \approx LU$. The latter expression can be made arbitrarily close to the original problem statement through tolerance τ_{ILU}, which is set to $1e-6$ for the present scheme.

3.5.4 Time-stepping

For time integration, the Theta Method is applied, a non-variable time-stepping method with a user-defined parameter Θ. For Θ-values of 0, 0.5 and 1, this method reduces to the Backward Euler method, Trapezoidal rule and Euler method, respectively. The implementation of this time-stepping method is provided by Badia et al. [4]. For an early version it was found that stability improved by setting Θ to 0.6, while this was later shown to drastically increase energy dissipation. Eventually, Θ was set to 0.5 amounting to the trapezoidal method, as shown below.

$$\begin{aligned}
& \boldsymbol{y}_{n+1} = \boldsymbol{y}_n + h\left[\theta \boldsymbol{f}\left(t_n, \boldsymbol{y}_n\right) + (1-\theta)\boldsymbol{f}\left(t_{n+1}, \boldsymbol{y}_{n+1}\right)\right], \quad n = 0, 1, \ldots \\
\text{and specifically:} & \\
\text{Euler: } \Theta = 1, \quad & \boldsymbol{y}_{n+1} = \boldsymbol{y}_n + h\boldsymbol{f}\left(t_n, \boldsymbol{y}_n\right), \\
\text{Backward Euler: } \Theta = 0, \quad & \boldsymbol{y}_{n+1} = \boldsymbol{y}_n + h\boldsymbol{f}\left(t_{n+1}, \boldsymbol{y}_{n+1}\right), \\
\text{Trapezoidal: } \Theta = \frac{1}{2}, \quad & \boldsymbol{y}_{n+1} = \boldsymbol{y}_n + \frac{1}{2}h\left[\boldsymbol{f}\left(t_n, \boldsymbol{y}_n\right) + \boldsymbol{f}\left(t_{n+1}, \boldsymbol{y}_{n+1}\right)\right].
\end{aligned} \tag{3.17}$$

The trapezoidal time-stepping scheme is an implicit method which induces the advantage of increased stability for larger time steps.

3.6 Discrete model and FE spaces

The model makes used of an Eulerian domain, with an equally-spaced mesh. The items from the previous sections are implemented on this uniform fixed mesh. The spacing of this mesh is based upon the Figure 4.3.1, built using Gridap's *DiscreteModel* function.

On the domain, a secondary model is defined on the upper boundary. This serves to facilitate the solution space where the surface elevation is defined upon. This leads to a 2D model for the entire domain, and a 1D surface boundary model, making the overall model mixed-dimensional.

Table 3.2: Finite element spaces defined on the domain.

Solution field	Var.	Space type	Order	Conf.	Notes
Velocity	u	Lagrangian, vector	2	H1	
Auxiliary stabilization var.	s	Lagrangian, vector	2	H1	Orthogonal projection velocity
Pressure	p	Lagrangian, scalar	1	C0	
Free surface elevation	η	Lagrangian, scalar	2	H1	On boundary Γ_{fs} only

In the model, the Finite Element spaces listed in Table 3.2 are linked together using Gridap's *MultiFieldFESpace*, which allows coupling of the variables through the weak form. Upon defining the FE Spaces, the boundary conditions can be partially integrated into the numerical setup already. The inflow boundary condition, with prescribed velocities for wave generation, and the zero-velocity seabed boundary, are implemented into the velocity trial space. This forces that any solution found by the solver will account for this boundary condition per definition.

The free-surface boundary condition is implemented in the weak form, see Equation 3.13, as this is dictated by the continuity of traction which cannot be hard-coded into the finite element spaces. Note that, as states in subsection 3.4.1, the FE space for velocity uses second order interpolation, while p has an interpolation order of 1 and C0-conformity.

4

Model Setup

The numerical framework presented in the previous chapter is supplemented with the setup as shown in this chapter. This includes input parameters regarding dimensions, wave conditions, grid resolution and timesteps. Analysis of the waveshape without any porous zone in place is done to evaluate the accuracy of wave production. In addition, the range of applicability in regards of input parameters is shortly discussed.

4.1 Model Parameters

Throughout the verification and validation process in this chapter, and the runs to generate the results in the following chapter, a set of model parameters are applied to represent realistic conditions.

4.1.1 *Standard Flume Model* settings

For the different purposes, the model is set-up to accommodate comparison to experimental results from literature. Therefore, in determination of the *Standard Flume Model* (SFM) parameters in Table 4.1, values are used that compare to the scale at which the majority of experiments on done in wave flumes. Reference is also made to Table C.3 from the literature review for an overview of typical experimental setups.

Table 4.1: *Standard Flume Model* parameters. Based on available experimental data.

Input parameter	Value or range	Unit
Total flume length	15	m
Sponge layer length	7.5	m
Water depth	1.0	m
Vegetation length	5.0	m
Vegetation height	0.2	m
Spatial resolution	5	cells/m
Timestep size	0.01	s
Simulation time	30	s
Standard wave height	0.015	m
Standard wave period	1.0	s
Standard wave length	1.54	m

4.1.2 Damping zone calibration

The sponge layer, used as a numerical beach and described in subsection 3.3.2, is calibrated to minimize reflections on the rightmost boundary that induce an error in the following analyses. Kim et al. [36] proposes to use a damping zone length of 1.5 times the wavelength. The damping coefficient, however, is dependent on wave input parameters, therefore it was calibrated on the regime of test for this research with a = 0.01 m and T = 1.0 s. Iteratively, the damping zone was shown to provide desired results for a damping coefficient of μ_0 = 10.

Table 4.2: Wave damping coefficient calibration.

Wave damping coefficient μ_0	Remaining after (x) m 0	2.5	5
25	100%	8.1%	0.1%
10	100%	12.0%	0.4%
2.5	100%	38.7%	1.0%

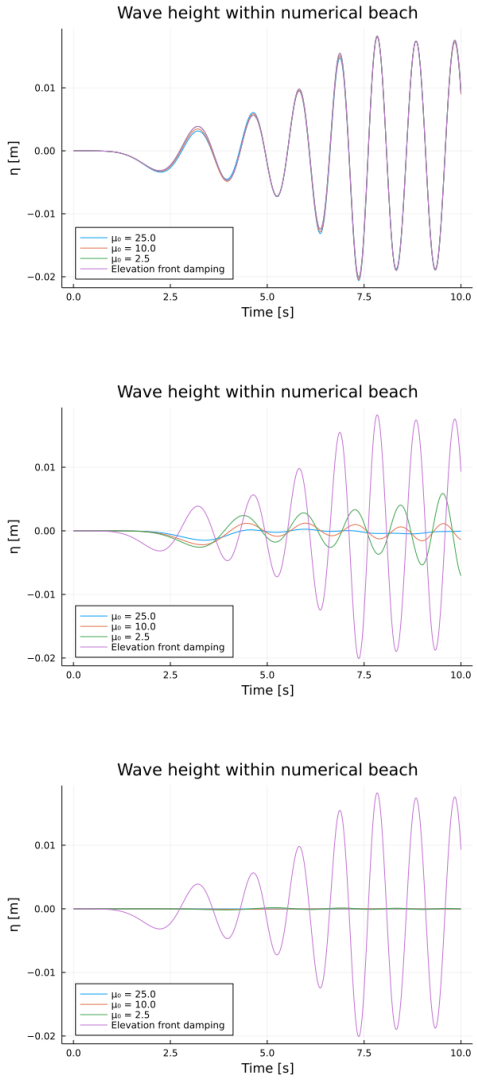

Figure 4.1: Calibration tests of the damping coefficient μ_0 for 1) wave heights at the damping zone front, 2) wave heights halfway through the damping zone, and 3) at the rightmost boundary. In purple, the undamped wave height is shown for reference.

For use of the model under a different regime of input waves, the calibration presented here is revised for optimal results. For the runs presented in the sensitivity studies and experiment reproductions, the damping zone length was parameterized to be 4λ, a conservative approach to ensure dissipation of all kinetic energy and reduction of all reflections.

4.2 Porous parameters used

In the model description presented in the next chapter, the vegetation is represented through the Darcy-Forchheimer terms α and β. These viscous and inertial terms are indicated in subsection 2.1.4, and more

thoroughly described in the literature review. As stated, Dupre [20] explains the parameters to be traditionally found through analysis of experimental data. However, as the present model aims to approximate behaviour for a wider range of conditions, a formulation is needed that can be found with minimal experimental data. To this end, the approach to define the parameters as a function of the conditions is used. The dependencies found in the limited research available are stated in the literature review.

Wave attenuation is influenced by numerous characteristics of plant and flow alike. It is only natural that the formulation of the Darcy-Forchheimer parameters follow from these dependencies. In Table 4.3, an indication is stated of what parameters are expected to be governing on the basis of the earlier research.

While the bulk drag coefficient C_d has found many different expressions for different applications, calibration of the porous parameters of the Darcy-Forchheimer equation is much less researched.

Table 4.3: Main parameters of influence on wave damping.

Category	Parameter	Description	Expected range
Dimensionless	Reynolds	Degree of inertial forces over viscous forces	10 < Re < 4700
Dimensionless	Keuler-Carpenter	Influence of oscillatory nature of flow	0.6 - 500
Dimensionless	Cauchy	Influence of flexibility	$\approx$ 1.0
Layout	N_v	Vegetation density in plants/m^2	0.15 - 5
Layout	L_m	Length of the meadow	up to 350 m
Layout	h_v/d	Relative plant height	0.1 - 0.5
Wave	T	Wave period/frequency	1-10 s
Wave	h_0	Incident wave height	0.1 - 5.0 m
Wave	d	Water depth	5 - 100 m
Plant	E	Elastic modulus plant	order 1-10 MPa
Plant	A_v	Leaf/blade surface area	500 cm^2, Saccharina
Plant	b_v	Frontal area of plant per unit height	0.2 m^2, Pyrifera

As stated, this research is focused on developing the numerical framework that enables further investigation of the porous parameters. Deriving the porous parameters themselves should be based upon the physical phenomena that govern the energy dissipation. Vortex shedding and vertical mixing transport the majority of the energy, general increase in turbulence intensity eventually dissipated the energy into heat. The formulations of α and β will have to be based upon the physical properties of the system that influence these phenomena.

4.3 Verification & Validation

The processes of verification and validation are essential steps in assessing credibility and accuracy of the outcomes of any numerical model. It should be noted that from a philosophical standpoint, in science, the veracity of a model cannot be proven. This contrasts the fallacy of any model or hypothesis, which is easily proven. Rather, this chapter comments on the credibility of the outcomes of the model that has been established and aims to confirm its applicability under certain conditions.

Verification refers to the mathematical side of the model. It is used to remove programming errors and verify the numerical algorithms used. Often, elements of the model are compared to systems of which an analytical solution is known. Congruence between the numerical and analytical results is often used to imply verification of the model.

On the other hand, validation concerns the physics of the model. It should conclude whether or not the implemented mathematics are a useful approximation of real-world phenomena. This means that validation considers a certain application, or range of applications. Generally, responsibility for verification lies with the software developer, while the end-user is meant to validate applicability to their use case. Within the present study, both steps are performed. Therefore, this section discusses both verification and validation of the model for its use with the desired application.

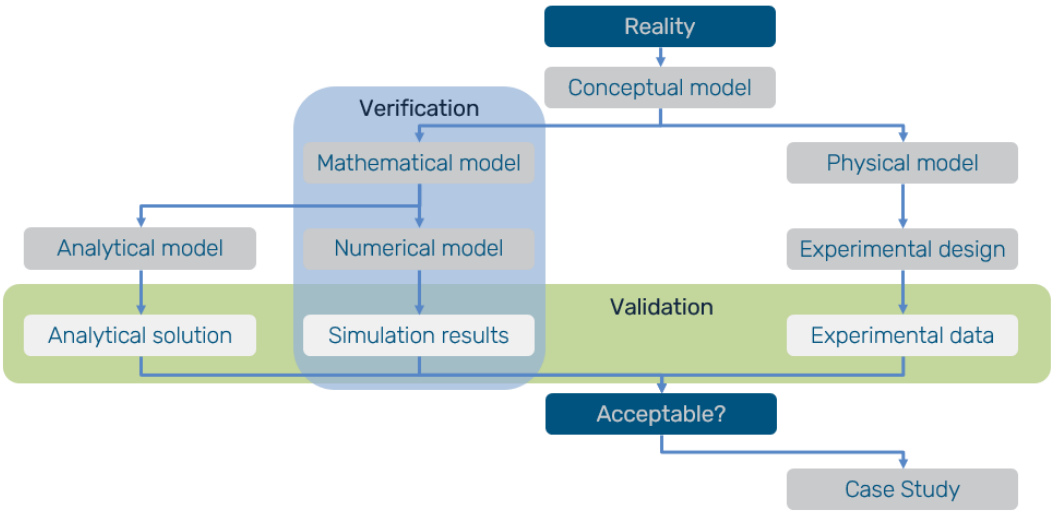

Figure 4.2: Graphical representation of validation and verification procedure.

4.3.1 Verification

The process of determining that a model implementation accurately represents the developer's conceptual description of the model and the solution to the model. - AIAA

Flow development and wave shape

One straightforward step in verification that the model represents the expected solution is comparison of the resulting surface elevation profile to the intended wave. In subsection 2.1.1, the analytical solution to the free surface boundary for the linear approximation is shown to be a pure sinusoidal. Comparing a simulation run without vegetated domain to a propagating harmonic wave establishes whether 1) the boundary condition functions as intended in generating the wave, and 2) the governing equations have been implemented correctly to allow for undisturbed propagation maintaining wave shape.

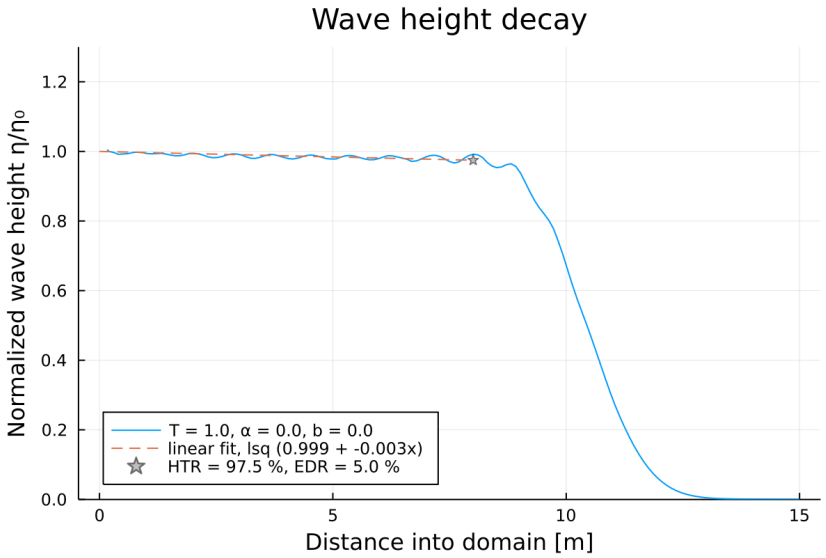

Figure 4.3: Surface elevation in domain without porous zone, with corrected $\theta = 0.5$.

Dissipative losses

The numerical method presented in this research induces some losses without activation of the porous zone. In other words, for an empty domain, some energy is still dissipated in the medium. This is a realistic scenario, as viscous losses can be present unless for an idealized situation. However, to justify the magnitude

of these losses, and compare them to expected results, empty runs are used to analyse the amount of energy dissipated. Wave height reduction for a run where the porous zone remains inactive can also be an indication of numerical errors, where implementation of the numerical methods leads to energy loss.

Initially, the generated waves were shown to dissipate a lot throughout the domain. It was found that the source of this numerical dissipation was the time-stepping method, where an interpolation constant of 0.6 provided erroneous results.

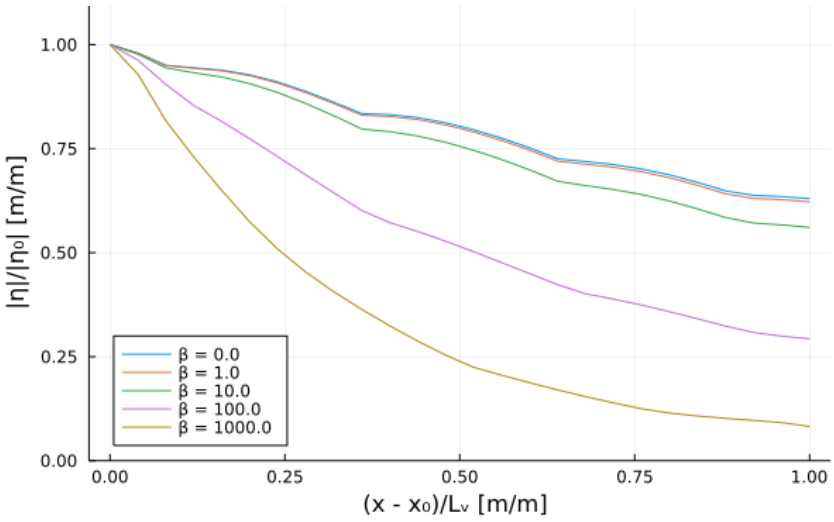

Figure 4.4: Example run that illustrates large losses by $\Theta = 0.6$ time interpolation.

The results show significant reduction in (normalized) wave amplitude over the vegetated domain, even though the run with $\beta = 0$ represents a simulation where the porous zone was not activated. This is a typical illustration of the importance of an elaborate validation and verification strategy.

After setting $\Theta = 0.5$, the model remained stable and provided more realistic results as shown in Figure 4.3. Amplitude reduction was reduced from 60% to 2.5%, the latter is considered acceptable.

Grid convergence

To determine what spatial resolution is needed for an optimal mesh - without needless computational cost - that does produce stable results, a grid convergence study is done. The performance of the model is tested for different numbers of cells per meter modelled in the domain.

Table 4.4: Grid convergence study

Run	Resolution cell/m	Total cells length x width, total	Cells per wavelength[1]	Computation time [2]
SEN_SPA_A1	1	40x4, 160	2.6	0.5 h
SEN_SPA_A2	2	80x8, 640	5.2	1.5 h
SEN_SPA_A3	5	200x20, 4000	13	6 h
SEN_SPA_A4	15	600x60, 36000	39	45 h

[1] Based upon the standard wavelength for SFM.
[2] On i5-4310U CPU at 2.0GHz - simulation time chosen as 30s

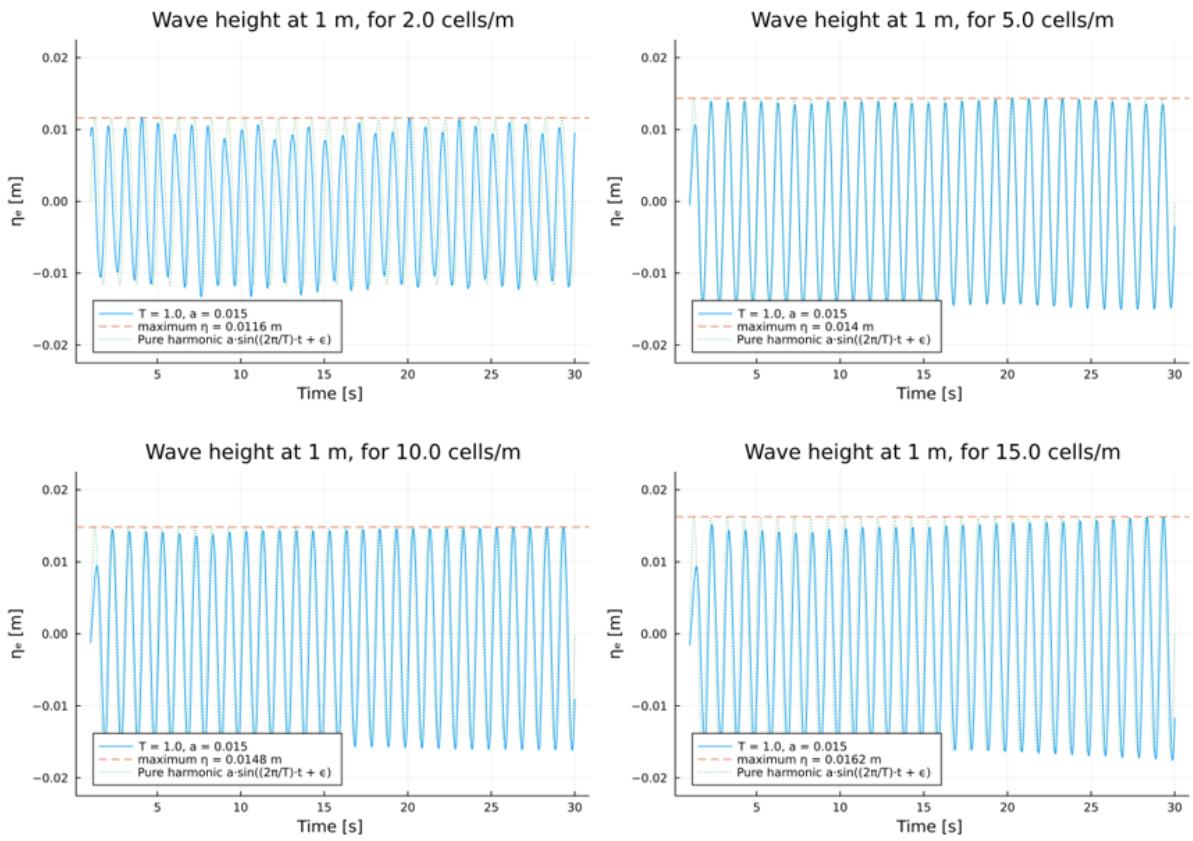

Figure 4.5: Grid convergence plots for values between 2 and 15 cells/m.

It should be noted that in simulations including free surface waves, a rule of thumb is often used that around 20 cells are needed per wavelength, to accurately capture the surface elevation profile. Given that the present models uses a second order polynomial to approximate the η-variable overt the mesh, the number of wavelengths needed are reduced.

In correspondence with the order of magnitude of the wavelengths that would realistically be produced in the model, this grid convergence study presented here needs no further adjustments to full fill the rule-of-thumb.

Time step convergence

Similar to how accuracy of the simulation results is dependent on spatial resolution, the time-stepping magnitude is also crucial to performance of the model. Again it is aimed to find a step-size that is computationally advantageous, but provides sufficient accuracy in results. Based upon an iterative approach this balance is sought for.

Table 4.5: Timestep convergence study for 20 seconds of simulated time.

Run	Step size [s]	Total timesteps [n]	Computation time [hh:mm]
SEN_TIM_A1	0.100	300	non-convergent
SEN_TIM_A2	0.050	600	non-convergent
SEN_TIM_A3	0.025	1200	00:45
SEN_TIM_A4	0.010	3000	02:00
SEN_TIM_A5	0.005	6000	03:30

[1] This run was erratically done without preconditioning the solver.

From the results of the runs displayed in Table 4.5, plots are displayed in Figure 4.6. Results were plot-

ted both in front of the vegetation patch (left-hand image) as well as within the vegetation field (right-hand image). It is shown that further in the domain, the difference in results for different step size diverge. Based upon the balance between computational time, and accuracy of the solutions, a standard timestep of 0.01 s was chosen.

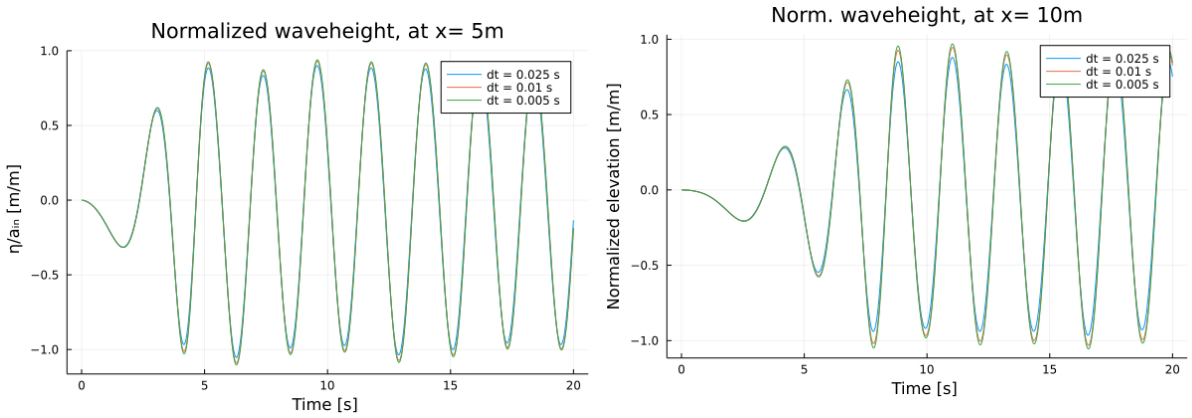

Figure 4.6: Timestep convergence plots for 1) before encountering the porous zone, and 2) within the porous zone.

4.3.2 Validation

The process of determining the degree to which a model is an accurate representation of the real world from the perspective of the intended uses of the model. - AIAA

Whether the model is an adequate representation of the real world is to be determined during sensitivity analysis presented in section 5.2. The findings of these runs are compared to known behaviour from experimental data, documented in the preceding literature review. Qualitative analysis will result in judgement if the findings from the numerical model represent measured data. This is a good indication if reality is correctly.

Key in the validation stage is commenting on the range of applicability of the model. Note that in order to provide clarity in the meaning of the modelling results, the *Standard Flume Model* - as described in section 4.1 is used as standard design. This results in the validation process being relevant to parameters close to the conditions expected in the representative farm.

5

Results and analysis

The validation method presented in Figure 4.2 provides a basis for comparing model results to existing data from literature. This chapter aims to compare the fluid-vegetation behaviour as modelled using the numerical model to a selected group of experiments from literature.

5.1 Analysis methodology

As the focus lies transmission and damping of the amplitude of propagating waves by the vegetation, the presentation of the results in this chapter aims to provide a clear overview of this phenomenon. Where relevant, the values have been normalized to facilitate comparison over different ranges of input. Normalization of amplitude with respect to incident magnitude is used. Furthermore, normalization with respect to vegetation length is used besides expression horizontal distance as a function of wavelength.

5.1.1 Main values of interest

One key parameter in analysing the model results is the wave height reduction per unit length of vegetation. This can be described as follows:

$$\Delta H_x = \frac{H(x) - H_0}{x} \tag{5.1}$$

where ΔH_x, $H(x)$, H_0 and x represent the wave height reduction per unit of vegetation, wave height at location x in the vegetation patch, wave height before entering the patch and distance into the vegetation patch. Closely related to this we can define the wave Height Transmission Ratio (HTR), the ratio between wave height along the vegetated patch H_{veg} and the incident wave height H_0.

$$HTR = \frac{H_{veg}}{H_0} \tag{5.2}$$

Another significant outcome of the simulations presented in this chapter is the ratio of decrease in energy that the waves contain after passing over vegetation. The derivation of wave energy is elaborated on in Equation 2.1.1. The term Energy Dissipation Rate (EDR) is used to express this ratio and determined as follows:

$$EDR = \frac{E_0 - E_{veg}}{E_0} \tag{5.3}$$

Substituting the overall wave energy, as derived in Equation 2.1.1 to be equal to $\frac{1}{2}\rho(\frac{H}{2})^2$ we obtain;

$$= \frac{\frac{1}{2}\rho(\frac{H_0}{2})^2 - \frac{1}{2}\rho\frac{H_{veg}}{2}^2}{\frac{1}{2}\rho\frac{H_0}{2}^2} \tag{5.4}$$

Finally, dividing over the common factors $\frac{1}{2}\rho$ and $\frac{1}{4}$ this results in

$$= \frac{H_0^2 - H_{\text{veg}}^2}{H_0^2} \tag{5.5}$$

For all simulations with activated porous zone, a run with identical wave conditions was with the porous parameters set to zero. This allows for compensation for energy dissipation unrelated to the porous zone, such as bottom friction and energy dissipation due to viscosity. See Figure 4.3.1 for more elaborate analysis.

5.1.2 Visualisation

The setup of the modelling code allows for saving the results as VTK-files that are ready to import to *ParaView* for visualisation. Development over time of all saved variables throughout the domain allows for a quick and rough check on whether the simulation qualitatively matches expected outcomes.

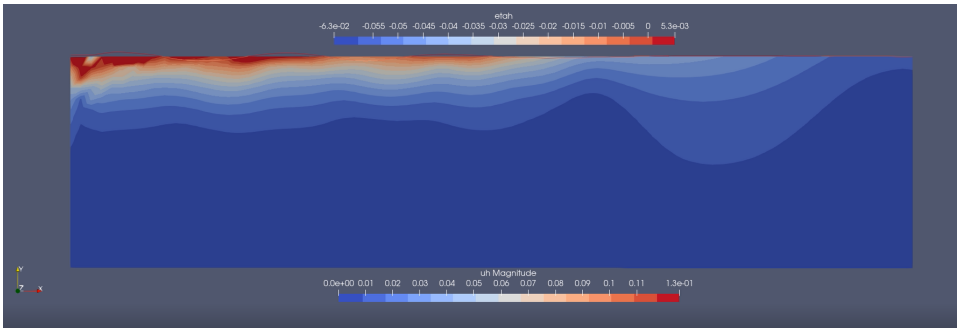

Figure 5.1: Visualisation of simulation results using ParaView.

5.1.3 Velocity profiles

For the deep water assumption used in this model, the velocity profile grows exponentially from seabed to still water level. In order to check that the wave generating boundary is effective in establishing the desired profile, the mean velocity, maximum and minimum can be plotted along the entire length of the domain.

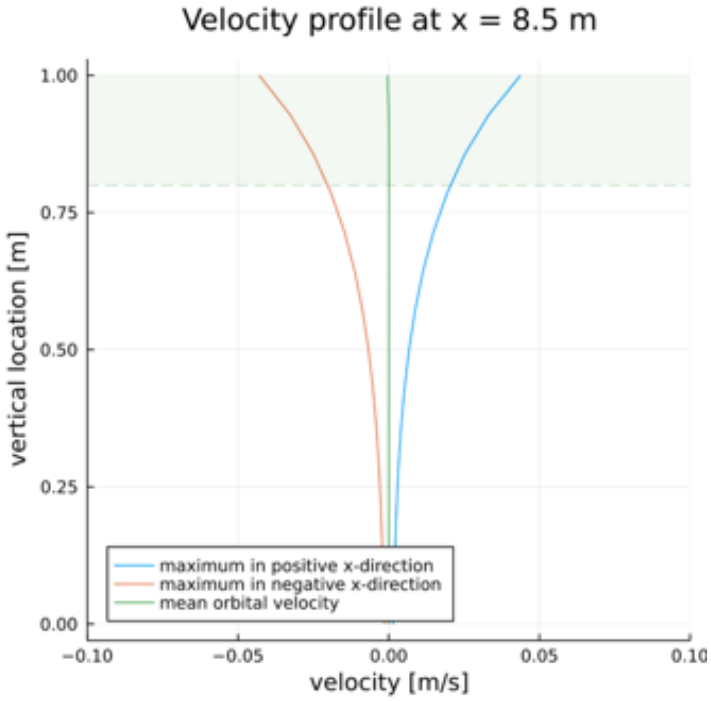

Figure 5.2: Vertical profile of minimum, maximum and mean velocity coefficient.

The results in Figure 5.2 indicate that the velocity profile is indeed generated as desired. Additionally, implementation of this analysis function allows for checking depth-dependent changes in the mean flow. Induced currents due to the shear layer on the underside of the vegetation can be detected. This is a recommended phenomenon to further investigate in following research.

5.1.4 Transient effects

As can be expected for time-domain simulations, the signal of wave height measured throughout the domain displays transient behaviour. To determine the effects of vegetation on wave damping, the steady-state behaviour is desired. To this end, the results presented in this report have all been subject to analysis of the steady-state result.

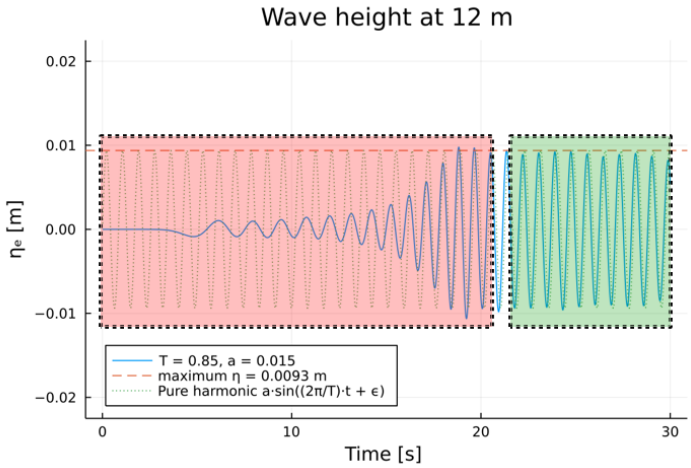

Figure 5.3: Graphical representation of transient effects and steady-state used in analysis.

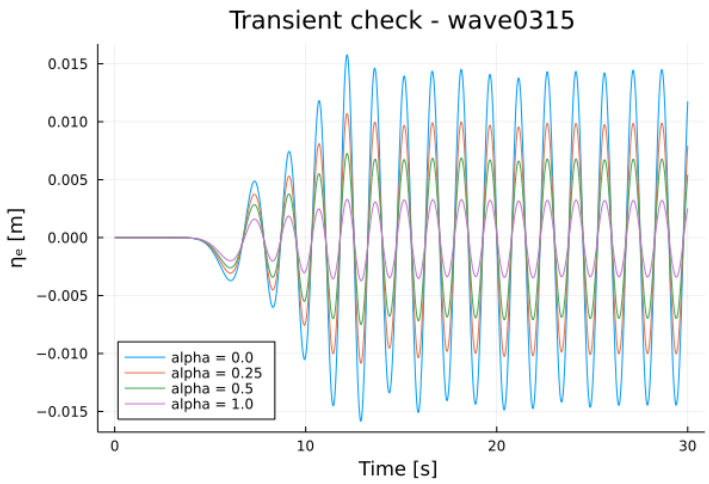

Figure 5.4: Analysis of transient effects.

For wave0315, the timeseries have been plotted in Figure 5.4 to provide an example of how the transient effects progress at one point in space. It was observed that during simulation, amongst the first set of waves arriving was one of significantly larger amplitude than the following waves during the steady state.

In analysis of the results, the amount of time cut-off at the beginning of the simulation was determined using the following function:

$$t_{\text{initial cutoff}} = L_{\text{tank}} / c_{\text{phase}} \tag{5.6}$$

Where the phase speed, or propagation velocity of a single wave component is found plugging $c = L/T = \omega/k$ into the dispersion relation;

$$c_{\text{phase}} = \frac{g}{\omega} \tanh kd \tag{5.7}$$

This was shown to reduce oscillations by the reflection of this wave significantly, see Figure 5.5 where the contribution of the first set is present. And Figure 5.6, where this has been filtered out using the data cut-off in Equation 5.6.

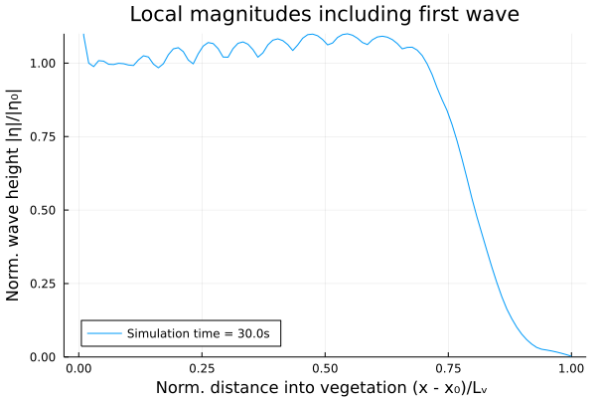

Figure 5.5: Distortions in local wave heights caused by reflection of initial wave.

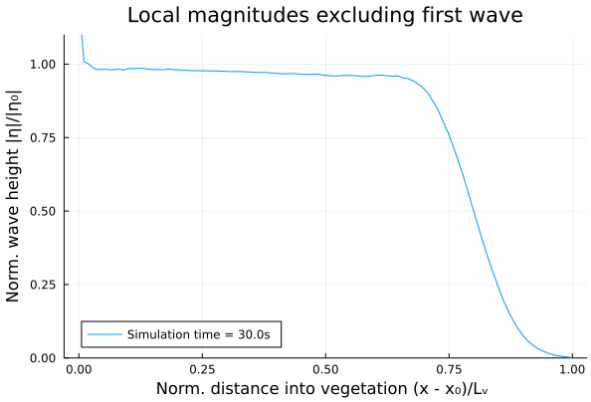

Figure 5.6: No distortions after exclusion of the initial wave.

It can be noted that after filtering away the time it takes for the initial wave set to cross the domain, some lower frequency oscillations are still present in the time series of wave elevation. These are assumed to be caused by the low-frequency and (relatively) low-amplitude initial excitation. As the period of this ramp-up set is longer than the intended waves, the damping zone has not been calibrated to filter them out. It is expected that these oscillations remain bouncing through the domain until crossing the damping zone often enough to lose all energy. They are not filtered out with the previous step, as their propagation speed is higher than the intended waves.

Furthermore, an additional damping zone at the generation BC could aid in solving this. Currently, the generating boundary condition forces velocity, but does not prescribe the free surface, thus allowing for a solution with increased pressure and surface elevation. This allows the wave to reflect off the leftmost boundary.

5.2 Sensitivity analysis

The model created aims to form the framework needed to find and calibrate the porous parameters that can represent the damping effects of vegetation accurately. In the present sensitivity analysis, a range of inputs is used to generate results. The results are than analysed to compare to expected outcomes of the model, to judge whether the linear and non-linear drag term behave as expected.

This helps to conclude on whether the system, which is inherently non-linear, can convey both the linear influence of the α-term and the non-linear influence of the β-term.

5.2.1 Wave period

To determine the influence of wave period on amplitude transmission, waves with periods from 1.0s to 2.0s, of 0.25s increments are analyzed. From Figure 5.7 it can be seen that for constant values of α, and for dimensions parameterized on the basis of wavelength, damping remains constant.

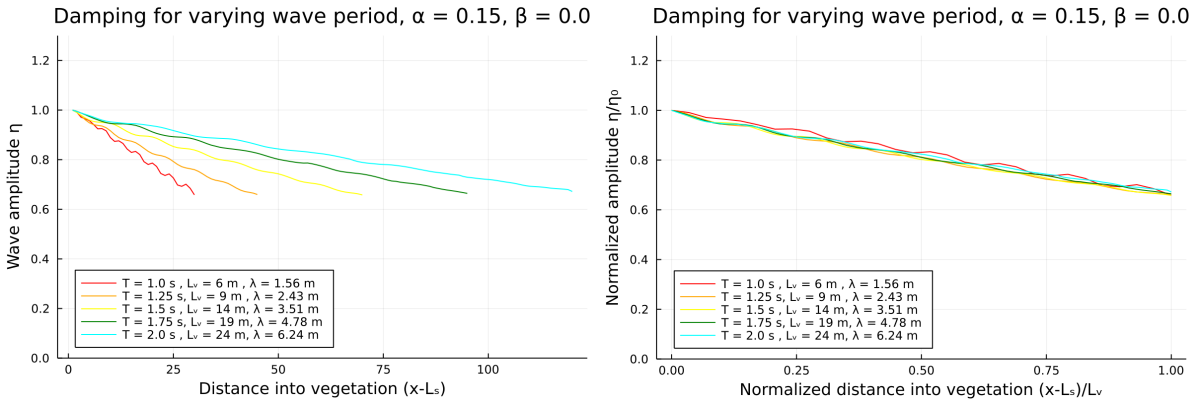

Figure 5.7: Amplitude transmission for different incident wave periods under linear damping.

In other words, when the wavelength becomes twice as large, the amount of damping remains the same if the farm is scaled to twice as large as well.

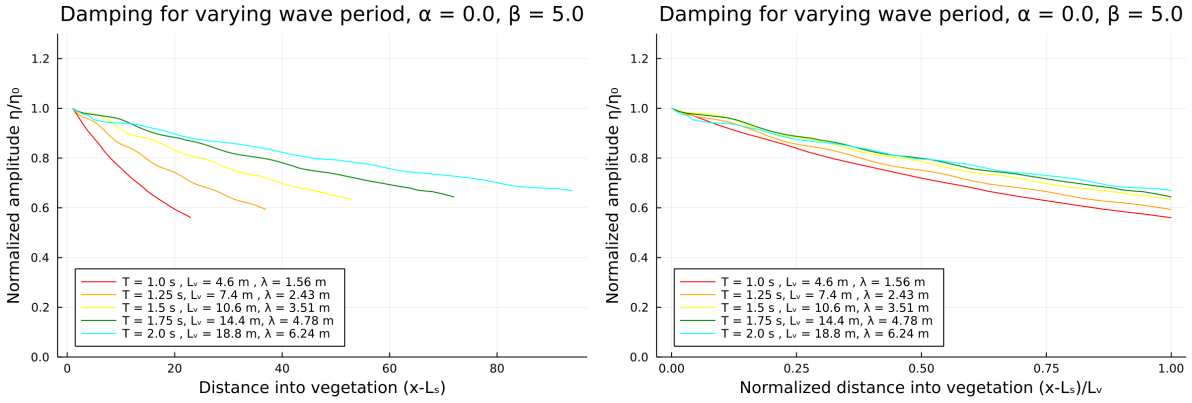

Figure 5.8: Amplitude transmission for different incident wave periods under quadratic damping.

This result indicates that, when normalized for wave length, the influence of the wave period on amplitude transmission is directly proportional to the vegetation patch length for linear drag terms, but not for quadratic drag.

5.2.2 Wave amplitude

The influence of wave amplitude was analysed for a range of $0.005 \leq a \leq 0.0175$ m, which corresponds to full-scale waves between 0.5 and 1.75m wave height due to the spatial scaling of factor 50. The remaining input parameters were left unchanged, which is considered an unrealistic scenario as wave height and period are correlated in physical oceanic wavetrains.

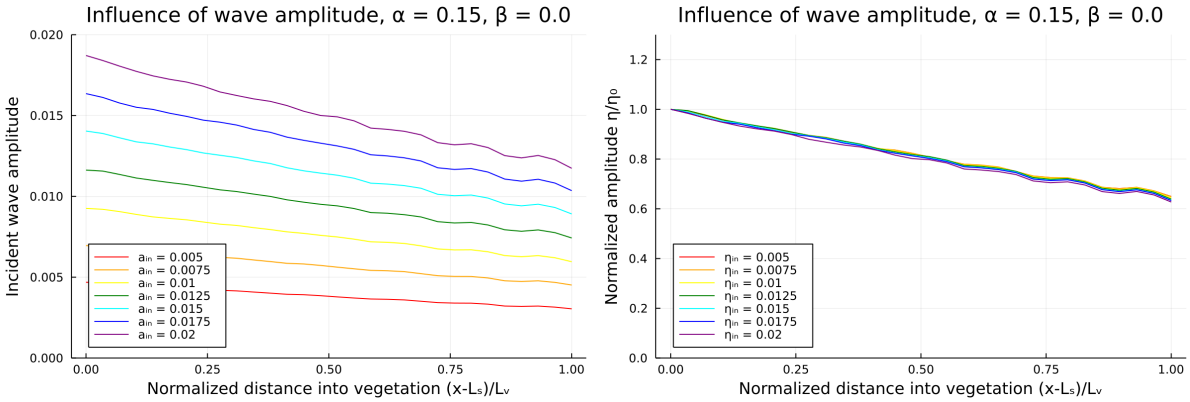

Figure 5.9: Amplitude transmission for different incident wave amplitudes under linear damping.

For the linear, Darcy resistance activated, the increased wave damping due to an increase in amplitude remains proportional. As can be seen from the normalized results on the right-hand-side of Figure 5.9. This shows that the attenuation of wave amplitude is not significantly influenced by a variation in the incident amplitude.

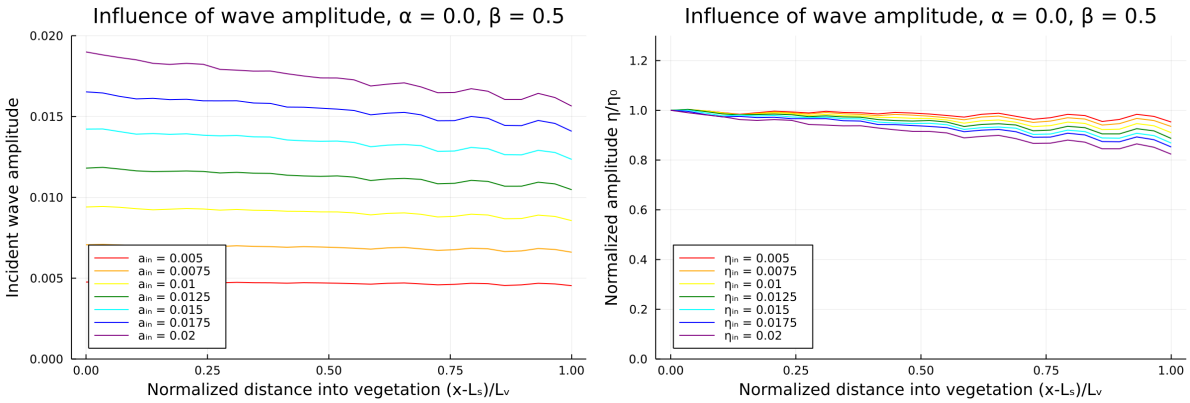

Figure 5.10: Amplitude transmission for different incident wave amplitudes under quadratic damping.

The results in Figure 5.10 show that, in contrast to the linear resistance term, the Forchheimer term does introduce a dependency on η_{in} (or H_0). This difference is elaborately tackled in Equation 5.2.5.

5.2.3 Vegetation vertical location

As described in the precursory literature review to this report, one of the novelties in modelling vegetation patches is focus on the vertical position within the water-column. To this end, the sensitivity analysis is supplemented with a study of the influence of the farm structure's depth on the wave attenuation properties. A comparative study is done to review the effects of submerged, suspended and floating vegetation.

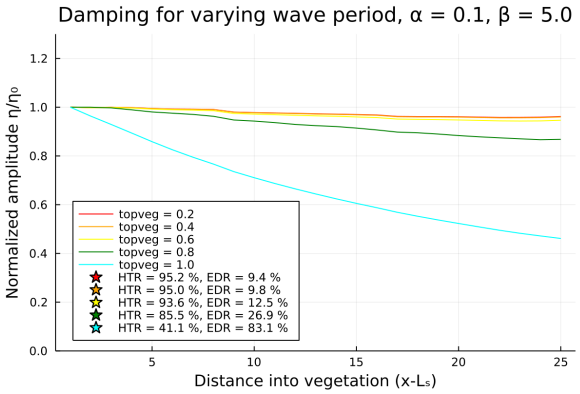

Figure 5.11: Normalized wave damping per vegetation distance for varying submergence depths of the meadow.

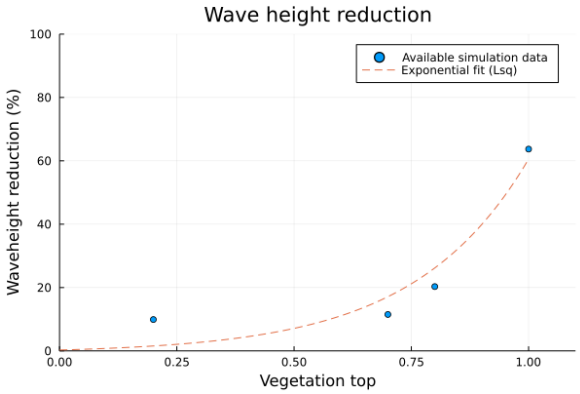

Figure 5.12: Rough trend of influence of the vertical position on wave damping.

The results can be explained because in the deep water regime, the wave kinematic energy concentrates in the top of the water column. Higher particle velocities near the surface increase the effect of the resistance terms in this area. See also the plot of the vertical velocity profile in Figure 5.2.

It is expected that this effect especially relevant for (relatively) short waves, as for those conditions kinematic energy further concentrates near the free surface, thus dissipating nearly all energy for a near-surface porous medium (i.e. floating canopies). While for longer waves, the exponential velocity profile penetrates deeper over water depth, potentially reaching a larger part of suspended or bottom founded dissipative zones.

Figure 5.13: Graphical representation of vertical velocity profile and different vegetation vertical positions.

Comparison with Figure 5.14 indicates that the wave energy transmission coefficient TE by the canopy at different locations are nearly the same at low frequency. However, as wave frequency increases, wave attenuation by canopies at different locations behaves differently. With increasing wave frequency, TE decreases to 0 when the canopy is floating on the surface while increases towards 1 when the canopy is situated at the bottom.

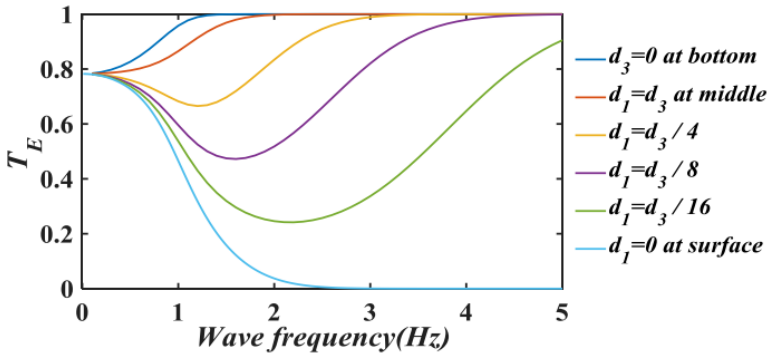

Figure 5.14: Influence of vegetation energy transmission coefficient T_E, for constant d_2.
Taken from Zhu and Zou [80]

It is also found that when the canopy is located at the upper half of the water column (d1<d3), TE first decreases and then increases to 1. The frequency range for TE less than 0.6 extends as well when the canopy

moves upwards, indicating that the canopy can effectively dissipate wave energy for a wider frequency range as it moves upwards.

5.2.4 Porous coefficients

For the standard wave of amplitude 0.015 m and period of 1 s, a range of Darcy and Forchheimer coefficients have been combined to illustrate the range in which the parameters should be sought during calibration efforts.

$$\begin{aligned} 0 \leq \alpha \leq 0.5 \\ 0 \leq \beta \leq 20 \end{aligned} \tag{5.8}$$

The range for values of the parameters represent situations under the following assumptions, that are deemed realistic for real life scenarios, and would be attainable in future calibration studies:

- Wave amplitude in range of $0 \leq H_0 \leq 2m$
- Wave period in range of $0 \leq T \leq 10s$
- Plant densities and spacing representative of current practice for Sugar Kelp
  - Elastic modulus $1 \leq E \leq 20$ MPa
  - Plant density $100 \leq N_{\text{plant}} \leq 700$ plants/m
  - Blade length $0 \leq l_b \leq 2$ m
- and for Giant Kelp
  - Representative diameter $0.1 \leq d_{\text{eq}} \leq 0.6$m
  - Plant spacing $0.5 \leq S_{\text{plant}} \leq 4$ m

These ranges are used throughout the different simulation runs that are based upon the same region of input wave conditions.

α-coefficient

Variation of the α coefficient under constant wave conditions and model dimensions results in a (near) linear increase. As shown on the leftmost plot of Figure 5.15, linear increments of α also induce linear increments in wave amplitude decay. Furthermore, the rightmost graph of the same figure displays the near linear decay per unit length of vegetated distance.

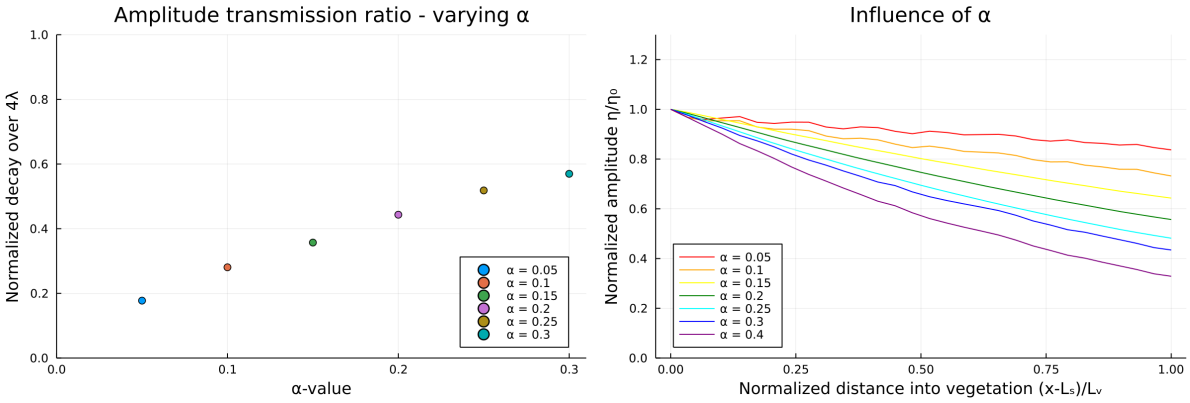

Figure 5.15: Amplitude transmission for different values of α.

β-coefficient

The influence of variation of the β-coefficient is isolated and analysed for its trend with increase by keeping the geometric set-up and wave conditions equal as well. Contrary to the influence of the α-term, this variational study indicates that the additional influence of the nonlinear damping factor decreases, relative to the increase of β. In Figure 5.16, the plot on the left indicates the nonlinear trend for varying β. The graph on the right displays the decreasing influence on wave height per unit length of vegetated distance.

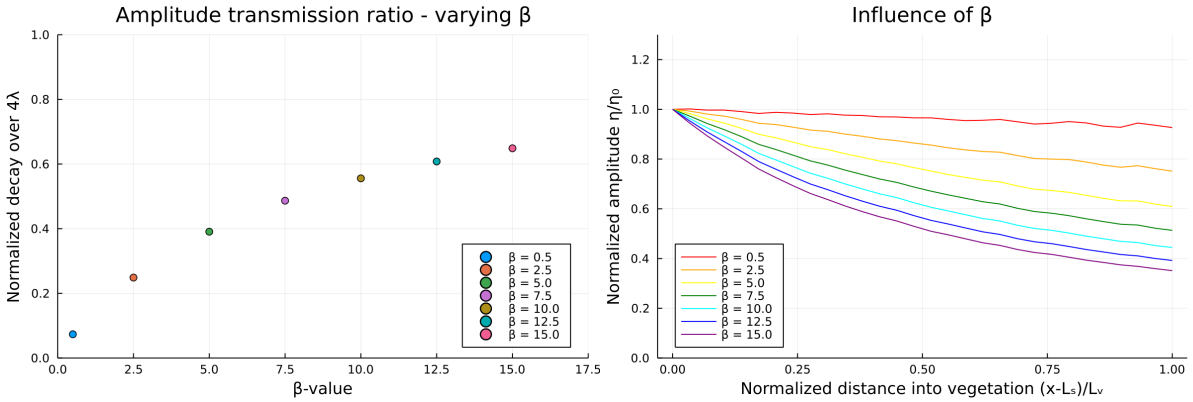

Figure 5.16: Amplitude transmission for different values of β.

Combined coefficients

In order to confirm the qualitative influence of the two resistance coefficients, and to judge the relative importance of their magnitude, a batch of simulations was performed with varying combinations of α and β.

The results in Figure 5.17 confirm that the β-coefficient is dominantly responsible for non-linear progression of wave height per unit distance.

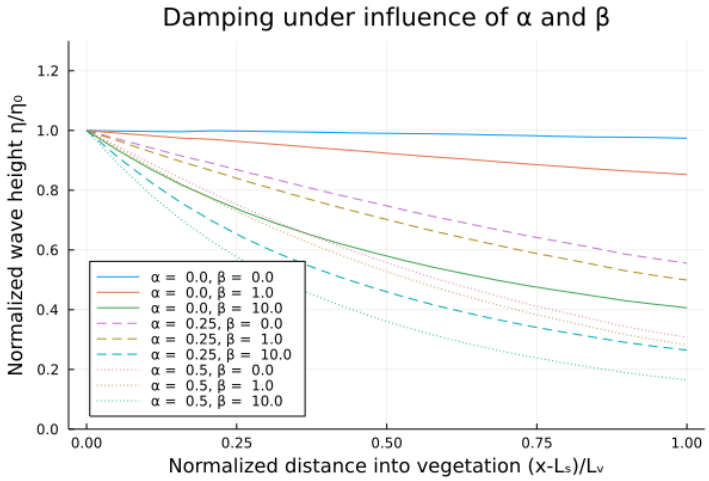

Figure 5.17: Amplitude transmission for different combinations of α and β.

5.2.5 Discussion sensitivity study

Velocity relations

The contribution of the Darcy-term and the Forchheimer-term are respectively linearly proportional, and quadratically related to the particle velocity as demonstrated in Equation 3.13. The sensitivity simulation runs related to the wave conditions are therefore compared to the expected outcomes using the analytical relation between the wave parameters and the particle velocities in the model.

For clarity, the velocity profiles in accordance with linear wave theory are restated first:

$$u = a\omega \frac{\cosh[k(d+z)]}{\sinh(kd)} \cos(\omega t - kx) \tag{5.9}$$

Adding to this the re-ordered dispersion relation - assuming deep water -, and the expressions of the wave frequency and wave number:

$$\begin{aligned} \text{for scaling with factor } s: \quad T &\rightarrow sT \\ \lambda = \frac{g}{2\pi}T^2 &\rightarrow \frac{g}{2\pi}(sT)^2 = s^2\lambda \\ \omega = 2\pi/T &\rightarrow 2\pi/(sT) = \frac{1}{s}\omega \\ k = 2\pi/\lambda &\rightarrow 2\pi/(s^2\lambda) = \frac{1}{s^2}k \end{aligned} \tag{5.10}$$

These can be combined to analytically define the proportional influence of amplitude and wave period on the velocity component. Where variation of wave period T increases wavelength λ quadratically, and decreases wave frequency ω linearly. This leads to a new expression for u:

$$\begin{aligned} u = a\omega\frac{\cosh[k(d+z)]}{\sinh(kd)}\cos(\omega t - kx) &\rightarrow a\frac{1}{s}\omega\frac{\cosh[\frac{1}{s^2}k(d+z)]}{\sinh(\frac{1}{s^2}kd)}\cos(\frac{1}{s}\omega t - \frac{1}{s^2}kx) \\ u = a\omega e^{kz} &\rightarrow a\frac{1}{s}\omega e^{\frac{1}{s^2}kz} \end{aligned} \tag{5.11}$$

And for the (more straightforward) amplitude scaling:

$$\begin{aligned} \text{for scaling with factor } s: \quad a &\rightarrow sa \\ u = a\omega\frac{\cosh[k(d+z)]}{\sinh(kd)}\sin(\omega t - kx) &\rightarrow sa\omega\frac{\cosh[k(d+z)]}{\sinh(kd)}\sin(\omega t - kx) \\ u = a\omega e^{kz} &\rightarrow sa\omega e^{kz} \end{aligned} \tag{5.12}$$

Furthermore, an isolated increase in amplitude a leads to a proportional increase of the amplitude of velocity u, as readily shown in Equation 5.9.

Energy dissipation

An energy balance can be established to compare the simulation relation results to the analytical formulation of the energy dissipated by the β-term-induced resistance. To this end, the formulation analogous to the Morison-type dissipation term in subsection 2.1.3 is considered.

$$\begin{aligned} W_{\text{drag}} &= \int_{-d}^{-d+h_v} F_D u dz \\ &= \int_{-d}^{-d+h_v} \beta|u|\cdot u u dz \end{aligned} \tag{5.13}$$

By using the energy balance in Equation 5.14, which relates the rate of change of energy transport per unit length, to the energy dissipated due to the resistance factor, as stated above, the following balance is found:

$$\frac{\partial Ec_g}{\partial x} = -\int_0^{l_{pm}} \overline{\beta|u|\cdot u u dz} \tag{5.14}$$

Splitting up the horizontal velocity components into the depth-independent part, and the vertical profile results in:

$$\begin{aligned} u &= u_d\Gamma \\ \text{provided} \quad \Gamma &= \cosh k(h+z)/\sinh kh \\ \text{and} \quad u_d &= \frac{H}{2}\omega\cos(kx-\omega t) \end{aligned} \tag{5.15}$$

Which enables working out the third power in the integral by plugging the height-dependent and height-independent terms from Equation 5.15 into Equation 5.13:

$$\begin{aligned} W_{\text{drag}} &= \beta \int_{-d}^{-d+h_v} \overline{|u| \cdot u^2} dz \\ &= \beta u_d^3 \int_{-d}^{-d+h_v} \overline{|\Gamma| \cdot \Gamma^2} dz \\ &= \beta \frac{1}{8} H_0^3 \omega^3 \int_{-d}^{-d+h_v} \overline{|\Gamma| \cdot \Gamma^2} dz \end{aligned} \tag{5.16}$$

Here the wave height, as found in the definition of the horizontal velocity according to linear wave theory, is taken to be equal to the incident wave height. Working out the integral over the vegetation height results in:

$$\begin{aligned} \int_{-d}^{-d+h_v} \overline{|\Gamma| \cdot \Gamma^2} dz &= \frac{1}{\sinh^3(kh)} \int_{-d}^{-d+h_v} \overline{\cosh^3 k(h+z)} dz \\ &= \frac{3}{4k \sinh^3(kh)} \left[\sinh(k(h+z)) + \frac{1}{9} \sinh(3k(h+z)) \right]_{-d}^{-d-h_v} \\ &= \frac{9\sinh(k(h-d)) + \sinh(3k(h-d)) - 9\sinh(k(d-h+l)) - \sinh(3k(d-h+l))}{12k \sinh^3(kh)} \end{aligned} \tag{5.17}$$

Referring back to Equation 5.14, we can now derive the decay ratio per unit length. For expansion of this term, reference is made to Zhu [79]. Note that this formulation is based upon quadratic drag. After ordering the terms this results in:

$$\frac{H(x)}{H_0} = \frac{1}{1 + k_d H_0 x} \tag{5.18}$$

Where wave decay coefficient k_d is expressed as:

$$k_d = \frac{16\beta}{H_0^3 \omega^3 \rho} \frac{k^2 \sinh^2 kh}{(2kh + \sinh 2kh)} \int_{-d}^{-d+h_v} \overline{|u| \, u^2} dz \tag{5.19}$$

And with consideration for how Equation 5.17 has worked out the integral we arrive at:

$$\begin{aligned} k_{d,\beta} &= \frac{16\beta}{H_0^3 \omega^3 \rho} \frac{k^2 \sinh^2 kh}{(2kh + \sinh 2kh)} \cdot \frac{1}{8} H_0^3 \omega^3 \ldots \\ &\quad \ldots \frac{9\sinh(k(h-d)) + \sinh(3k(h-d)) - 9\sinh(k(d-h+l)) - \sinh(3k(d-h+l))}{12k \sinh^3(kh)} \\ &= \beta \frac{k}{6\rho} \frac{9\sinh(k(h-d)) + \sinh(3k(h-d)) - 9\sinh(k(d-h+l)) - \sinh(3k(d-h+l))}{\sinh(kh)(2kh + \sinh 2kh)} \\ &= \beta \cdot f(k, \omega, d, l, h, rho) \end{aligned} \tag{5.20}$$

Note that the H_0^3-term from the definition of k_d in Equation 5.19 and the same term from expansion of the integral in Equation 5.22 cancel each other out in the final formulation of k_d. This results in the wave height reduction $H(x)/H_0$ being a linear function of H_0.

The same derivation can be made for the linear resistance α-term. The work done by the drag now reduces one order in u, this leads to a new conservation equation:

$$\frac{\partial E c_g}{\partial x} = -\int_0^{l_{pm}} \overline{\alpha |u| \cdot u} dz \tag{5.21}$$

This, in turn, reduced the order of the expansion of the integral as well:

$$W_{\text{drag}} = \alpha \frac{1}{4} H_0^2 \omega^2 \int_{-d}^{-d+h_v} \overline{|\Gamma| \cdot \Gamma} dz \tag{5.22}$$

And consecutively, the overall formulation of $k_{d,\alpha}$ will decrease one order in H_0:

$$\begin{aligned} k_{d,\alpha} &= \frac{16\alpha}{H_0^3\omega^3\rho}\frac{k^2\sinh^2 kh}{(2kh+\sinh 2kh)}\cdot\frac{1}{4}H_0^2\omega^2\cdot\ldots \\ &\quad\ldots\frac{9\sinh(k(h-d))+\sinh(3k(h-d))-9\sinh(k(d-h+l))-\sinh(3k(d-h+l))}{12k\sinh^3(kh)} \\ &= \alpha\frac{k}{3H_0\omega\rho}\frac{9\sinh(k(h-d))+\sinh(3k(h-d))-9\sinh(k(d-h+l))-\sinh(3k(d-h+l))}{\sinh(kh)(2kh+\sinh 2kh)} \\ &= \alpha\cdot\frac{1}{H_0}\cdot f(k,\omega,d,l,h,\rho) \end{aligned} \tag{5.23}$$

The wave decay coefficient found for the linear term can be filled in into the $H(x)/H_0$ expression, which shows that for a variation in H_0, the wave decay per unit length will not change.

Comparing the wave decay coefficients for α and β with each other, we note that the wave decay per unit length should be independent of H_0 for the linear drag term, while dependence remains for the non-linear drag term. This is in correspondence to the results found in the sensitivity study.

Wave steepness

In the previous two sections, the results of varying wave height and wave period are analyzed separately. Under constant amplitude, variation of wave period induces different wave steepness among the runs. In Table 5.1, the wave steepness of analyzed conditions are included by expression of the Ursell number, Ur $= \frac{\text{steepness}}{\text{relative depth}^3} = HL^2/d^3$.

Table 5.1: Wave steepness of simulation runs.

Run -	Amplitude m	Period s	Length m	Ursell $m\cdot m^2/m^3$	Steepness m/m
waveT1	0.015	1.00	1.56	0.073	0.019
waveT2	0.015	1.25	2.43	0.177	0.012
waveT3	0.015	1.50	3.51	0.370	0.009
waveT4	0.015	1.75	4.78	0.685	0.006
waveT5	0.015	2.00	6.24	1.168	0.005
waveA1	0.005	1.00	1.56	0.024	0.006
waveA2	0.0075	1.00	1.56	0.037	0.01
waveA3	0.010	1.00	1.56	0.049	0.013
waveA4	0.0125	1.00	1.56	0.061	0.016
waveA5	0.015	1.00	1.56	0.073	0.019
waveA6	0.0175	1.00	1.56	0.085	0.022

The general rule of thumb that waves remain symmetric, and linear, for Ur ≤ 5.0 remains true for all runs in the previous two sensitivity variations. This indicates that the resulting simulation outcomes should not be obscured by inaccurate representation, we know that waves to remain in the regime that the model was developed for.

It is argued in Hedges [23], that for the deep water regime, the influence of water depth should be considered negligible, as this forms part of initial assumptions of the deep water regime. Wave steepness remains a good indication of applicability of linear wave theory, where a steepness $H/L = 1/25 = 0.04$ will still only introduce a deviation of 6% between Stokes' 2nd order theory and Airy waves [23]. As shown in Table 5.1 this also holds for all conditions tested.

5.3 Comparison to experimental results

The goal of the model is to represent the physical process of waves propagating though a kelp field. As discussed in Chapter 4 of the anterior literature review, a multitude of laboratory experiments have been published that aim to quantify the hydrodynamic effects of (flexible) vegetation. A selection of experimental result of interest to wave damping by kelp is collected in Table C.3. The large spread in input values and approaches of these experiments warrants a focus on the experiments that can 1) comment on the generality and applicability of the present model, and 2) approach the situation aimed for in the case study presented in chapter 6.

5.3.1 Periodic waves through a suspended canopy

In Hu et al. [28], the passing of small-amplitude waves through a suspended canopy is studied, it contains new measurements as well as data from Hu et al. [29]. The experiment makes use of the idealized representation of solid cylinders in an ordered array. The setup has a porosity of 97.2% ($n = 1 - \pi(d/l)^2$), the canopy length is 5m and the cylinder have a diameter of 0.015m. The setup is shown in Figure 5.18.

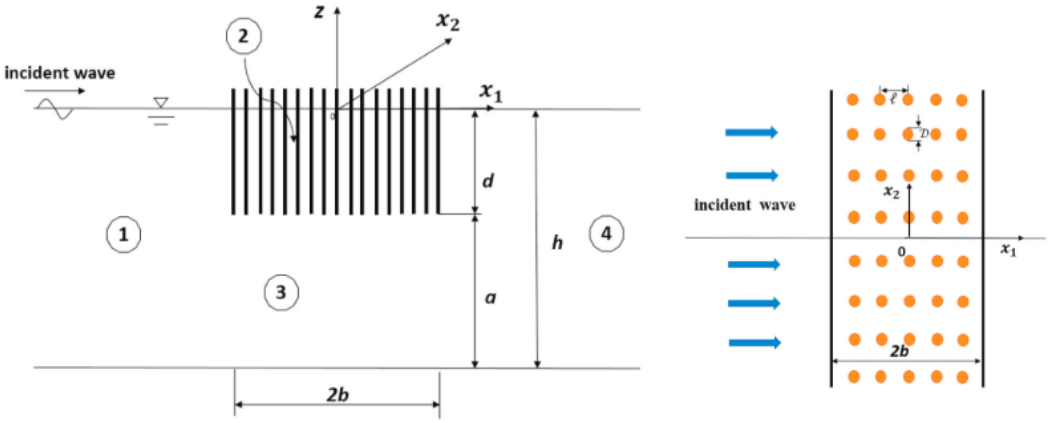

Figure 5.18: Experimental setup of Hu 2021.

The wave flume used was 36m long and 1.3m deep, to investigate the effect of varying wave conditions, an elaborate set op generated waves have been tested. A complete view of the applied waves is presented in Table 5.2.

Table 5.2: Selected wave conditions from Hu et al. [28] for comparison.

Case name	h m	d m	T s	A cm	k_0 1/m	L m
wave0310	0.6	0.22	1.0	1.5	4.0	1.5
wave0610	0.6	0.22	1.0	3.0	4.0	1.5
wave0910	0.6	0.22	1.0	4.5	4.0	1.5
wave0315	0.6	0.22	1.5	1.5	2.1	2.9
wave0615	0.6	0.22	1.5	3.0	2.1	2.9
wave0915	0.6	0.22	1.5	4.5	2.1	2.9

The setup as stated has been reproduced in the numerical framework, and selected wave conditions have been applied to test performance. Some results are presented here in Figure 5.19 and Figure 5.19 to illustrate successful reproduction.

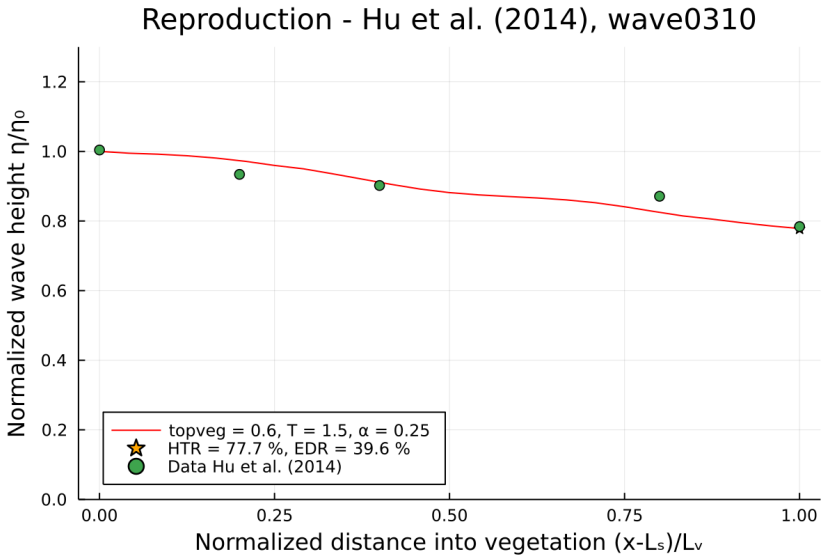

Figure 5.19: Wave 0310 (Hu 2014) reproduction.

In Figure 5.19, it can be seen that the experimental results and the numerical reproduction seem to align very well. For these specific conditions the α value of 0.25 represents the cylinder array very well. Note that this simulation has run under the assumption that the linear resistance coefficient is a good presentation. Given the fairly accurate fit of the trend to the data points this seems acceptable.

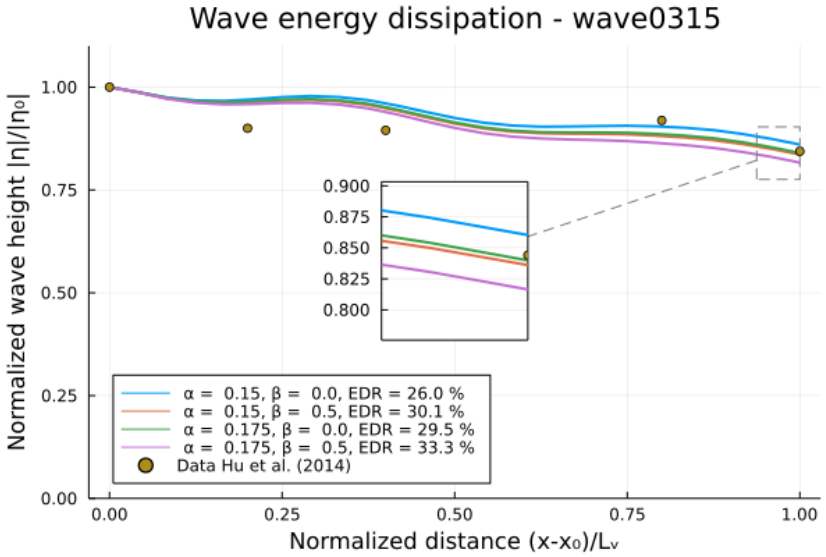

Figure 5.20: Wave 0315 (Hu 2014) reproduction.

A range of α and β coefficients has been plotted to represent the results of wave 0315. Again, the linear term with a value of $\alpha = 0.175$ provides the closes result over the entire vegetation length. However, it must be noted that calibration of β alone could have also reproduced with similar accuracy. The data points of wave0315 do not seem to follow a specifically linear or more quadratic trend.

5.3.2 Wave attenuation by suspended canopies with cultivated kelp

The publication by Zhu et al. [82] makes use of a more complex model to represent sugar kelp. A 1:10 dynamically scaled model of Saccharina Latissima on longlines is installed in a 24m long wave tank. It is among the most realistic studies found to represent offshore kelp cultivation farms, due to its highly realistic sugar kelp mimics and the the setup using a frame that allows for adjusting cultivation depth.

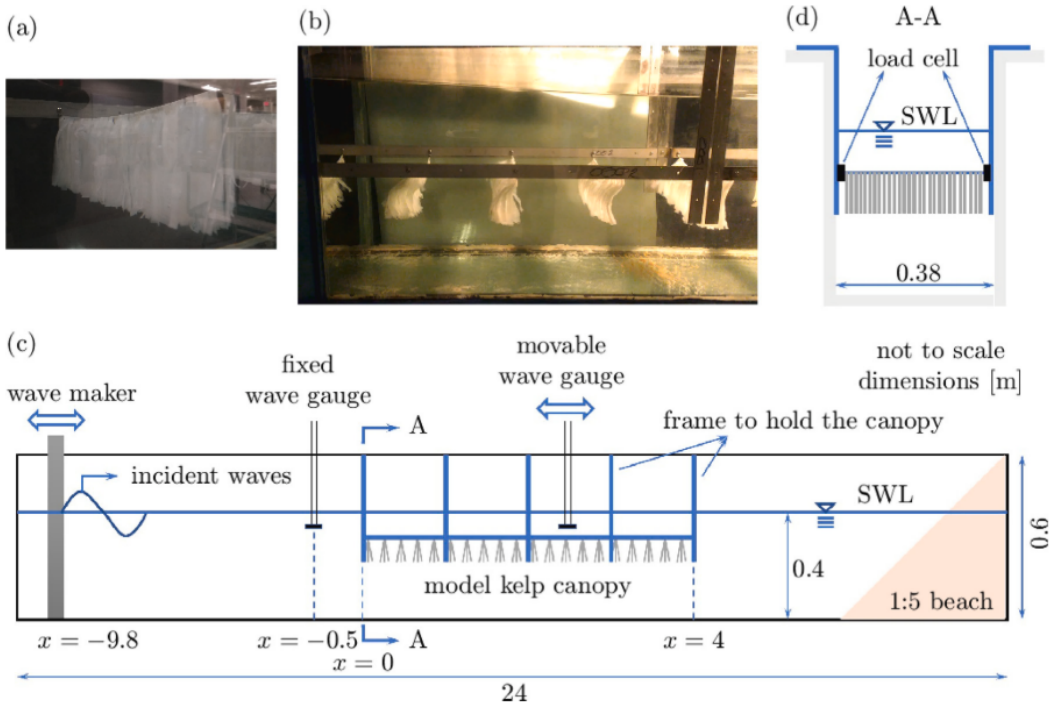

Figure 5.21: Experimental setup of Zhu 2021.

The wave conditions corresponded to full-scale wave heights of $0.18 \leq H_0 \leq 0.38$ and periods between 2.6 and 6.3 seconds. For brevity, one comparison simulation is displayed in Figure 5.22.

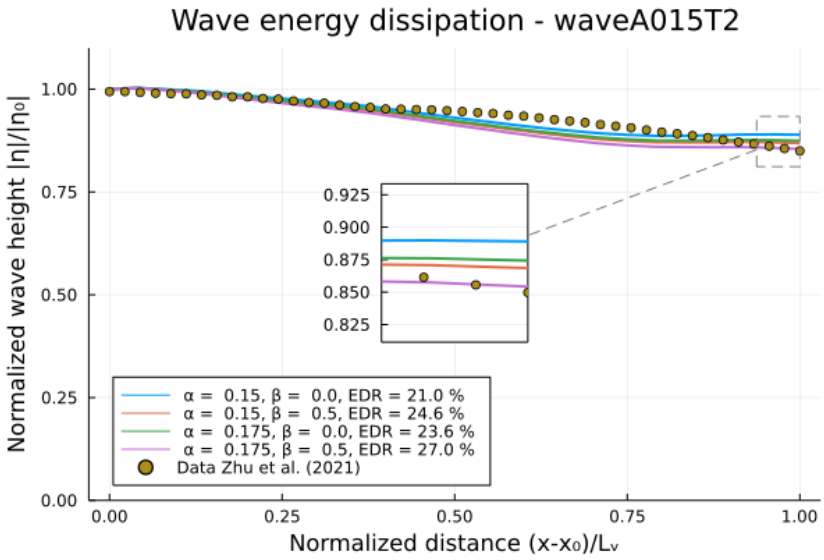

Figure 5.22: Normalized wave damping per normalized vegetation distance for E21n700.

The presented run with wave015T2 makes use of the most dense seeding line setup, with fairly stiff models over sugar kelp. In order to provide some insight of the influence of this seeding density and stiffness, a

comparison is provided in Figure 5.23. This forms the basis for calibration of the model that is used to provide the case study.

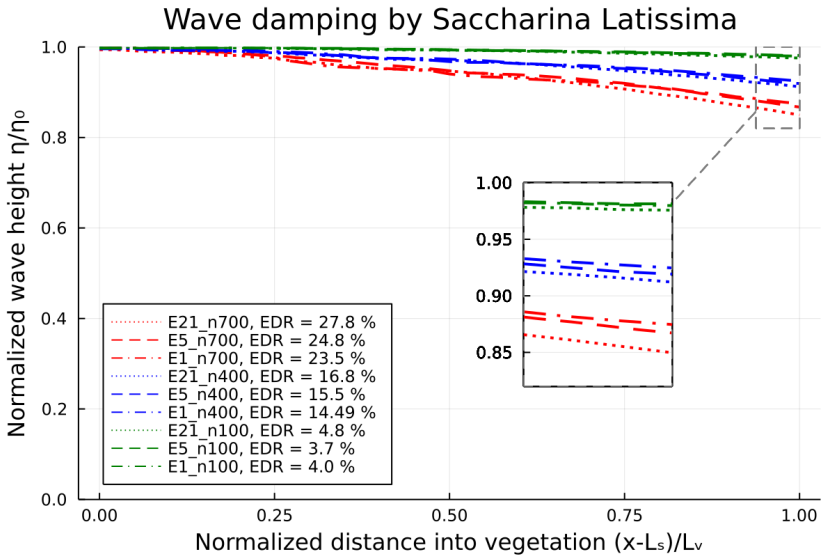

Figure 5.23: Influence of plant characteristics on Energy Dissipation Ratio.

6

Case study offshore kelp farm

Borssele III & IV is currently the largest operational wind park offshore the Dutch coastline. It has designated areas where the option for multi-use is kept open for passive fishing, nature-development and mariculture. For the case study, Borssele III & IV is considered an exemplary site to explore the opportunities of large scale kelp farms. This section shortly sums up the layout of the proposed farm and aims to quantify what the effects of seaweed farms could be in this area regarding wave damping. Supplementary information can be found in Appendix A.

Table 6.1: Key characteristics of the Borssele III & IV windfarm.

Parameter	Value	Remarks
Operator	Blauwwind consortium	Shell, Van Oord, Eneco, Partners Group, DGE
No. of turbines	77	Type V164 9.5 MW
Installed power	731.5 MW	
Total area	344 km^2	90 km^2 designated for multi-use
Distance from shore	22 km	Nearest port Vlissingen

6.1 Case set-up

6.1.1 Location and layout

Available space for secondary uses in the wind farm is based upon assumption, making use of the estimated distance between turbines, necessity for waterways for operations and a safety margin around the turbines. Turbine spacing is based upon efficiency optimization and generally set at around 7 times the rotor diameter. With the 164m rotor diameter of the turbines used in the wind farm, this amounts to around one kilometer.

Turbines are assumed to be spaced in a squared pattern, leading to a grid of 1000x1000m patches with turbines at the nodes. This is a strong deviation from patterns that realistically used, based upon optimization for yield and cable layouts within the available (non-rectangular) space.

To account for conservative requirements on space around turbines, and to somewhat account for the disordered grid found in wind parks, it is assumed that the maximum dimensions of vegetation patches within the wind park are 500m width by 500m length. This leads to an idealized layout, presented in Figure 6.1.

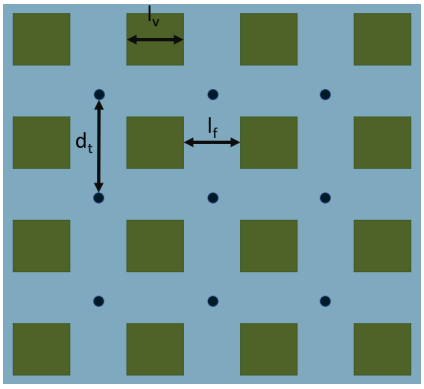

Figure 6.1: Assumed idealized layout of Case Study wind park.
Turbine distance $d_t = 1000m$, Vegetation length l_v and free length l_f both equal 500m.

Saccharina Latissima is chosen as vegetation species for this case study. Besides it being native to the North Sea area, it is also one of the better-researched species. This makes it a realistic choice and allows for more credible validation. For the characteristics of the seaweed reference is made to Table 6.2.

Table 6.2: Mechanical and morphological characteristics of Saccharina Latissima, from Zhu et al. [81].

	Mass density ρ_v [g/cm^3]	Elastic modulus E[MPa]	Blade length l_f[cm]	Blade width b[cm]	Blades per meter [m^{-1}]
Model kelp 1:10	1.2	2.04	9.66	0.95	1000
Full-scale Zhu et al. [81]	1.23	21.0	96.6	9.5	100
Fredriksson et al. (2020)	1.3 ± 0.3	1.3 ± 0.4	Up to 300	–	–
Vettori and Nikora (2017)	1.09 ± 0.09	4 ± 3	15 – 65	3.6 – 13.1	–
Augyte et al. (2017) I	–	–	220.4	4.67	330
Augyte et al. (2017) II	–	–	147.4	2.76	400
Peteiro and Freire (2013)	–	–	152.9	12.1	745

6.1.2 Environmental conditions

In determination of representative environmental conditions, the potential application should be kept in mind. Effectiveness of wave damping by seaweed is influenced largely by wavelength, as shown in both the literature review, as well as the sensitivity analysis in section 5.2. Taking fatigue into consideration as well, it would be beneficial to decrease wave energy for the waves that are most common at the location. In further research it could be investigated whether this hypothesis is correct, and to what degree these benefits might hold. In the context of this study it is considered merely a relevant sea state for analysis.

From the data of RVO [59] the key conditions have been imported to Appendix A. Based upon the mean values from the Normal Sea States occurrence table, it was assumed that a wave with a period of 6s and wave height of 1.5m is representative for the majority of the time. This is a crude approach to determination of the simulation conditions. In further research it is recommended to reproduce local wave spectra in the numerical flume for a more accurate representation.

Furthermore, even though currents are known to be part of the environment at the Borssele wind park, they are neglected in this example. Current blockage is unlikely due to the relatively small portion of the water column being occupied. Further investigation is required to determine whether currents significantly alter the damping characteristics.

6.1.3 Simulation setup

Based upon the scaling proposed in Rosman et al. [58] and the dynamic similarity discussed in Zhu et al. [82], the farm characteristics as defined in the previous sections, are transferred to the numerical flume scale. The input parameters used for quantification of the damping potential are presented in Table 6.3, it is verified that through this scaling method, the Froude numbers remain the same and Reynolds numbers are different, but remain in the same regime.

Table 6.3: Full scale and simulation dimensions of the model kelp farm.

Parameter	Full scale	Simulation scale	Unit
Vegetation length	500	10	m
Vegetation height	5.0	0.1	m
Water depth	40	0.8	m
Wave height	1.5	0.03	m
Wave period	6.0	0.85	s
Wave length	56.2	1.12	m
Wave number	0.11	5.59	m^{-1}
Angular frequency	1.05	7.4	rad/s
Maximum orbital velocity	0.79	0.11	m/s

Darcy-Forchheimer coefficient calibration

In order to establish what α- and β-coefficients are appropriate values for application under the conditions in the wind park, the following steps were taken:

- ☐ Find suitable vegetation characteristics in existing test data (Sacch.Lat.)
- ☐ Focus on appropriate wave conditions (wave frequency main driver)
- ☐ Simulate closely reproduced scaled experiment
- ☐ Calibrate α and β to match wave height reduction/EDR
- ☐ Re-scale numerical flume to Case Study dimensions
- ☐ Check results with analytical solution based on provided Cd

The porous parameters have been determined for this case through calibrating on the data available in the dynamically scaled experiments of Zhu et al. [82]. The Darcy and Forchheimer coefficients found to represent the Saccharina Latissima, are applied to a scaled version of the Case Study.

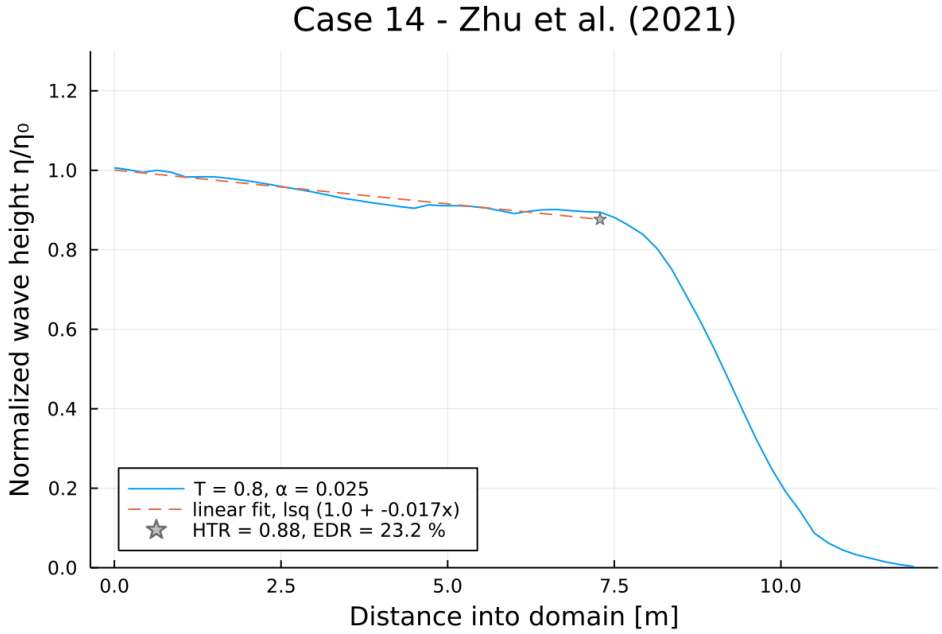

Figure 6.2: Simulation run calibrated with $\alpha = 0.025$ to represent case 14 [82].

6.2 Results

Based upon the calibration data that is displayed in section 5.3, four combinations of α and β have been identified that could reflect the influence of the original experimental study. These combinations have varying

contributions of the linear and quadratic terms. Based upon the limited measurements in the experimental data, the trend-line could not be accurately reproduced, therefore the combinations provide an indication of what effects the different combinations have on the outcome.

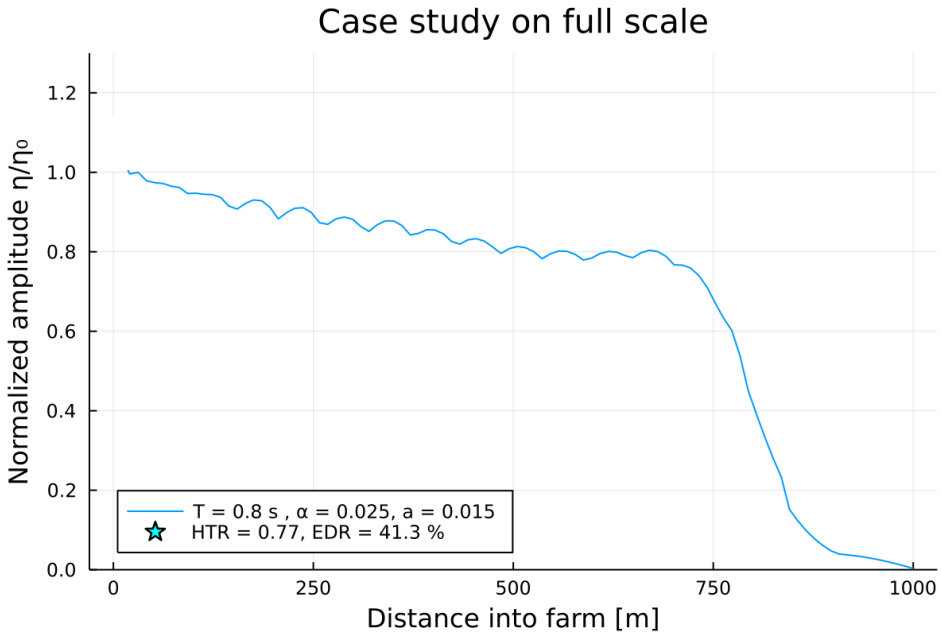

Figure 6.3: Wave height reduction over 500m of cultivated sugar kelp. Based on the simulation parameters provided in Table 6.3.

As seen in Figure 6.3, the calibrated coefficient provides an estimation of around 40% of total energy reduction over the entire vegetation length. This simulation indicate that over the length of the vegetation patch of 500m, around 40% of wave energy in 1.5m, 6s waves can be dissipated if the farm provides seeding densities of $N > 100$ plants/m.

An important realisation is that this result has been obtained through calibration of only the linear resistance term α. In the calibration case of Figure 4.1, the reduction per unit length follows a fairly linear trend, this indicates that extrapolation to the larger dimensions would also be appropriate through the α-coefficient.

As this study concerns Saccharina Latissima, a kelp species that is expected to contribute to drag mainly through its large amount of surface area, viscous drag should be a good approximation. Besides this, the expected difference between applying the Darcy or Forchheimer term for extrapolation is expected not to be governing in accuracy. Rather, the introduction of wake-effects and wave shielding is expected to have a larger influence at this scale. Since these phenomena are not represented in the scaling method, incongruence is expected to arise from this mainly. The result is therefore only an indication, albeit one that coincides with estimates made in literature.

From a design perspective, these insights can be used to develop a farm specifically tuned to the desired waves to be attenuated. The local peak period of the wave spectrum would be a logical design parameter, this could lead to designing the farm to cover the following length:

$$L_{\text{veg}} > \frac{H_{\text{inc}}/H_{\text{trans}} - 1}{k_d(\omega_p)} \tag{6.1}$$

The remaining wave height after passing through the farm, i.e. the transmitted wave height is denoted by H_{trans}. Here $k_d\omega_p$ corresponds to the frequency-dependent decay coefficient, a function of α and β, as shown in Equation 5.2.5. Furthermore, $\omega_p = 2\pi/T_p$ signifies the angular frequency of the waves at peak period.

7

Discussion & conclusions

This chapter provides a discussion on the findings and results presented in the report, and the conclusions that are derived from them. The different elements are individually commented upon in the following sections. Care has been taken to relate the results from previous chapters and their interpretation to the implementation methods and assumptions made. Therefore, this chapter demonstrates the link between expected results, observed simulations and a reasoning for their interpretation.

In short, the research presented in this report shows that the numerical framework is a good alternative to existing modelling methods. The framework has been tested for a variety of realistic input parameters; wave conditions, geometric layout and porous characteristics. This has provided consistent results in terms of convergence and stability of the numerical method, reproducible simulation results and acceptable simulation times.

The framework is a versatile solution to modelling complex interaction with sufficient accuracy at relatively low computational cost. The conceptual simplicity of the approach avoids unnecessary complexities in translating the real life situation into modelling input. It is therefore deemed that the Darcy-Forchheimer terms are an adequate method to capture the influence of vegetation on the wave climate, generalizing the geometry without losing essential phenomena of the interaction, and accounting for wider range off flows than existing methods.

7.1 Limitations of mathematical formulation and model assumptions

The model consists of mixed order ODEs, as is demonstrated in this chapter. Furthermore, it couples multiple variables in the same grid; it links together multiple FE spaces. The method of defining the free surface introduces the need for multi-dimensionality, as wave height is defined on a 1D boundary of the 2D domain.

For reference, the modelling objectives, as stated in the objectives of this research are repeated here:

- ☐ Mathematical formulation of flow through a porous domain
- ☐ Numerical methods for solving the problem
- ☐ Implementation of the numerical methods in FEM using *Gridap*
- ☐ Verification and validation of the numerical model
- ☐ Reproduction of existing experiments in the numerical wave tank
- ☐ Execution of a hypothetical farm case study
- ☐ Visualisation, analysis and interpretation of simulation results

7.1.1 Incompressible, viscous Navier-Stokes

Several numerical wave models exist to describe the evolution of surface waves, with or without the influence of any structures in the flow. Different approaches all have their advantages and disadvantages. The use of incompressible, viscous Navier-Stokes as the basis of the numerical method allows for analysis of more phenomena than models based upon potential theory, shallow water equations or spectral wave models.

Viscous effects, rotationality and small-scale phenomena can be captured using a full Navier-Stokes description. This comes at computational cost however, compared to the other methods. Furthermore, the framework established is a nonlinear system due to the use of Navier-Stokes, which has its own implications. The convective term in the NS-equations is a non-linear term, stability issues and numerical challenges are often introduces by this term. The introduction of the sponge layer that dissipated energy for all simulation runs, as well as the stabilizing term in the weak form result in consistently stable behaviour of the model.

7.1.2 Free surface definition

As stated above, the Navier-Stokes basis allows for detailed analysis of hydrodynamic phenomena. These options, however, are greatly limited in the present numerical model due to the free surface boundary condition. Linearization of the traction equilibrium on the free-surface limits the ability to capture large fluctuations of the surface elevation per unit horizontal distance into the domain.

Practically, this means wave steepness becomes a bottleneck. Phenomena like wave breaking cannot be modelled with this approach. The single-phase linearized transpiration condition is sufficiently accurate for the desired application to small-amplitude deep water waves based on linear wave theory. However, it is expected that deviation from this regime to waves of increased steepness will introduce instabilities in the method resulting in inaccurate results.

7.1.3 Porous domain

The initial objective of implementation of the porous medium formulation to represent vegetation in a fluid flow was to capture the influence, while greatly reducing computational complexity compared to full micro-scale FSI modelling. This research has indicated successful implementation of this method, thus reaching the objective, however this directly implies a downside as well, namely loss of information within the domain.

Generalization of the complex geometry inside a porous medium is analogous to the loss of information on any scale other than the macro-scale (overall patch-dimensions). This discards any fluctuation within the medium that is related to heterogeneity, for instance the influence of variable seeding density.

In development of this model, fairly high porosities are assumed, this approaches real-life situations the best. This has lead to the assumption that phenomena on the interface between free-flowing fluid and medium are irrelevant and have not been considered. The assumption leads to inability to accurately depict induced currents in the model, and clear representation of the effects of shear layers (including phenomena like monami and detailed description of large-scale Kelvin-Helmholtz vortices).

Conclusions: Performance of numerical framework

According to the research objective, a 2D FEM modelling framework was developed to analyse the influence of vegetation on wave propagation through a porous medium. Analysis of the surface elevation without activation of the porous zone shows adequate wave generation that adheres to the intended wave shapes. Propagation through the domain follows linear wave theory and displays expected behaviour. The set-up is shown to cope well with the variety of wave conditions that is representative for waves on realistic cultivation sites. Further investigation into the limits of wave non-linearity is required to conclude on what the extremes are regarding the allowed regime of generated waves.

Although computational cost is difficult to compare to existing results, mainly due to lack of detailed documentation of existing methods, all runs in this research were performed without computational power beyond a personal laptop. Together with comparison to existing studies that do state computational cost, this shows that the framework is a feasible method in terms of required resources.

The model is considered robust, as variation of the input parameters is shown to continuously produce results that are consistent with expectations. Instabilities by errors in the approximation methods of the discretization schemes are not magnified, this implies a stable system over the range of intended inputs.

All in all, the performance of the numerical framework provides an adequate basis for further investigation of the porous parameters, and generates simulation results without the need for excessive computational resources.

7.2 Determination of porous medium parameters

Part of the research objective was defined to be analysis of how the porous parameters should be defined to accurately represent the effect of a vegetation patch. It was found that a conclusive definition of these parameters on the basis of physical processes is not feasible within the limited time-frame, considering the defined scope. Additionally, from literature review it was concluded that the elaborate data, including detailed variational analysis needed for validation, are not currently available. This greatly limits the opportunity to provide a credible physics-based parameter definition.

However, in an effort to narrow down the range of magnitudes of the parameters, it was established that for wave transmission coefficients that follow existing research, ranges could be established for the values of α and β. Namely, the former was found to lie between 0 and 0.5, while the latter can attain values between 0 and 20. In addition, an overview has been created in Table 4.3 of the characteristics of the vegetation and flow that are found to be most likely to significantly influence the degree of attenuation by large-scale offshore kelp farms.

7.3 Interpretation of simulation results

A series of simulations have been performed to test sensitivity of the modelling framework to variations in input parameters. This allows to 1) verify that the numerical implementation follows the conceptual model and physical behaviour, 2) compare results to existing models and experimental data, 3) test the ability of the model to display linear and non-linear relations and 4) perform calibration and execution for a case study.

7.3.1 Sensitivity analysis

The sensitivity study illustrates the behaviour of the model under influence of incremental variation of input parameters. Foremostly, the results of the α- and β-coefficients are of interest as their performance dictates the added value that the porous medium formulation might have. Furthermore, wave amplitude and period are analysed, as well as the depth at which the medium is modelled.

8. Can a numerical model using a Darcy-Forchheimer porous zone reproduce existing experiments?
9. How can resistance parameters be determined to accurately describe fluid-vegetation interaction?

While these questions cannot be directly answered through sensitivity analysis of the Darcy-Forchheimer coefficients, it does indicate their influence and form the basis of further analysis in follow-up research.

Darcy-Forchheimer coefficients

The linear and quadratic resistance terms were varied over the ranges $0 \leq \alpha \leq 0.5$ and $0 \leq \beta \leq 20$, as this corresponds to the situations between no damping occurring to absorption of all wave energy over a vegetation patch of 3λ. These ranges are considered realistic and found for the representative conditions provided the *Standard Flume Model*, discussed in subsection 4.1.1.
It is observed that variation of the α-coefficients results in a linearly proportional variation in amplitude transmission for constant vegetation patch length. This means that Darcy resistance term provides a linear effect on wave damping potential in the medium, as supported by derivation of the formulation of dissipation by drag in Equation 5.2.5.

On the other hand, the β coefficients is shown to display nonlinear trends in the outcomes of a linearly increasing coefficient. This is illustrated by two observations:

1. for an incrementally increasing magnitude of β on vegetation length proportional to the incident wave length, wave amplitude transmission is shown the decrease quadratically, and
2. per unit distance into the vegetated domain the contribution of the β-term quadratically decreases. In other words; the effect of β quadratically decreases with linear increase in coefficient magnitude, as well as per unit length of vegetation.

The findings stated here indicate that the model is successful at displaying both the linear contribution of the Darcy-term, as well as the nonlinear Forchheimer-contribution. Additionally, combination of the parameters also produces results that indicate that both linear drag effects, as well as quadratic drag can be combined effectively in simulations. In turn, this observation implies that the framework is indeed capable of simulating a larger range of flows by capturing both linear and quadratic drag regimes, as stated in the objectives.

Wave amplitude and period, and vertical location

Besides the Darcy-Forchheimer terms, the effects of variation of wave period and wave amplitude have been investigated. This provides insights into the research questions:

3. How does wave damping by kelp relate to incoming wave conditions?
4. How does vertical position within the water column influence attenuation?

In congruence with most studies from existing academic literature, the amount of damping is significantly influenced by the period of the incident waves. Wave damping of high-frequency waves is more pronounced than for long waves. Proportionality of the particle velocity u with incident wave period as demonstrated in subsection 5.2.5, is shown to explain this behaviour, in combination with the direct linear and quadratic dependence on u. The first explains dependence in itself, while the second exposes the different degrees of influence.

It can, however, be observed that when the vegetation patch length is made proportional to wavelength, the relation remains constant. In other words, dissipation is proportional to length normalized with wave length. This goes for situations where the remaining variables are kept constant. In a practical application this might mean that to absorb wave energy from the longest waves, the most efficient measure would be to increase the farm dimensions in the prevailing wave-direction.

Sensitivity analysis for the incident wave amplitude shows that under influence of the linear resistance term only, the influence of H_0 does not affect wave damping. For the non-linear resistance term, $H(x)$ is shown to decay proportionally quicker for increasing incident wave height. Formulation of the wave decay coefficients $k_{d,\alpha}$ and $k_d d, \beta$ in subsection 5.2.5 confirm this finding through mathematical derivation.

Regarding the influence of the vertical location, the results illustrate theory accurately. Situations were analysed from $d_{\text{veg, top}} = d_{\text{MSL}}$ (just under surface) to $d_{\text{veg, top}} = h_{\text{veg}}$ (bottom-founded). The exponential decay of velocity components from mean sea level to seabed is reflected in the exponential increase of wave amplitude transmission with relocation of the vegetated medium downwards in the water column. This indicates that the framework is suitable to judge the effects of changing the installation depth of a farm. Therefore it could be used in the case a trade-off needs to be made between growth-efficiency, mooring loads and wave damping effects in the design of a large-scale kelp farm.

Conclusions: Simulation results

Simulation results presented in this research indicate that the wave period of incident waves influences the degree of amplitude attenuation significantly. As amplitude reduction remains constant when vegetation length is proportional to wavelength, a linear increase in wave periods requires a proportionally increasing vegetation length to dissipate the same amount of wave energy. For simulations making use of the β-factor

Wave amplitude is shown not to influence the degree of attenuation directly for linear drag. For higher waves, no additional amplitude damping is observed when only the α-term is activated. Dissipation by the quadratic drag term, however, does increase with higher H_0. It should be noted that during sensitivity analysis, wave amplitude and wave period have been varied separately, while in reality they would be correlated. Thus an increase in wave height would in reality be accompanied by longer waves, and reduced attenuation per unit length of vegetation would be observed.

Furthermore, the vertical location of the vegetation patch in the water column is shown to be highly influential to the degree of amplitude attenuation. Consistent with the velocity profile found in deep water regimes, attenuation follows a close to exponential trend with respect to vegetation depth.

Lastly, sensitivity analysis using a linear-spaced set of α- and β-coefficients demonstrates that the degree of energy dissipation follow a linear and quadratic pattern for respectively an increase in Darcy and Forchheimer coefficients. This indicates that the implementation of the Darcy-Forchheimer terms indeed provide the opportunity to represent dissipation through drag in wider regimes than currently available methods.

7.3.2 Reproduction experiments

Current literature provides no extensive analysis of the influence of separate vegetation characteristics and farm dimensions on wave damping potential. This has made it impossible to compare simulation results to experimental results for a continuous set of parameters. In order to still provide illustration of the capabilities of the modelling framework, studies have been selected to represent different use-cases.

Comparison to the idealized situation of waves through rigid cylinders in an ordered array was done. The simulations indicate that for vegetation that can be represented by equivalent cylinders - which is often the case for Macrocystis Pyrifera in current literature - the model can be calibrated to reproduce experimental results. Similar to this, the more complex situation of flexible strips - representing the long blades of Saccharina Latissima - was reproduced successfully using the Darcy-Forchheimer framework as well.

Currently, calibration of the α and β parameters was needed to reach agreement between experimental results and simulation outcomes. For added value of the framework, it would be beneficial to determine these coefficients on the basis of the plant characteristics, farm layout and potentially wave conditions. This would enable the formulation of Darcy-Forchheimer terms on the basis of physical phenomena.

Conslusions: Reproduction of experimental data

In the process of validating the framework, a number of physical experiments have been reproduced in the numerical wave flume. Simulation results illustrate that after calibration, the framework is successful in reproduction of the damping effects as presented in the respective studies. This includes the studies by Hu et al. [28], Zhu et al. [82], Hu et al. [29] and Wu et al. [74].

Both the idealized representation of kelp through an array of solid cylinders, as well as the more complex mimics using thin sheets that represent flexible sea-growth, could be successfully reproduced using the numerical framework. It was found that the objective to quickly and straightforwardly implement set-ups with different geometry in terms of vegetation dimensions and wave conditions was met with success.

The ease of set-up for reproduction of existing experimental observations not only provides the opportunity to validate outcomes, it also implies that the framework can be of good use in applications where calibration is required. Sets of runs with varying input parameters are quickly set up, to allow for analysis of batches of results and calibrate with minimal effort.

7.3.3 Case study

Application of the numerical framework to the hypothetical kelp farm described in chapter 6 forms an indication of wave damping in future kelp farms. This is used to answer part of the initial research questions;

1. What could a future offshore kelp farm look like?
2. Could large-scale offshore wave farms be effectively used for wave damping?

The first question has been mostly investigated through industry reviews, where professionals in the kelp cultivation sector have shared their views on current developments. The dominant view was that the kelp sector is expected to grow a lot in the near future, however, some key challenges remain in obstructive legislation, governance practices, financial feasibility and the lack of a clear winning technology regarding support structures needed.

In line with the ambitions of currently operating companies, and the Klimaatakkoord by the Dutch government, multi-use of a windpark was identified as a plausible opportunity of kelp cultivation. Based upon this, a theoretical farm was developed using input parameters gathered in conjunction with the Borssele III & IV site. Simulation of waves through this hypothetical farm was based upon extrapolation using a calibrated wave tank-scale experiment using similar (scaled) wave conditions and vegetation parameters. Scaling was done in accordance with literature recommendations, keeping Froude number equal and Re in the same range. The chosen approach is still heavy on assumptions and should only be considered a rough indication, mainly due to the following:

1) Extrapolation from wave tank scale to large-scale does not include additional effects like large-scale wake production and wave shielding effects.
2) Micro-scale behaviour of the seeded plants has not been verified to remain identical for the jump from laboratory scale to real-life conditions.
3) Validation of the overall modelling results is not possible due to lack of measurement data on this scale.
4) Calibration of the model-test was done assuming the α term is governing for sugar kelp in mild conditions, extensive investigation of the linear and non-linear resistance contributions is recommended.

Conclusions: Wave attenuation in future offshore kelp farm

Based upon limit data regarding real-scale kelp forests it is difficult to predict wave damping by offshore kelp cultivation farms with useful accuracy.

The simulation results have indicated that, based upon scaling of a calibrated model-scale experiment, the wave reduction in a sugar kelp farm - with a seeding density of 100 plants/m, vegetated height of 5 m in 40 m waterdepth, and an elastic modulus of the blades of 21 Mpa - can reduce the energy of 1.5m, 6s waves with up to 40% over a length of 500 m. The dimensions of this farm are considered realistic, and seeding density has been assumed conservatively. In relation to the second research question stated it can be concluded that large-scale validation is recommended, but preliminary results indicate that large-scale offshore kelp farms are expected to be effective at wave energy reduction.

7.4 List of condensed conclusions

The framework is a versatile solution to modelling complex interaction with sufficient accuracy at relatively low computational cost. The conceptual simplicity of the approach avoids unnecessary complexities in translating the real life situation into modelling input. It is therefore deemed that the Darcy-Forchheimer terms are an adequate method to capture the influence of vegetation on the wave climate, generalizing the geometry without losing essential phenomena of the interaction, and accounting for wider range off flows than existing methods.

In Table 7.1 the main findings in the three different categories are presented that work towards the main research objective:

A numerical model to simulate the influence of large-scale offshore kelp farms on the wave climate, using a porous medium approach.

Table 7.1: Summary of the main conclusions in this report.

Subject	Findings
The presented numerical framework	... allows for modelling of linear and non-linear damping effects, enabling further research into porous parameters ... creates the opportunity to easily model and analyse different conditions for the complex problem of vegetation-flow interaction ... allows for analysis of more complex hydrodynamic phenomena than State-of-the-art methods with limited computational resources ... displays robust behaviour within realistic ranges of input parameters
Wave energy dissipation in kelp farms	... increases significantly for near-surface floating farm structures ... is strongly influence by wave period, with higher dissipation for short waves ... is not significantly influence by incident wave amplitude ... decreases with increased relative water depth
The porous medium approach	... can represent a wide range of flow regimes, through a combination of linear and quadratic resistance ... is a robust approach for the representation of vegetation ... can reproduce experimental results when implemented in a numerical method

8

Suggestions for further research

In the relatively limited timespan available for conduction of this research, a hydrodynamic model was built from scratch with implementation of a porous zone that is shown to be capable of reproducing experimental results of wave damping by vegetation. The setup is such that batches of runs using variable inputs can be run subsequently and post-processing of the results including diverse visualisations are implemented. The method is shown to use acceptable computational resources within the intended range of use, although significant further optimizations are expected to be within reach.

However, as with any research - and especially for an inexperienced researcher such as this author - more questions have been uncovered than answered. And the limitations of the findings and the established model, that have been largely posed in chapter 7, are obvious. Thus, further research has the potential to improve insights, the key recommendations are posed in this chapter.

8.1 Framework-related recommendations

Development of the numerical framework has provided the bulk of the work of this research project. Still, within the limited scope, sufficient possible supplements to the model remain to improve its performance and applicability. The recommended additions are presented below.

8.1.1 Free surface modelling technique

The single-phase linearized boundary condition that is applied to the free surface to solve for a virtual elevation has been stated as one of the most limiting components in the numerical framework. It allows for mild conditions only and will not be able to capture waves of significant steepness or capturing phenomena like wave-breaking. One step in the right direction would be more detailed analysis of the maximum range of wave steepness using the current approach.

Implementation of free surface modelling method that allows for a wider range of free-surface geometries would expand the applicability of the model to waves that are not accurately captured in the linearized transpiration boundary condition. It is recommended to supplement the current numerical framework with e.g. a level-set method based free surface capturing method to increase modelling abilities.

8.1.2 Introduction of combined wave-current simulation

The setup provided in this study does not directly allow for modelling of combined waves and current. Reason for this lies with the boundary conditions implemented at the outflow boundary; currently no outflow is permitted. Enabling the combination of current and waves would enable the inclusion of plant-reconfiguration in the model. This phenomenon is known to reduce overall drag when a current is applied alongside incoming waves, and would be interesting to include.

Through implementation of a traction equilibrium at the rightmost boundary, it would be possible to apply a net positive current. It is recommended to combine this new boundary condition with a more elaborate method of free surface-modelling, as during testing a traction equilibrium was shown not to cope well with the current virtual elevation definition. A VOF-type method or a level-set implementation is recommended for further advancement of the model.

8.1.3 Derivation of porous medium terms

The objective of the modelling framework was to develop a framework that enables representation of vegetation through a porous medium. In that sense it can be seen as the basis for further research into the porous medium terms. Therefore, the recommendations regarding this follow up research deserves mention.

The recommendations are twofold; 1) Derivation on the basis of physical phenomena is recommended, and 2) a research strategy that processes more elaborate experimental results to be able to calibrate the porous parameters more accurately is recommended.

For the second recommendation broad experimental measurements are the essence, but the first recommendation would also greatly benefit from an elaborate dataset that enables validation of the physics-based formulations. Current experimental data is considered insufficient as variation of input parameters (e.g. separate plant characteristics) doesn't often consider the needed resolution and combination for thorough checking of hypothesized linear and quadratic parameters. The studies that do enable calibration focus on the classical $C_{\mathrm{d,\,bulk}}$ formulation.

Lastly, regarding the first recommendation above, physical phenomena are not sufficiently understood to derive formulations on the basis of physics. Through dimensional analysis, close analysis of experiments and by combing insights over a large range of experimental and numerical studies, these insights could be supplemented in future research.

8.1.4 Expansion of analysis functions

Throughout this report, mention has been made of some interesting phenomena that could aid in the understanding of the physical processes around wave damping by large-scale offshore kelp farms. The numerical framework provided in this study allows for analysis of a number of these phenomena in the current state, however the analysis methods put in place have not been focused on them.

Among them are the analysis of *vorticity* that can aid in researching the velocity structures that are for instance generated by the shear layers around the porous medium. Additionally, *vertical mixing* due to the presence of a velocity gradient over the vertical dimension under/in the porous medium could be studied using the current set up. Furthermore, it is expected that *wake production* could be analyzed without too much additions to the model since convection and viscous effects can be captured in the current numerical setup.

Following currents are identified in literature to be a relevant result of incident waves experiencing resistance from a vegetated patch. It could induce reconfiguration of the vegetation and might result in net sediment transport, which is a crucial phenomena when deep water assumptions are relaxed. In short, the current setup has not yet been fully exploited in the results shown in this report. Additional analysis functions and validation of the representation of the mentioned phenomena could further elaborate the benefits of this framework.

8.2 General recommendations

Besides the recommendations regarding the model, further progress in the understanding and modelling of waves through large-scale offshore kelp farms could be made with the following suggestions for research.

8.2.1 Alternative applications of the framework

In the category of porous structures interacting with waves and currents, floating porous breakwaters are an area of research that might benefit from the proposed numerical framework. Opposed to their static counterparts, floating breakwaters are generally considered a more environmentally friendly solution to wave damping. Porous structures have been proposed as transmitted wave heights are decreased, especially at resonance frequencies. Also mooring forces are favorable influenced by porous structures versus impermeable breakwaters.

The developed framework would have to be redeveloped, as for correct modelling of a floating breakwater, the fluid-structure interaction should include the dynamic behaviour of the structure itself. This introduces coupled equations of motion that includes description of the motions of the breakwater. The Darcy-Forchheimer description, however, should form a reasonable method to model for this application as well.

8.2.2 Elaborate experiments at scale

Although a significant body of experimental publications is available for the problem of bottom-founded vegetation interacting with waves, floating and suspended experiments are less numerous. Expansion of validation data through experiments that make use of a setup that represents a cultivation farm, instead of naturally occurring patches in shallow water would contribute to future studies. In addition, laboratory experiments, contrary to field tests, allow for the use of PIV-methods to provide a detailed picture of the velocity field through a section of farm, a bundle of plants or around a single plant. Even though the strength of the modelling framework in this study relies on generalization of these small-scale interactions, it was found that many unknowns remain on the small scale as well.

Furthermore, it is recommended to conduct practical experiments that keep in mind the validation strategy of a numerical model. To avoid collection of sub-optimal data it is recommended to experiment specifically focused on the parameters that are suggested by physics-based coefficient determination. Before that time, the suggestions made in Table 4.3 are recommended as a basis for investigation.

8.2.3 Full scale measurements

In any further application of the numerical framework, the outcomes would improve from calibration on more realistic experimental data. Currently, experiments almost all depend on the use of relatively small-scaled wave tanks. In the future, measurement campaigns in full-scale kelp forests would contribute immensely to the possible accuracy that can be reached with this framework.

Furthermore, full-scale data would allow for analysis of phenomena that are now left unknown. This includes the occurrence of wave-shielding, wake production, and induced currents. As current developments quickly scale up, it might be possible to facilitate elaborate measurement campaigns around pilot farms and eventually full scale cultivation projects.

In any such measurement campaign, it would be beneficial to recover data regarding biomass growth, plant dimensions and mechanical/morphological characteristics. Since the morphology of kelp is site-specific and highly dependent on species, this is essential information. Variation over time would aid in determination of the seasonal effects over the course of growth from seedling to fully grown crops. Through collection of these parameters, the findings regarding wave damping can be compared to the vegetation, this could aid validation of any full-scale model when resistance terms are defined as characteristic-dependent parameters.

Data should be collected around the field using a setup of multiple wave buoys. The most basic requirement is the ability to compare wave height data set from before entering the farm with wave heights after damping. For cost-saving this setup could be based upon the prevalent direction of wave propagation, however damping along multiple direction would be interesting to capture. Especially for farms where width and length of the vegetation field differ significantly, as this would allow for some insight into the dependence of transmitted wave heights as a function of farm length. Besides data on wave height reduction over the length of the farm, the line stress of the mooring configuration would make for interesting data. Mooring loads can be be related to the overall drag induced by the farm.

A

Case study background information

The layout of the hypothetical offshore kelp cultivation farm is based upon multi-use in combination with a wind farm. In chapter 6 the basics of the farms are justified, this appendix supplements further information regarding the on-site conditions. The information is based upon the publicly available data from RVO [59].

Location

The existing location of the Borssele III/IV wind park is chosen, it is located in the EEZ of the Netherlands and lays in the Southern part of the Dutch North Sea territory. The site has already been appointed by the Dutch authorities for multi-use pilots. Furthermore, the site is representative in terms of conditions for the North Sea.

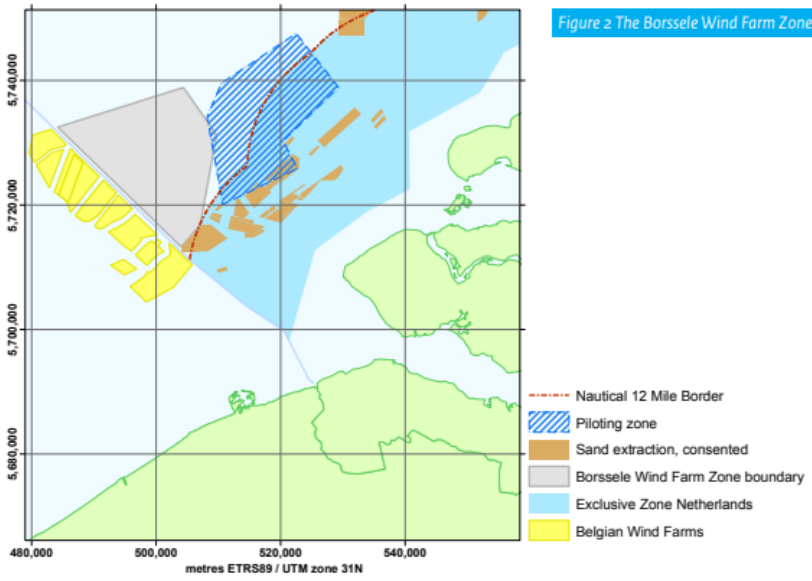

Figure A.1: Location of the Borssele III & IV windfarm.

Environmental Conditions

The case study focusses on the prevailaing conditions instead of extreme values of the metocean conditions. To this end, the significant wave height for a 50-year return period is considered representative. Figure A.2 is used in conjunction with Figure A.3 to determine what wave conditions to use in the case study.

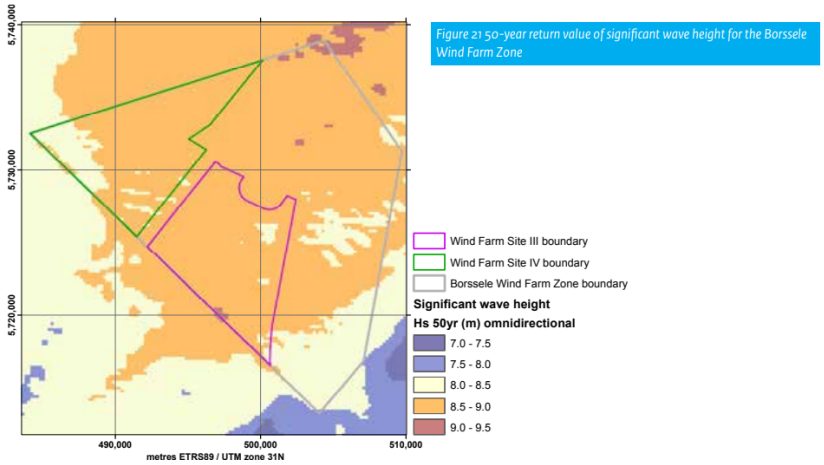

Figure A.2: Significant wave height for 50-yea return period, Borssele III & IV windfarm.

$Wind_{10m}$ (m/s)	H_s (m)	T_p (s)	Spectrum (-)	Gamma γ (-)	duration (%)	T (s) min - max
< 4	0.6	6.0	JONSWAP	1.44	19.42	(2.8 - 3.6)
4 - 5	0.8	5.8	JONSWAP	1.44	10.99	(3.1 - 4.0)
5 - 6	0.9	5.7	JONSWAP	1.44	11.84	(3.3 - 4.3)
6 - 7	1.0	5.7	JONSWAP	1.44	11.15	(3.6 - 4.6)
7 - 8	1.2	5.8	JONSWAP	1.44	9.96	(3.9 - 5.0)
8 - 9	1.4	6.0	JONSWAP	1.44	8.58	(4.2 - 5.4)
9 - 10	1.6	6.2	JONSWAP	1.44	6.90	(4.5 - 5.8)
10 - 11	1.8	6.4	JONSWAP	1.44	5.59	(4.8 - 6.2)
11 - 12	2.1	6.6	JONSWAP	1.44	4.38	(5.1 - 6.6)
12 - 13	2.3	6.8	JONSWAP	1.44	3.33	(5.4 - 7.0)
13 - 14	2.6	7.1	JONSWAP	1.44	2.55	(5.8 - 7.4)
14 - 15	2.9	7.3	JONSWAP	1.44	1.78	(6.0 - 7.8)
15 - 16	3.2	7.5	JONSWAP	1.44	1.31	(6.3 - 8.2)
16 - 17	3.4	7.6	JONSWAP	1.44	0.89	(6.6 - 8.5)
17 - 18	3.7	7.8	JONSWAP	1.44	0.62	(6.8 - 8.8)
18 - 19	4.0	8.0	JONSWAP	1.44	0.31	(7.1 - 9.1)
19 - 20	4.3	8.2	JONSWAP	1.44	0.18	(7.3 - 9.5)
20 - 21	4.5	8.4	JONSWAP	1.44	0.10	(7.5 - 9.7)
21 - 22	4.7	8.4	JONSWAP	1.44	0.07	(7.7 - 9.9)
22 - 23	5.0	8.6	JONSWAP	1.44	0.02	(7.9 - 10.2)
23 - 24	5.3	8.9	JONSWAP	1.44	0.02	(8.1 - 10.5)
24 - 25	5.3	8.8	JONSWAP	1.44	0.01	(8.2 - 10.5)
25 - 27	5.9	9.3	JONSWAP	1.44	0.01	(8.6 - 11.1)
> 27	6.6	10.0	JONSWAP	1.44	0.00	(9.1 - 11.7)

Figure A.3: Normal Sea States, given values are means. They form a good indication of expected waves [59].

Water depth at the location of installation is the final crucial parameter to an indicative simulation on site.

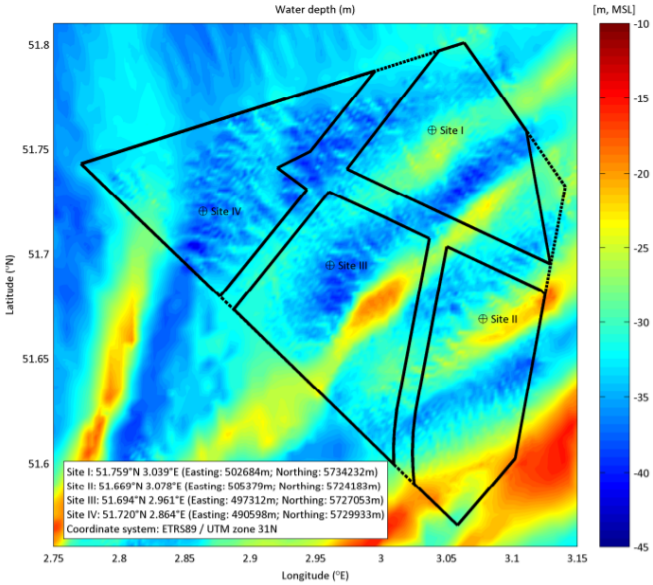

Figure A.4: Waterdepth at Borssele wind park [59].

Farm dimensions & seeding density

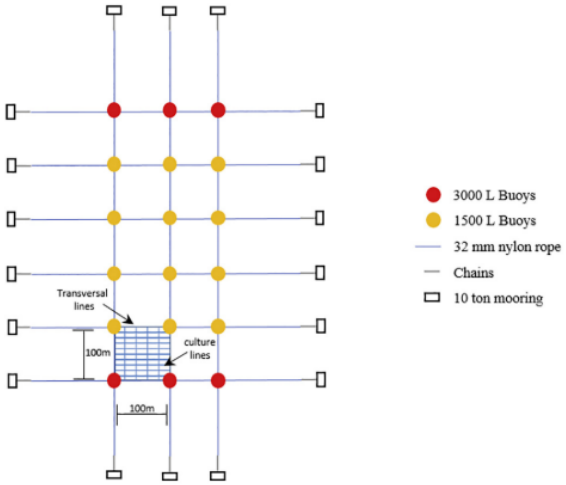

Figure A.5: Layout of 10ha cultivation system, Camus (2019).

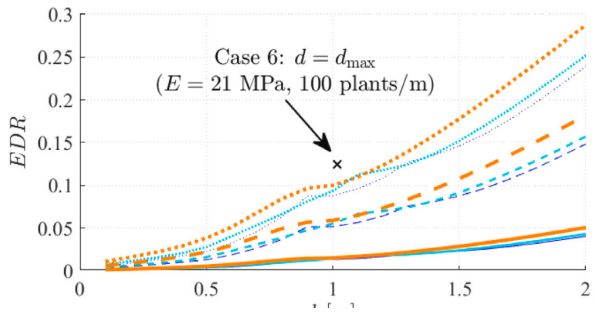

Figure A.6: Seeding density influence on attenuation Zhu et al. [82].

B

Industry Interviews

Interviewed parties

Academic relevance of the research is guarded by thorough analysis of exiting literature, and the gap analysis on scientific publications. To supplement this with relevance to the industry, and maximize the potential benefit of this research to technological developments and societal impact, an additional industry review was performed.

The main focus of the interviews done was to verify findings from the scientific literature review. In other words, the conversations with parties directly involved in the industry - either from commercial or research-perspective - helped guide in the right direction. Furthermore, the insights gained in the industry review provide valuable knowledge on the current state of the industry. The outcomes of the conversations are used throughout the industry prospects.

Table B.1: Interviews within kelp farming industry

Organisation	Role	Position	Topics
Aqitec	Marine engineering & construction	Owner and Chief Engineer	Support structure modelling, drag force calibration
Kelp Blue	Cultivation company	Project engineer	Engineering challenges, data collection, structural designs
Kelson Marine	Aquaculture engineering consultancy	Hydrodynamic engineer	Engineering challenges, model validation, hydrodynamic behaviour
MARIN	Research and testing	Manager offshore projects	Hydrodynamic experiments, state of the sector, data acquisition
North Sea Farmers	Sector network	Manager operations	Scaling difficulties, Market integration, current initiatives
Ocean Rainforest	Cultivation company	Production & Quality manager	Scaling challenges, state of the sector, operational challenges
Witteveen+Bos	Engineering	Graduate student	Research approach, modelling efforts
Reshore	Start-up concept design	Founders	Status of sector, model testing
WUR	Research	Senior Researcher & Project manager marine ecology	Biological implications scaling, data acquisition for model validation

The elaborate meeting notes have been omitted as to not disclose any sensitive information on the current state of ongoing research and commercial projects.

Main insights

The input from industry parties has been processed throughout the literature review and this report. Their main contribution has been in establishing a proper image of the current state of affairs, besides this some data has been supplied that aids in developing the Case Study that is done using the numerical model.

Most of the material provided during personal communication with industry parties is considered sensitive and is therefore not included in the public version of this report.

Farm dimensions

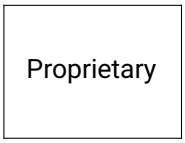

Figure B.1: Design overview of the pilot farm under construction by Kelp Blue.

Living Breakwater (Reshore)

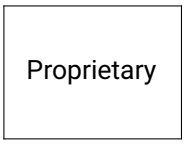

Figure B.2: Graphical representation of the living breakwater concept by Reshore.

Representative conditions

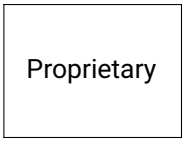

Figure B.3: Representative conditions in a non-sheltered pilot site.

Biomass and load correlation

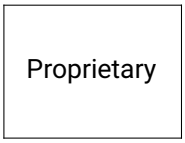

Figure B.4: Amount of biomass over time plotted vs significant wave height.

Lumped mass model (MATLAB)

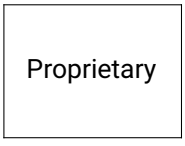

Figure B.5: Visual impression of results generated by currently in-use MATLAB model for North Sea longline.

C

Modelling methods, drag formulations and experimental data

Modeling methods of wave-vegetation interaction

Table C.1: Overview of representative numerical modeling methods. Expansion of the review in Suzuki et al. [63].

Source	Governing equations	Wave condition	Vegetation model	Comp. cost
Price et al. [56]	Viscous bottom friction	Regular wave	Effective viscosity	Minimal
Kutija and Thi Minh Hong [38]	Horizontal momentum conservation	Steady uniform flow	Timoshenko beam	
Dalrymple et al. [17] & Mendez and Losada [50]	Energy flux conservation	Regular/irregular	Rigid cylinders	Low
Suzuki et al. [62]	Spectral action balance	Regular/irregular	Rigid cylinders	Low
Cao et al. [8], Tang et al. [65]	Mid-slope equation	Regular/irregular	Rigid cylinders	Low
Kobayashi [37], Mei et al. [49]	Shallow Water Equations	Regular/irregular	Rigid/fixable	Low
Liu et al. [41]	RANS, multi-scale	Regular	Rigid	Low
Phan et al. [55]	Shallow Water Equations	Regular/irregular (breaking)	Rigid	Medium
Mendez et al. [51]	Potential flow (eigen-function expansion)	Regular waves	Rigid	Low
Augustin et al. [2], Huang et al. [30] & Yang et al. [77]	Boussinesq equations	Regular/irregular	Rigid cylinders	Medium
Li and Yan [40], Ma et al. [45], Maza et al. [47], Chen et al. [10], Maza et al. [48]	RANS equations	Regular/irregular	Rigid cylinders	High
Soares [60]	RANS equations	Regular waves	Porous zone	Medium
van Rooijen et al. [68]	Nonlinear shallow water	Irregular waves	Rigid cylinders	Low
Suzuki et al. [63]	Nonlinear shallow water	Regular/irregular	Rigid cylinders	Medium
Hadadpour [22]	RANS equations	Waves & current	Porous medium	
Hu et al. [27]	Homogenization FE (micro) and FD (macro)	Regular waves	flexible cantilever cylinder	High

Drag coefficient formulations

Table C.2: Formulations of bulk drag coefficient and their applicable range, adapted from Chen et al. [9].

Reference	Mimic Type	Flow	C_D relation	Method
Kobayashi et al. (1993)	Flexible strips	Waves	$C_D = 0.08 + (2200/Re)^{2.4}$ $2200 < Re < 18,000$	Calibration
Méndez et al. (1999)	Flexible strips	Waves	$C_D = 0.08 + (2200/Re)^{2.2}$ $2000 < Re < 15,500$ (no swaying) $C_D = 0.40 + (4600/Re)^{2.9}$ $2300 < Re < 20,000$(swaying)	Calibration
Mendez et al. (2004)	Flexible real	Waves	$C_D = 0.47\exp(-0.052KC)$ $R^2 = 0.76$ $3 \leq KC \leq 59$	Calibration
Bradley, Houser (2009)	Flexible real	Waves	$C_D = 253.9KC^{-3.0}$ $R^2 = 0.95$ 0<K C<6	Calibration
Jadhav et al. (2013)	Flexible real	Waves	$C_D = 70KC^{-0.86}$ $R^2 = 0.95$ 25<K C<135	Calibration
Anderson Smith (2014)	Flexible real	Waves	$C_D = 1.10 + (27.4/KC)^{3.08}$ $R^2 = 0.88$ $26 < KC < 112$ $C_D = 0.76 + (744.2/Re)1^{.27}$ $R^2 = 0.94$ $533 < Re < 2296$	Calibration
Ozeren et al. (2014)	Rigid wood	Waves	$C_D = 1.5 + (6.785/KC)^{222}$ $R^2 = 0.21$ $N_v = 156\ m^{-2}$, $h_v = 0.63$ m $C_D = 2.1 + (793/Re)^{2.39}$ $C_D = 0.683 + (12.07/KC)^{2.25}$ $N_v = 350\ m^{-2}$, hv = 0.48 m	Calibration
Infantes et al. (2011)	Flexible real	Waves	$\lg C_D = -0.6653 * \lg Re + 1.1886$ $R^2 = 0.77$	Direct meas.
Hu et al. (2014)	Rigid wood	Wave + current	$C_D = 1.04 + (730/Re)^{1.37}$ 300 < Re < 4700	Direct meas.
Loasada et al. (2016a,b)	Flexible real	Waves ± current	$C_D = 0.08 + (50,000/Re)^{2.2}$ $R^2 = 0.60$ (regular waves) $C_D = 0.25 + (75,000/Re)^9$ (regular waves + currents) $C_D = 0.50 + (50,000/Re)^9$ (regular waves-currents)	Calibration

Physical experiments from literature

Table C.3: Overview of publications with experimental data

Source *[ref]*	Flow type -	Vegetation model -	Patch size[1] l x h [m]	Focus experiment -
Lowe et al. [42]	Current & waves	Rigid coral	1.8 x 0.1	Velocity profile
Nezu and Sanjou [53]	Current	Strip plates	9 x 0.05	Flow structures for variable density
Rosman et al. [57]	Current	1:25 scale kelp	2 x 0.6	Influence kelp spacing & floating canopy
Manca et al. [46]	Wave spectra	Elastic seagrass mimics	10.7 x 0.55	Wave attenuation
John et al. [33]	Regular waves	Full scale seagrass mimics	2 x 0.22	Wave attenuation
John et al. [34]	Regular waves	Full scale seagrass mimics	3.66 x 0.63	Effect submergence/ emergence & density
Wu et al. [75]	Wave spectra	Rigid/flexible seagrass mimics	2 x 0.22	Wave attenuation
Dubi and Tørum [19]	Current & waves	1:10 scale hyperborea	9.3 x 0.2	Wave force and attenuation
Rosman et al. [58]	Current & waves	1:25 scale kelp	2/3.2 x 0.6	Wave/current interaction
Zhu et al. [82]	Waves (perpendicular)	1:10 Silicon film	3.8 x 0.1	Wave attenuation
van Rooijen et al. [69]	Regular waves	Rigid dowels	2.5 x 0.3	Wave forces & velocity profile
Hu et al. [28]	Waves	Suspended rigid cylinders	5.2 x 0.22	Wave attenuation
Luhar et al. [44]	Waves	Flexible seagrass mimics	5 x 0.2	Wave attenuation
Luhar et al. [43]	Linear waves	Flexible seagrass mimics	5 x 0.2	Wave attenuation
Hu et al. [29]	Waves & current	Rigid rods	6 x 0.36	Cd calibration
Ozeren et al. [54]	Regular & irregular	Rigid, flexible & live	3.66 x 0.48	Wave attenuation
Asano et al. [1]	Waves	Flexible kelp mimics	8 x 0.25	Wave attenuation
van Veelen et al. [70]	Regular waves	Rigid, flexible & real	1.5 x 0.3	Wave attenuation
Phan et al. [55], Wu and Cox [73]	Regular & irregular, non-linearity	Rigid	17.5 x 0.3	Influence of wave non-linearities

[1] The patch size is described through length of the vegetation patch and its (mean) height.

D

Julia language & model tutorial

This appendix includes a short description of the Julia Programming Language, the main packages used in setting up the numerical model of this research and a tutorial on the step-by-step development of the model. The latter can also be found through the online library at oriolcg.github.io/GridapOffshore.jl.

Julia Programming Language

Julia is an open source programming language which combines the performance of compiled languages like C/C++, with the productivity of scripting languages such as Python and it is therefore one of the fastest languages at the moment, while providing a high-level user front-end [6].

Figure D.1: Julia Programming Language graphic.

Through Gridap's expressive API, Julia Language facilitates almost one-on-one copying of the generally accepted notation for e.g. weak forms of PDE's. This makes for well-structured code for the writer, and transparent implementation for the reader.

As Julia is a compiled language running as fast as Fortran or C. Simultaneously, it has the look and feel of scripting languages like Matlab and Python. Making it an easy-to-use language that does not compromise in performance. Julia's comparatively (still) modest user-base results in online documentation providing less guidance than longer-established counterparts. This seems to be on a pivotal point with a growing body of academic work being done with the support of Julia Language.

Packages

In order to credit the work of contributors to valuable additions to the Julia Language community, and as overall reference, the most significant packages used during development of the numerical code are presented in Table D.1. This excludes the native functions included in Julia Language's stdlib library which comes with any Julia distribution.

Table D.1: Main packages used in model besides Julia stdlib components.

Package	Description	Reference
DrWatson	Scientific help in structuring research endeavours that include the development of code and analysis of simulation results.	Datseris et al. [18]
Gridap	A set of tools for the grid-based approximation of partial differential equations. Optimized for easy implementation and great performance.	Badia and Verdugo [3]
GridapODEs	Time-integration tools for the Gridap package.	Badia et al. [4]
JuliaNLSolvers	A family of packages to solve nonlinear equations (in this project includes LineSearches, LsqFit, NLsolve)	Contributors [15]
WriteVTK	For writing VTK XML files that allow for visualisation of simulation results using ParaView.	Ignacio Polanco and Ekre [31]
JuliaIO	A famliy of packages developed to unify IO infrastructure within Julia (for this project includes FileIO, JLD2)	Contributors [16]
DataFrames	A set of tools for working with tabular data. Comparable to the functionality of pandas in Python.	JuliaData-collaborators [35]
IncompleteLU	Implementation of the left-looking version of the Incomplete Lower-Upper factorization.	Stoppels and Montoison [61]
IterativeSolvers	Provides iterative algorithms for solving linear systems, eigensystems and singular value problems. Part of JuliaLinearAlgebra.	Contributors [14]

Tutorial

Development of this framework is encouraged to continue after this research, using the recommendations provided in **??**. To this end, a tutorial is created to help in development of similar code in the future. This tutorial can be found online for the latest update (oriolcg.github.io/GridapOffshore.jl). An export is included on the following pages.

Flow through porous zone

Authors: *Joël Ruesen* and *Oriol Colomés Gené*

Published: January 2022

Gridap version: Gridap@0.16.5

This tutorial shows how wave-progression through a porous medium is modelled. The model uses viscous incompressible Navier Stokes in combination with Darcy-Forchheimer resistance terms in the momentum balance, implemented using the Gridap library.

Problem statement

Large-scale offshore kelp farms have the beneficial side-effect that they can be used for coastal protection, increasing workability, and potentially reduce design requirements regarding fatigue life. All of this is possible through the wave damping potential of densely seeded grow lines or nets in seaweed cultivation areas.

Wave height reduction over a vegetated area is due to the dissipation of wave energy. Different methodologies exist to capture this problem in a model. Some models are able to capture even individual plant dynamics, they are computationally way too expensive for modelling on a farm scale. Other methods rely on calibrating a bulk drag coefficient, which captures the effects for a limited range of conditions and vegetation characteristics.

The following model generalizes the complex geometry on a small scale by approaching the farm as a porous medium. Hereby, the effect of the kelp on incident waves can be modelled through a porous medium, described by the Darcy-Forchheimer resistance terms in the momentum equation.

Numerical model

The mathematical equations posed above are captured in a numerical scheme to be able to simulate the resulting system. The structure of the numerical method, with all components needed to arrive at a solution is presented below.

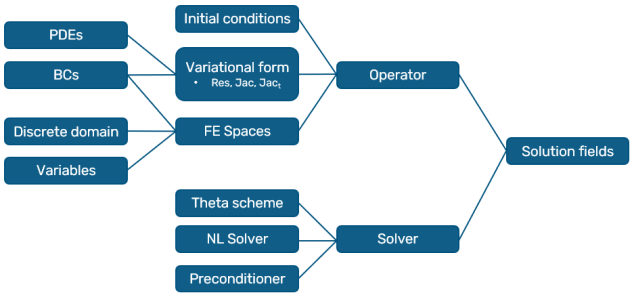

Structure of numerical components

Before setting up and code, all packages are called to include their functions in the following code.

```
using DrWatson
@quickactivate "PorousMediumFlow"
# Load packages
using Gridap
using Gridap.Geometry
using GridapODEs
using GridapODEs.ODETools
using GridapODEs.TransientFETools
using LineSearches: BackTracking
using WriteVTK
using LinearAlgebra
using DelimitedFiles, FileIO, Dates
using JLD2, DataFrames, TimerOutputs
using IncompleteLU, IterativeSolvers
include("LinearSolvers.jl")
```

Input variables

The constants that remain the same for each simulation and thus do not need to be user-defined are defined first. Additionally, the variables that are direct functions of the input variables can be stated already.

```
## Establish constants:
    theta = 0.5
    g = 9.81
    n_z = VectorValue(0.0,1.0)
    ρ = 1025.0
    p_atm = (1.013*10^5)/ρ
    ν =  0.001/ρ
    f_g = VectorValue(0.0, -g)
```

```
λ_in = g*(T_in^2)/(2*π)
k_in = 2*π/λ_in
ω_in  = sqrt(g*k_in)

## Geometry and meshing
dampinback = length_damp
dampoutfront = length_tank-length_damp
dampoutback = length_tank
n = cellm*length_tank
m = (cellm)*depth_tank
h_cell = 1/cellm
dampinfront = 0.0
vegbottom = vegtop-vegheight
vegback = vegfront+veglength

## Alternatively, dimensions can be parameterized
# vegfront = round(λ_in, digits = 1, base = 5)
# length_tank = round(10*λ_in, digits = 1, base =5)
# veglength = round(4*λ_in, digits = 1, base =5)
# length_damp = round(4*λ_in, digits = 1, base =5)
```

Domain

The equations stated above are impemented onto the domain. The model essentially makes use of a stationary, evenly-spaced mesh, but *Gridap* allows for more complex definitions as well.

```
## Domain and model set-up
    domain = (0,length_tank,0,depth_tank)
    partition = (n,m)
    model = CartesianDiscreteModel(domain,partition)
    writevtk(model,model_dir*"\\$runname _domain")

    k = 2
    Ω = Triangulation(model)
    degree = 2*k
    dΩ = Measure(Ω,degree)

    labels = get_face_labeling(model)
```

Boundaries

The boundaries need to be defined (and tagged) in order to implement the boundary conditions on them later on.

```
add_tag_from_tags!(labels,"diri_in",[3,7,])
    add_tag_from_tags!(labels,"freesurf_in",[3,])
    add_tag_from_tags!(labels,"free_surf",[3,4,6,])
    add_tag_from_tags!(labels,"neum_out",[4,8,])
    add_tag_from_tags!(labels,"diri_wall",[1,2,5])

    ## Prepare free surface discrete model
    bgface_to_mask = get_face_mask(labels,[6],1)
    Γface_to_bgface = findall(bgface_to_mask)
    model_Γ = BoundaryDiscreteModel(Polytope{1},model,Γface_to_bgface)
    writevtk(model_Γ,model_dir*"\\$(runname)_boundary")

    Γ_fa = Triangulation(model_Γ)
    dΓ_fa = Measure(Γ_fa,degree)
    n_fa = get_normal_vector(Γ_fa)

    Γ_out = BoundaryTriangulation(model,tags="neum_out")
    dΓ_out = Measure(Γ_out,degree)
    n_Γout = get_normal_vector(Γ_out)
```

Zones within domain

For the damping zone and actual porous medium, where the porous parameters are activated, the coordinates must be specified:

```
function is_inveg(coords)
        midx = (coords[1][1] + coords[2][1])/2
        midy = (coords[1][2] + coords[3][2])/2
        midx >= vegfront && midx <= vegback && midy <= vegtop && midy >= vegbottom
    end

    function is_indampout(coords)
        midx = (coords[1][1] + coords[2][1])/2
        midy = (coords[1][2] + coords[3][2])/2
        midx >= dampoutfront && midx <= dampoutback
    end

    oldcell_to_coods = get_cell_coordinates(Ω)
    oldcell_to_is_inveg = [lazy_map(is_inveg, oldcell_to_coods)[i] for i in 1:length(lazy_map(is_inveg, oldcell_to_coods))]
    oldcell_to_is_indampout = [lazy_map(is_indampout, oldcell_to_coods)[i] for i in 1:length(lazy_map(is_indampout, oldcell_to_coo
    incell_to_cellveg = findall(oldcell_to_is_inveg)
    incell_to_celldampout = findall(oldcell_to_is_indampout)
    outcell_to_cell = findall(iszero,(oldcell_to_is_inveg+ oldcell_to_is_indampin+ oldcell_to_is_indampout))

    model_veg = DiscreteModel(model,incell_to_cellveg)
    model_dampout = DiscreteModel(model,incell_to_celldampout)

    Ωveg = Triangulation(model_veg)
    dΩveg = Measure(Ωveg,degree)
    Ωdampout = Triangulation(model_dampout)
    dΩdampout = Measure(Ωdampout,degree)

    # Vegetation parameters (currently user-defined in input)
    α_veg = a_cons
    β_veg = b_cons

    # Sponge damping zone
    α_dampout(x::VectorValue) = C1*(1-((depth_tank-x[2])-depth_tank)/(depth_tank))*((x[1]-(length_tank-length_damp))/(length_tank-
```

Inflow conditions

As stated, wave generation is implemented by forcing particle velocity at the leftmost boundary. This is done using the orbital velocities as defined using Linear wave theory.

```
# #### Boundary conditions and porous zone
    # Velocity profile inlet
    u_hor(x,t) = a_in*ω_in*((cosh(k_in*x[2]))/(sinh(k_in*depth_tank)))*sin(x[1]*k_in - ω_in*t - theta_in)
    u_ver(x,t) = a_in*ω_in*((sinh(k_in*x[2]))/(sinh(k_in*depth_tank)))*cos(x[1]*k_in - ω_in*t - theta_in)

    # Boundary conditions at inlet and wall
    u_in(x, t::Real) = VectorValue(u_hor(x,t), u_ver(x,t))
```

```
    u_wall(x, t::Real) = VectorValue(0.0, 0.0)
    u₀(x, t::Real) = VectorValue(0.0,0.0)
    #u₀(x, t::Real) = VectorValue(a_in*w_in*((cosh(k_in*x[2]))/(sinh(k_in*depth_tank))), 0.0)       #Initial conditions can be ch

    u_in(t::Real) = x -> u_in(x, t)
    u_wall(t::Real) = x -> u_wall(x, t)
    u₀(t::Real) = x -> u₀(x, t::Real)
```

FE Spaces

The spaces are defined on which the functions will need to be found that provide the eventual solution fields. This is in line with the Gridap tutorials.

```
# ## Numerical Scheme
    # Velocity FE space
    reffeᵤ = ReferenceFE(lagrangian,VectorValue{2,Float64},k)
    V₀ = TestFESpace(model, reffeᵤ, conformity=:H1, dirichlet_tags=["diri_wall", "diri_in"])
    U = TransientTrialFESpace(V₀, [u_wall, u_in])

    # Stabilization variable Space
    reffe_s = ReferenceFE(lagrangian,VectorValue{2,Float64},k)
    S₀ = TestFESpace(model, reffe_s, conformity=:H1)
    S = TrialFESpace(S₀)

    # Pressure FE space
    reffe_p = ReferenceFE(lagrangian,Float64,1)
    Q = FESpace(model, reffe_p, conformity=:C0)
    P = TrialFESpace(Q)

    # Free surface space
    reffe_η = ReferenceFE(lagrangian,Float64,k)
    H₀ = TestFESpace(model_Γ, reffe_η, conformity=:H1)
    H = TrialFESpace(H₀)

    # Combining in multi-field
    Y = MultiFieldFESpace([V₀,S₀,Q,H₀])
    X = TransientMultiFieldFESpace([U,S,P,H])
```

Weak form

Before going on to implementing the physics, some auxiliary functions are defined:

```
@timeit timesave "weak form setup" begin
    nl_floor(u) = max((u⋅u).^(1/2), 1e-10)
    c₁    = 12.0*p           # algorithmic constant (John,Kindl2007)
    c₂    = 2.0
    ca    = c₁*ν/(h_cell^2)  # aux. constants
    cb    = c₂/h_cell
    τₘ(u)       = 1/( ca + cb*((u⋅u).^(1/2)) )                                    # Stabilization parameter (CoLomes2016)
    τlin(u,du)  = -((cb)/( (ca + cb*((u⋅u)^(1/2)) )^2)) * ((1/(nl_floor(u)))*(u⋅du))      # Linearized stabilization parameter # u⋅
    hN(x)       = VectorValue(p_atm + g*(depth_tank-x[2]), 0.0)                   # hydrostatic pressure
```

Weak Residual

The governing equations are captured through the weak form:

```
#RESIDUAL
    a((u,ut,p),(v,q))       = ∫( v⋅ut + v⋅((∇(u)')⋅u) + 2*ν*(ε(v)⊙ε(u)) - (∇⋅v)*p + q*(∇⋅u) )dΩ        # Original transient NS
    b((u,p),(v,q))          = ∫( v⊙(αu)+ v⊙(β((u⋅u).^(1/2))*u) )dΩveg                                  # Darcy and forchheimer ter
                              ∫( v⊙(C_damp*u))dΩdampout                                                # Sponge layer
    c((u,p,η),(v,q,w))      = ∫( ( (-p_atm - g*η)*n_fa)⋅v )dΓ_fa                                       # traction equilibrium air/
    d((u,η,ηt),(v,w))       = ∫( ( (u⋅n_z) - ηt)*w )dΓ_fa                                              # traction equilibrium
    l(v)                    = ∫( v⋅f_g )dΩ                                                           # Gravity throughout domain
    e(v,u,p)                = ∫( v⋅(hN) )dΓ_out                                                      # 'Outflow' pressure profil
    tbt_oss((u,s),(v,ϵ))    = ∫( τₘ*((∇(u)')⋅u - s)⋅( (∇(v)')⋅u - ϵ ) )dΩ                             # Stabilization projection

    res(t,((u,s,p,η),(ut,st,pt,ηt)),(v,ϵ,q,w)) = a((u,ut,p),(v,q)) + b((u,p),(v,q)) - l(v) + e(v,u,p) - c((u,p,η),(v,q,w)) + d((u,
```

Jacobian

Since Backtracking line search will be used in the solver, the derivative of the weak form is also needed; the jacobian:

```
julia
    #JACOBIAN
    jac_a(u,(du,dp),(v,q))      = ∫( v⋅((∇(du)')⋅u) + v⋅((∇(u)')⋅du) + 2*ν*(ε(v)⊙ε(du)) - (∇⋅v)*dp + q*(∇⋅du))dΩ
    jac_b(u,du,v)               = ∫( v⊙(αdu) + (β*v⋅((1/(nl_floor∘(u)))(u⊗u)⋅du + (u⋅u).^(1/2)*du)) )dΩveg +
                                  ∫( v⊙(C_damp*du)  )dΩdampout
    jac_c(dη,v)                 = ∫( ((-g*dη)*n_fa)⋅v )dΓ_fa
    jac_d(ηt,du,w)              = ∫( ( (du⋅n_z) - ηt)*w )dΓ_fa
    jac_tbt_oss(u,s,du,ds,v,ϵ)  = ∫( τₘ*( ((∇(v)')⋅du)⋅((∇(u)')⋅u - s) + (((∇(v)')⋅u-ϵ)⋅((∇(u)')⋅du +(∇(du)')⋅u -ds)))
                                  + (τlin∘(u,du))*(((∇(u)')⋅u - s)⋅( (∇(v)')⋅u - ϵ ) )dΩ

    jac(t,((u,s,p,η),(ut,st,pt,ηt)),(du,ds,dp,dη),(v,ϵ,q,w))        = jac_a(u,(du,dp),(v,q))  + jac_b(u,du,v) + jac_c(dη,v) + jac_
    jac_t(t,((u,s,p,η),(ut,st,pt,ηt)),(dut,dst,dpt,dηt),(v,ϵ,q,w))  = ∫( v⋅dut )dΩ - ∫( dηt*w )dΓ_fa
```

The resulting system provides the operator:

```
op = TransientFEOperator(res,jac,jac_t,X,Y)
```

Initial conditions

```
# ###### Stokes operator
    res_stokes((u,p),(v,q)) = ∫( 2*ν*(ε(v)⊙ε(u)) - (∇⋅v)*p + q*(∇⋅u) )dΩ
    jac_stokes((u,p),(du,dp),(v,q)) = res_stokes((du,dp),(v,q))
    op_stokes = FEOperator(res_stokes,jac_stokes,X(0.0),Y(0.0))
    #global xh0 = solve(op_stokes)
    xh0 = interpolate_everywhere([VectorValue(0.0,0.0),VectorValue(0.0,0.0),0.0,0.0],X(0.0))
    #xh0 = interpolate_everywhere([u₀(0.0),VectorValue(0.0,0.0),0.0,0.0],X(0.0))
    #writevtk(Ω,datadir("sims", "$runname")*"\\$runname _initial_up",cellfields=["u"=>xh0[1],"p"=>xh0[2]])
```

Solver

```
# ## Solver
    ls = LinearSolvers.GmresSolver(verbose=false,preconditioner=ilu;τ=1e-6)
    nl_solver = NLSolver(ls, show_trace = true,method = :newton,linesearch = BackTracking())
```

```
    ## Without preconditioning
    # nl_solver = NLSolver(show_trace = true,method = :newton,linesearch = BackTracking())

    ode_scheme_1 = ThetaMethod(nl_solver, dt1, theta)
    solver_1 = TransientFESolver(ode_scheme_1)
    xh_1 = solve(solver_1, op, xh0, t0, T)

    pvd = paraview_collection(datadir("sims", stage)*"\\$runname collection_ups", append=false)
    pvd_Γ = paraview_collection(datadir("sims", stage)*"\\$runname collection_eta", append=false)

    for (xh_tn, tn) in xh_1
        uh, sh, ph, ηh = xh_tn
        t_doc = round(tn; digits=3)
        pvd[tn] = createvtk(Ω, datadir("sims",stage)*"\\$runname FS$t_doc.vtu", cellfields = ["uh" => uh, "ph" => ph, "sh" => sh])
        pvd_Γ[tn] = createvtk(Γ_fa,datadir("sims",stage)*"\\$runname _FS_surf$t_doc.vtu",cellfields = ["etah" => ηh]) #
        # global xh0
        # xh0 = xh_tn
    end
```

The code above will produce a solution that's immediately written to VTK files. By writing the solution to variable `xh0`, this can now be loaded as the intial conditions for a new solution.

Essentially this provides the option to first run a small timespan with large timesteps to provide a rough solution. The following run can then performed at higher temporal resolution, while it can skip the (uninteresting) initial start-up behaviour.

```
pvd = paraview_collection(datadir("sims",stage)*"\\collection_ups_$(runname)", append=false)
    pvd_Γ = paraview_collection(datadir("sims",stage)*"\\collection_eta_$(runname)", append=false)

    # Same solver method, new inputs for Phase 2
    ode_scheme_2 = ThetaMethod(nl_solver, dt2, theta)
    solver_2 = TransientFESolver(ode_scheme_2)
    xh_2 = solve(solver_2, op, xh0, t0_2, T_2)

    global ηns = []
    global uhs1 = []
    global uhs2 = []
    global uhs3 = []
    global uhs4 = []
    global phs = []
    for (i, (xh, t)) in enumerate(xh_2)
        uh, sh, ph, ηh = xh

        global cell_values_ηn = get_cell_dof_values(ηh)
        surface = []
        len_FS = length(cell_values_ηn)
            for j in 1:len_FS
                push!(surface, cell_values_ηn[j][3])
            end
        push!(ηns, surface')

        global cell_values_uh = get_cell_dof_values(uh)
        surface_uh1 = []
        surface_uh2 = []
        surface_uh3 = []
        surface_uh4 =[]
        len_UH = length(cell_values_uh)
            for j in 1:len_UH
                push!(surface_uh1, cell_values_uh[j][1])
                push!(surface_uh2, cell_values_uh[j][2])
                push!(surface_uh3, cell_values_uh[j][3])
                push!(surface_uh4, cell_values_uh[j][4])
            end
        push!(uhs1, surface_uh1')
        push!(uhs2, surface_uh2')
        push!(uhs3, surface_uh3')
        push!(uhs4, surface_uh4')

        global cell_values_ph = get_cell_dof_values(ph)
        surface_ph = []
        len_pH = length(cell_values_ph)
            for j in 1:len_pH
                push!(surface_ph, cell_values_ph[j][1])
            end
        push!(phs, surface_ph')

        t_doc = round(t; digits=4)
        pvd[t] = createvtk(Ω, datadir("sims",stage)*"\\$runname _FS$t_doc.vtu", cellfields = ["uh" => uh, "ph" => ph, "sh" => sh])
        pvd_Γ[t] = createvtk(Γ_fa,datadir("sims",stage)*"\\$runname _FS_surf$t_doc.vtu",cellfields = ["etah" => ηh])
    end

    vtk_save(pvd)
    vtk_save(pvd_Γ)
```

We now have the desired solution as variable `xh`, as timeseries in the variables `ηns, uhs1, uhs2, uhs3, uhs4` and `phs`, and as the saved VTK files. To be able to process the solution at a later moment as wel, JLD2 files are created. Native julia datafiles that allow for storing the generated solution. To this end, the arrays are written into a library that is then saved in the `.jld2` format.

```
@timeit timesave "Data build & save" begin

    dat_total = Dict()
    dat_total["eta"] = ηns
    dat_total["uh1"] = uhs1
    dat_total["uh2"] = uhs2
    dat_total["uh3"] = uhs3
    dat_total["uh4"] = uhs4
    dat_total["ph"] = phs
    dat_params = Dict(
        "stage" => [stage],
        "runname" => [runname],
        "rundate" => [start_time],
        "Lwave"=> [λ_in],
        "dt1"=> [ dt1],
        "t0" => [ t0],
        "T"  => [T],
        "dt2" => [dt2],
        "t0_2"  => [t0_2],
        "T_2"  => [T_2],
        "a_in" => [ a_in],
        "T_in" => [ T_in],
        "theta_in" => [theta_in],
        "a_cons" => [a_cons],
        "b_cons" => [b_cons],
        "C1" => [ C1],
        "cellm"  => [cellm],
        "length_tank"  => [length_tank],
        "depth_tank"  => [depth_tank],
        "length_damp" => [length_damp],
```

```
        "vegtop" => [vegtop],
        "vegbottom" => [vegbottom],
        "vegheight" => [vegheight],
        "vegfront" => [vegfront],
        "vegback" => [vegback],
        "veglength"=>[veglength]
        )
    dat_total["params"] = dat_params

    save(datadir("data",stage)*"\\$(runname).jld2",dat_total)

    println("Starttime was: $(start_time), current time is ", Dates.format(Dates.now(),"HH_MM_SS"))
    return true
end
end
```

Plotting

Julia has many options for graphically presenting results. Most are julia-versions of software you may have used before (think matplotlib). Plots is a visualization interface and toolset. It sits above other backends, like GR, PyPlot, PGFPlotsX, or Plotly.

For the numerical model, a series of functions was defined to plot various insights. An indication of the core functions is provided here.

```
using Plots; gr()
function plot_wave(loadedruns,region,starttime,saveorshow,plotaddition)
    global params1 = loadedruns[1]
    plotname = "Damping_$(plotaddition)"
    titlename = "Reproduction - Zhu et al. (2021), waveAT015T2"
    xaxisname = "Normalized distance into vegetation (x-Lᵥ)/Lᵥ"
    yaxisname = "Normalized Wave height η/η₀"
    yaxisname = "Wave height η [m]"
    labelsname = ["Hs = 1.5 m ,T = 6 s, α = $(params1["params"]["a_cons"][1])"]#, θ = $(params1["params"]["b_cons"][1])"]#,"T = $(
    labelsname = ["a_in = $(params1["params"]["a_in"][1]),T = $(params1["params"]["T_in"][1]), α = $(params1["params"]["a_cons"][1
    global max_at_coord1 = []

    global finalcell = []
    global cellm_list = []
    global cphase = (params1["params"]["Lwave"][1]/params1["params"]["T_in"][1])
```

```
if starttime ==1000
        temp_time = 2*trunc(Int,params1["params"]["length_tank"][1]/cphase)
        if temp_time >= params1["params"]["T_2"][1]
            println("initial wave travelling time is $(temp_time)s, choosing last 2s of simulation")
            global start_time = 2*trunc(Int,params1["params"]["length_tank"][1]/cphase)-1
        else
        global start_time = 2*trunc(Int,params1["params"]["length_tank"][1]/cphase)
        println("No measurement starttime inserted: using c=$(cphase)m/s -> t=$(start_time)")
        end
    elseif starttime ==0
        global start_time = 1
    else
        global start_time = starttime
    end

    if length(params1) == 0
        println("no data loaded yet, commencing now")
        global params1 = load(datadir("data",foldername,runs[1]))
        # global xcoord_cell = trunc(Int,(params1["params"]["vegfront"][1]+params1["params"]["veglength"][1])*params1["params"]["c
    else
        println("data already loaded, skipping step")
    end
        println("Houston, we have data")

        # for i in 1:length(runs)
        # global run_dict = load(datadir("data",foldername,runs[i]))
        # icellm = run_dict["params"]["cellm"][1]
        # push!(cellm_list, icellm)
        # ifinalcell = run_dict["params"]["length_tank"][1]*icellm
        # push!(finalcell, ifinalcell)
```

Depending on what type of plot is desired, the entire domain, or just part of it can be shown.

```
if region == "veg"
        startcell = trunc(Int,params1["params"]["vegfront"][1]*params1["params"]["cellm"][1])
        endcell = trunc(Int,startcell + params1["params"]["veglength"][1]*params1["params"]["cellm"][1])
        totalcells = endcell-startcell
        EDRfirstcell = startcell
        EDRlastcell = totalcells
        x_axis = LinRange(params1["params"]["vegfront"][1], (params1["params"]["vegfront"][1]+ params1["params"]["veglength"][1]),
        k=1
        xaxisname = "Normalized distance into vegetation (x-Lᵥ)/Lᵥ"

    elseif region == "domain"
        startcell = 3 #was1
        endcell = trunc(Int,params1["params"]["length_tank"][1]*params1["params"]["cellm"][1])
        EDRfirstcell = trunc(Int, params1["params"]["vegfront"][1]*params1["params"]["cellm"][1])
        EDRlastcell = EDRfirstcell + trunc(Int,(params1["params"]["veglength"][1]*params1["params"]["cellm"][1]))
        totalcells = endcell-startcell
        x_axis = LinRange(0,params1["params"]["length_tank"][1],totalcells)
        # x_axis = LinRange(0,750,totalcells)

        k=4
        xaxisname = "Distance into domain [m]"

    else
        println("No region selected")
    end
```

Next up is looping through the timesteps to build the arrays that will be plotted eventually.

```
for j in 1:totalcells
            global timeseries = []
            for ts in trunc(Int,(start_time)/params1["params"]["dt2"][1]):(trunc(Int,(params1["params"]["T_2"][1])/params1["params
                temp_val = params1["eta"][ts][j+startcell]
                push!(timeseries, temp_val')
            end
            temp_max_at_coord = maximum(timeseries)
                push!(max_at_coord1, temp_max_at_coord)
        end
    # end

    norm_run1 = (max_at_coord1/max_at_coord1[k])
```

```
    #If desired, a linear fit can be added:
    linearizedfit, coef1, coef2 = poly_fit(x_axis[EDRfirstcell:EDRlastcell],max_at_coord1[EDRfirstcell:EDRlastcell])
    coefn1, coefn2 = [coef1, coef2] ./ max_at_coord1[k]
    linearizedfitnorm = linearizedfit/max_at_coord1[k]

    MP1, MP2 = x_axis[EDRlastcell], linearizedfitnorm[EDRlastcell-EDRfirstcell]
    perc1 = round((1-(linearizedfit[EDRlastcell-EDRfirstcell]/max_at_coord1[k])^2)*100, digits = 1)
    HTRend = round(linearizedfit[EDRlastcell-EDRfirstcell]/max_at_coord1[k], digits = 2)
    # lenslo = 0.95*minimum([norm_run1[end], norm_run2[end], norm_run3[end], norm_run5[end], norm_run5[end], norm_run6[end]])#, no
    # lenshi = 1.05*maximum([norm_run1[end], norm_run2[end], norm_run3[end], norm_run5[end], norm_run5[end], norm_run6[end]])#, no
    # lensleft = 7.5/8
    # lensright = 1
    # xlens = 0.4
    # ylens = 0.3
    # lenswidth = 0.2
    # lensheight = 0.35

    global labels = labelsname
    global p_total1 = plot(x_axis, norm_run1, label = labels[1], dpi=200, legend = :bottomleft, ylim=(0,1.3))
    # plot!(x_axis[EDRfirstcell:EDRlastcell], linearizedfitnorm, ls=:dash, label="linear fit, lsq ($(trunc(coefn1,digits=3)) + $(t
    scatter!(xpoint_exp_wave, values_exp_wave, label = "Data Hu et al. (2014)")
    scatter!([MP1], [MP2], markershape=:star5, color=:grey, alpha=0.5, label = "HTR = $(HTRend), EDR = $(perc1) %")
    xlabel!(p_total1,xaxisname)
    ylabel!(p_total1, yaxisname)
    title!(p_total1, titlename)
    # lens!([lensleft,lensright], [lenslo, lenshi], inset = (1, bbox(xlens, ylens, lenswidth, lensheight)), xticks = false, frames

    if saveorshow == "save"
        savefig(p_total1, plotsdir("$(plotname).png"))
        println("figure saved as $( plotsdir("$(plotname).png"))")
    elseif saveorshow == "show"
        println("not saved")
    else
        println("please define show or save")
    end
    p_total1
end
```

Fitting a polynomial

For the analysis of data and for further development of the framework, it is useful to be able to fit user-specified function types to the simulation data. This can be done using many packages, LsqFit is one convenient option.

```
using Polynomials
using LsqFit
function poly_fit(xdata,ydata)

    p0 = [0.1, 0.1]
    model(t,p)= p[1] .+ p[2]*t
    xlin = range(xdata[1], xdata[end], length =100)

    fitcurve = curve_fit(model, xdata, ydata, p0)
    residuals = fitcurve.resid

    global linydata = ydata .+ residuals
    param = fitcurve.param
    println("$(param)")

    return linydata, param[1], param[2]
end
```

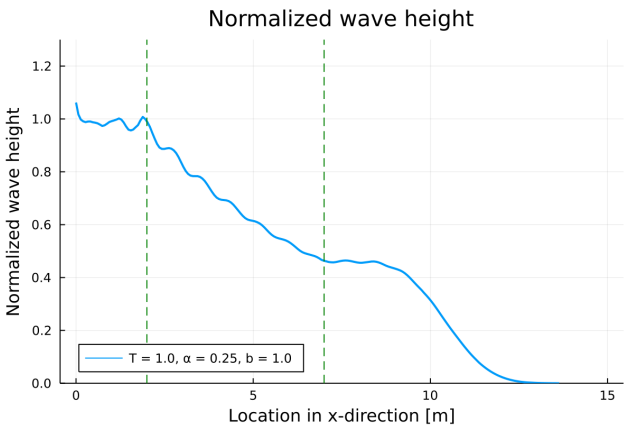

Structure of framework components

Workflow tools

To structure the work around setting up a model, running simulations, analysing data and collaborating on code through Github, the following tools are recommended.

Research project structuring

The package DrWatson.jl automatically creates a folder-structure/repository that includes everything you need to develop code in a research project and allows for collaboration through GitHub easily. The set-up includes infrastructure dedicated to ignore some folders during commits to avoid overloading your repo. It lets anyone duplicate all package versions and dependencies for reproducing your work without running into errors. Furthermore, provide clear naming conventions and prevent double work by checking whether the same input parameters have already been used in an earlier run.

It is worth checking out and investing a little bit of time in beforehand, as it will make your life significantly easier.

```
using DrWatson
@quickactivate "PorousMediumFlow" # defines what environment (ie. versions etc) is activated
include(projectdir("src","Sim_PM.jl")) #projectdir() is an example of DrWatson's helpful tools
```

Simulating in batches

With simulations that take more than a couple of seconds, automation is your friend. DrWatson allows to setup a library of input parameters that are fed into the simulation script when the last run is done.

```
allparams = Dict(
    "stage"=>["numerical_methods"],
    "dt1"=> [ 0.005],   #timestep of first solving round
    "t0" => [ 0.0],     #starttime of first solving round
    "T"  => [ 0.01],    #end time of first solving round

    "dt2" => [0.01],
    "t0_2"  => [0.01],
    "T_2"  => [5.0], #30

    "a_in" => [0.015, 0.01],  #m 0.05
    "T_in" => [1.0],

    "a_cons" => [ 0.15 0.2, 0.1, 0.05],
    "b_cons" => [ 5.0],
    "C1" => [ 7.5],

    "cellm"  => [5.0],
    "length_tank"  => [15.0],
    "depth_tank"  => [1.0],
    "length_damp" => [7.0],
    "vegtop" => [1.0],
    "vegheight" => [0.1],
    "vegfront" => [1.0],
    "veglength" => [6.0]
)
dicts = dict_list(allparams)
```

We have now set up the dictionary that contains all variables we desire for input. We run `sim_prep(d:Dict)` to build a series of *all* combinations of these variables.

> ⚠ **Warning:**
>
> For the large number of input variables of this model, the possible combinations grow quickly. Make sure to carefully think about what runs (and combinations) are essential.

```
function sim_prep(d::Dict)
    @unpack stage, dt1, t0, T, dt2, t0_2, T_2, a_in, T_in, theta_in a_cons, b_cons, C1, cellm, length_tank, depth_tank, length_dam
    etahs = sim_run(stage, dt1, t0, T, dt2, t0_2, T_2, a_in, T_in, theta_in, a_cons, b_cons, C1, cellm, length_tank, depth_tank, l
    return true
end

for (i, d) in enumerate(dicts)
    f1 = sim_prep(d)
end
```

The julia file that runs the simulations can then make used of the created dictionaries of input parameters:

```
function sim_run(stage, dt1, t0, T, dt2, t0_2, T_2, a_in, T_in, theta_in, a_cons, b_cons, C1, cellm, length_tank, depth_tank, leng
    ######################
    # Actual simulations #
    ######################
end
```

Timing outputs

TimerOutputs.jl is a minimal, basic tool that helps to gain some insights into the resources your simulations demands.

```
using TimerOutputs

timesave = TimerOutput()
@timeit timesave "Total simulation time" begin

    ####################################
    # Setting up a batch of simulation #
    ####################################

    @timeit timesave "Simulation time 1 run" begin

        ######################
        # Actual simulations #
        ######################

    end
end
show(timesave)
```

The image below provides an example of what the results look like when a .jl uses multiple timers throughout:

```
Timestep: 5.009999999999938 with start time:  14_13
Starttime was: 14_13, current time is 15_44_26
 ──────────────────────────────────────────────────────────────────────────────────────────────────
                                                  Time                    Allocations
                        Tot / % measured:         5452s / 100%            387GiB / 100%

 Section                                ncalls     time   %tot     avg     alloc   %tot      avg
 ──────────────────────────────────────────────────────────────────────────────────────────────────
 total script                                1     5452s   100%   5452s    387GiB   100%    387GiB
   enumerate over dicts                      1     5451s   100%   5451s    387GiB   100%    387GiB
     weak form setup                         1     5449s   100%   5449s    387GiB   100%    387GiB
       loop pushing data xh2                 1     5350s  98.1%   5350s    383GiB  99.1%    383GiB
       Data build & save                     1     2.30s  0.04%   2.30s    152MiB  0.04%    152MiB
     FE space building                       1     38.3ms  0.00%  38.3ms   4.73MiB  0.00%   4.73MiB
     check/create folder                     1     2.37ms  0.00%  2.37ms   50.5KiB  0.00%   50.5KiB
   load Sim_PM function(s)                   1      370ms  0.01%   370ms   2.01MiB  0.00%   2.01MiB
   unpack input for sim                      1     69.1µs  0.00%  69.1µs   5.33KiB  0.00%   5.33KiB
 ──────────────────────────────────────────────────────────────────────────────────────────────────
                                                                                          Main.PMTP
```

TimerOutputs summary

Bibliography

[1] T.S. Asano, Tsutsui, and T. Sakai. Wave damping characteristics due to seaweed, (in Japanese),. *Thirty-Fifth Coastal Engineering in Japan, Japan Soc. Of Civil Engineering*, January 1988:138–142, 1988.

[2] Lauren N. Augustin, Jennifer L. Irish, and Patrick Lynett. Laboratory and numerical studies of wave damping by emergent and near-emergent wetland vegetation. *Coastal Engineering*, 56(3):332–340, 2009. ISSN 03783839. doi: 10.1016/j.coastaleng.2008.09.004. URL http://dx.doi.org/10.1016/j.coastaleng.2008.09.004.

[3] Santiago Badia and Francesc Verdugo. Gridap: An extensible finite element toolbox in julia. *Journal of Open Source Software*, 5(52):2520, 2020. doi: 10.21105/joss.02520. URL https://doi.org/10.21105/joss.02520.

[4] Santiago Badia, Oriol Colomes, and Francesc Verdugo. GridapODEs, 9 2021. URL https://github.com/gridap/GridapODEs.jl.

[5] Urd Grandorf Bak, Agnes Mols-Mortensen, and Olavur Gregersen. Production method and cost of commercial-scale offshore cultivation of kelp in the Faroe Islands using multiple partial harvesting. *Algal Research*, 33(April):36–47, 2018. ISSN 22119264. doi: 10.1016/j.algal.2018.05.001. URL https://doi.org/10.1016/j.algal.2018.05.001.

[6] Jeff Bezanson, Alan Edelman, Stefan Karpinski, and Viral B. Shah. Julia: A fresh approach to numerical computing. *SIAM Review*, 59(1):65–98, 2017. doi: 10.1137/141000671.

[7] Moisés Brito, João Fernandes, and João Bento Leal. Porous media approach for RANS simulation of compound open-channel flows with submerged vegetated floodplains. *Environmental Fluid Mechanics*, 16(6):1247–1266, 2016. ISSN 15731510. doi: 10.1007/s10652-016-9481-0.

[8] Haijin Cao, Weibing Feng, Zhan Hu, Tomohiro Suzuki, and Marcel J.F. Stive. Numerical modeling of vegetation-induced dissipation using an extended mild-slope equation. *Ocean Engineering*, 110:258–269, 2015. ISSN 00298018. doi: 10.1016/j.oceaneng.2015.09.057. URL http://dx.doi.org/10.1016/j.oceaneng.2015.09.057.

[9] Hui Chen, Yan Ni, Yulong Li, Feng Liu, Suying Ou, Min Su, Yisheng Peng, Zhan Hu, Wim Uijttewaal, and Tomohiro Suzuki. Deriving vegetation drag coefficients in combined wave-current flows by calibration and direct measurement methods. *Advances in Water Resources*, 122(October):217–227, 2018. ISSN 03091708. doi: 10.1016/j.advwatres.2018.10.008. URL https://doi.org/10.1016/j.advwatres.2018.10.008.

[10] Xuebin Chen, Qin Chen, Jiemin Zhan, and Don Liu. Numerical simulations of wave propagation over a vegetated platform. *Coastal Engineering*, 110:64–75, 2016. ISSN 03783839. doi: 10.1016/j.coastaleng.2016.01.003. URL http://dx.doi.org/10.1016/j.coastaleng.2016.01.003.

[11] Chung-Ren Chou, John-Z Yim, and Ruey-Syan Shih. Optimizing deployment of sponge zone on numerical wave channel. *Journal of the Chinese Institute of Engineers*, 25(2):147–156, 2002. doi: 10.1080/02533839.2002.9670689. URL https://doi.org/10.1080/02533839.2002.9670689.

[12] Oriol Colomés, Santiago Badia, Ramon Codina, and Javier Principe. Assessment of variational multiscale models for the large eddy simulation of turbulent incompressible flows. *Computer Methods in Applied Mechanics and Engineering*, 285:32–63, 2015. ISSN 00457825. doi: 10.1016/j.cma.2014.10.041.

[13] Oriol Colomés, Santiago Badia, and Javier Principe. Mixed finite element methods with convection stabilization for the large eddy simulation of incompressible turbulent flows. *Computer Methods in Applied Mechanics and Engineering*, 304:294–318, 2016. ISSN 00457825. doi: 10.1016/j.cma.2016.02.026.

[14] Various Contributors. Iterativesolvers:iterative algorithms for solving linear systems, eigensystems, and singular value problems, 2021. URL https://github.com/JuliaLinearAlgebra/IterativeSolvers.jl.

[15] Various Contributors. Nlsolvers: family of various repositories for nonlinear solvers and supporting functions, 2021. URL https://github.com/JuliaNLSolvers.

[16] Various Julia Contributors. Juliaio: group for a unified io infrastructure, 2021. URL https://https://github.com/JuliaIO.

[17] Robert A. Dalrymple, James T. Kirby, and Paul A. Hwang. Wave Diffraction Due to Areas of Energy Dissipation. *Journal of Waterway, Port, Coastal, and Ocean Engineering*, 110(1):67–79, feb 1984. ISSN 0733-950X. doi: 10.1061/(ASCE)0733-950X(1984)110:1(67). URL http://ascelibrary.org/doi/10.1061/%28ASCE%290733-950X%281984%29110%3A1%2867%29.

[18] George Datseris, Jonas Isensee, Sebastian Pech, and Tamás Gál. Drwatson: the perfect sidekick for your scientific inquiries. *Journal of Open Source Software*, 5(54):2673, 2020. doi: 10.21105/joss.02673. URL https://doi.org/10.21105/joss.02673.

[19] Alfonse Dubi and Alf Tørum. Wave Damping by Kelp Vegetation. In *Coastal Engineering*, pages 142–156, New York, NY, aug 1995. American Society of Civil Engineers. ISBN 9780784400890. doi: 10.1061/9780784400890.012. URL https://doi.org/10.9753/icce.v24.%25phttp://ascelibrary.org/doi/10.1061/9780784400890.012.

[20] R. Kathleen Dupre. Relating Porous media structure to the darcy-forchheimer model. 2020.

[21] Marco Ghisalberti and Heidi M. Nepf. Shallow flows over a permeable medium: The hydrodynamics of submerged aquatic canopies. *Transport in Porous Media*, 78(2):309–326, 2009. ISSN 01693913. doi: 10.1007/s11242-008-9305-x.

[22] Sanaz Hadadpour. Numerical Modelling & New Prediction Formulae for Wave and Wave-Current Attenuation By Vegetation As a Natural Shore Protection. (October 2015):1–20, 2020.

[23] T S Hedges. Regions of validity of analytical wave theories. *Proceedings of the Institution of Civil Engineers - Water, Maritime and Energy*, 112(2):111–114, 1995. doi: 10.1680/iwtme.1995.27656.

[24] Pablo Higuera, Javier L. Lara, and Inigo J. Losada. Realistic wave generation and active wave absorption for Navier-Stokes models. Application to OpenFOAM®. *Coastal Engineering*, 71:102–118, 2013. ISSN 03783839. doi: 10.1016/j.coastaleng.2012.07.002. URL http://dx.doi.org/10.1016/j.coastaleng.2012.07.002.

[25] Leo H. Holthuijsen. *Waves in Oceanic and Coastal Waters*. Cambridge University Press, Cambridge, 2007 edition, 2007. ISBN 9780511618536. doi: 10.1017/CBO9780511618536. URL http://ebooks.cambridge.org/ref/id/CBO9780511618536.

[26] M. Shahadat Hossain, S.M. Sharifuzzaman, M. Nur Nobi, M. Shah Chowdhury, Subrata Sarker, Sheikh Aftab Uddin, Sayedur Rahman Chowdhury, M. Mizanur Rahman, M. Shajjadur Rahman, Faisal Sobhan, and et al. Seaweeds farming for sustainable development goals and blue economy in bangladesh. *Marine Policy*, 128:104469, Jun 2021. doi: 10.1016/j.marpol.2021.104469.

[27] Jie Hu, Chiang C. Mei, Che-Wei Chang, and Philip L-F. Liu. Effect of flexible coastal vegetation on waves in water of intermediate depth. *Coastal Engineering*, 168(June):103937, 2021. ISSN 03783839. doi: 10.1016/j.coastaleng.2021.103937. URL https://doi.org/10.1016/j.coastaleng.2021.103937.

[28] Jie Hu, Xiaochun Tang, Pengzhi Lin, and Philip L.F. Liu. Periodic water waves through suspended canopy. *Coastal Engineering*, 163(November 2020), 2021. ISSN 03783839. doi: 10.1016/j.coastaleng.2020.103809.

[29] Zhan Hu, Tomohiro Suzuki, Tjerk Zitman, Wim Uittewaal, and Marcel Stive. Laboratory study on wave dissipation by vegetation in combined current-wave flow. *Coastal Engineering*, 88:131–142, 2014. ISSN 03783839. doi: 10.1016/j.coastaleng.2014.02.009. URL http://dx.doi.org/10.1016/j.coastaleng.2014.02.009.

[30] Zhenhua Huang, Yu Yao, Shawn Y. Sim, and Yao Yao. Interaction of solitary waves with emergent, rigid vegetation. *Ocean Engineering*, 38(10):1080–1088, 2011. ISSN 00298018. doi: 10.1016/j.oceaneng.2011.03.003. URL http://dx.doi.org/10.1016/j.oceaneng.2011.03.003.

[31] Juan Ignacio Polanco and Frederik Ekre. Writevtk: allows to write vtk xml files for visualisation in tools like paraview, 2021. URL https://github.com/jipolanco/WriteVTK.jl.

[32] Bjarne Jensen, Niels Gjøl Jacobsen, and Erik Damgaard Christensen. Investigations on the porous media equations and resistance coefficients for coastal structures. *Coastal Engineering*, 84:56–72, feb 2014. ISSN 03783839. doi: 10.1016/j.coastaleng.2013.11.004. URL http://dx.doi.org/10.1016/j.coastaleng.2013.11.004https://linkinghub.elsevier.com/retrieve/pii/S0378383913001816.

[33] Beena Mary John, Kiran G. Shirlal, and Subba Rao. Effect of Artificial Sea Grass on Wave Attenuation- An Experimental Investigation. *Aquatic Procedia*, 4(Icwrcoe):221–226, 2015. ISSN 2214241X. doi: 10.1016/j.aqpro.2015.02.030. URL http://dx.doi.org/10.1016/j.aqpro.2015.02.030.

[34] Beena Mary John, Kiran G. Shirlal, and Subba Rao. Laboratory investigations of wave attenuation by simulated vegetation of varying densities. *ISH Journal of Hydraulic Engineering*, 25(2):203–213, 2019. ISSN 21643040. doi: 10.1080/09715010.2017.1398112. URL http://doi.org/10.1080/09715010.2017.1398112.

[35] JuliaData-collaborators. Dataframes: tools for working with tabular data in julia, 2021. URL https://github.com/JuliaData/DataFrames.jl.

[36] Min Woo Kim, Weoncheol Koo, and Sa Young Hong. Numerical analysis of various artificial damping schemes in a three-dimensional numerical wave tank. *Ocean Engineering*, 75:165–173, 2014. doi: 10.1016/j.oceaneng.2013.10.012.

[37] Nobuhisa Kobayashi. FORMULATION z Wave Gages. *J. Waterway, Port, Coastal, Ocean Eng*, 119(1):30–48, 1993.

[38] Vedrana Kutija and Hoang Thi Minh Hong. A numerical model for assessing the additional resistance to flow introduced by flexible vegetation. *Journal of Hydraulic Research*, 34(1):99–114, jan 1996. ISSN 0022-1686. doi: 10.1080/00221689609498766. URL https://www.tandfonline.com/doi/full/10.1080/00221689609498766.

[39] Jiarui Lei and Heidi M. Nepf. Wave damping by flexible vegetation: Connecting individual blade dynamics to the meadow scale. *Coastal Engineering*, 147(January):138–148, 2019. ISSN 03783839. doi: 10.1016/j.coastaleng.2019.01.008. URL https://doi.org/10.1016/j.coastaleng.2019.01.008.

[40] C W Li and K Yan. Numerical Investigation of Wave–Current–Vegetation Interaction. *Journal of Hydraulic Engineering*, 133(7):794–803, jul 2007. ISSN 0733-9429. doi: 10.1061/(asce)0733-9429(2007)133:7(794). URL http://ascelibrary.org/doi/10.1061/%28ASCE%290733-9429%282007%29133%3A7%28794%29.

[41] Philip L.F. Liu, Che Wei Chang, Chiang C. Mei, Pedro Lomonaco, Francisco L. Martin, and Maria Maza. Periodic water waves through an aquatic forest. *Coastal Engineering*, 96:100–117, 2015. ISSN 03783839. doi: 10.1016/j.coastaleng.2014.11.002. URL http://dx.doi.org/10.1016/j.coastaleng.2014.11.002.

[42] Ryan J. Lowe, Jeffrey R. Koseff, and Stephen G. Monismith. Oscillatory flow through submerged canopies: 1. Velocity structure. *Journal of Geophysical Research C: Oceans*, 110(10):1–17, 2005. ISSN 01480227. doi: 10.1029/2004JC002788.

[43] M. Luhar, E. Infantes, and Heidi M. Nepf. Seagrass blade motion under waves and its impact on wave decay. *Journal of Geophysical Research: Oceans*, 122:2647–2651, 2017. doi: 10.1002/2017JC012731. Received.

[44] Mitul Luhar, Sylvain Coutu, Eduardo Infantes, Samantha Fox, and Heidi M. Nepf. Wave-induced velocities inside a model seagrass bed. *Journal of Geophysical Research: Oceans*, 115(12), 2010. ISSN 21699291. doi: 10.1029/2010JC006345.

[45] Gangfeng Ma, James T. Kirby, Shih Feng Su, Jens Figlus, and Fengyan Shi. Numerical study of turbulence and wave damping induced by vegetation canopies. *Coastal Engineering*, 80:68–78, 2013. ISSN 03783839. doi: 10.1016/j.coastaleng.2013.05.007. URL http://dx.doi.org/10.1016/j.coastaleng.2013.05.007.

[46] Eleonora Manca, Vasiliki Stratigaki, and P. Prinos. Large scale experiments on spectral wave propagation over Posidonia oceanica seagrass. *Environmental Hydraulics - Proceedings of the 6th International Symposium on Environmental Hydraulics*, 1(2009):463–468, 2010. doi: 10.1201/b10553-74.

[47] Maria Maza, Javier L. Lara, and Iñigo J. Losada. A coupled model of submerged vegetation under oscillatory flow using Navier-Stokes equations. *Coastal Engineering*, 80:16–34, oct 2013. ISSN 03783839. doi: 10.1016/j.coastaleng.2013.04.009.

[48] Maria Maza, Javier L. Lara, and Iñigo J. Losada. Tsunami wave interaction with mangrove forests: A 3-D numerical approach. *Coastal Engineering*, 98:33–54, 2015. ISSN 03783839. doi: 10.1016/j.coastaleng.2015.01.002. URL http://dx.doi.org/10.1016/j.coastaleng.2015.01.002.

[49] Chiang C. Mei, I. Chi Chan, Philip L.F. F Liu, Zhenhua Huang, and Wenbin Zhang. Long waves through emergent coastal vegetation. *Journal of Fluid Mechanics*, 687:461–491, 2011. ISSN 00221120. doi: 10.1017/jfm.2011.373.

[50] Fernando J. Mendez and Iñigo J. Losada. An empirical model to estimate the propagation of random breaking and nonbreaking waves over vegetation fields. *Coastal Engineering*, 51(2):103–118, 2004. ISSN 03783839. doi: 10.1016/j.coastaleng.2003.11.003.

[51] Fernando J. Mendez, Iñigo J. Losada, and Miguel A. Losada. Hydrodynamics induced by wind waves in a vegetation field. *Journal of Geophysical Research: Oceans*, 104(C8):18383–18396, 1999. ISSN 2169-9291. doi: 10.1029/1999jc900119.

[52] J.R. Morison, J.W. Johnson, and S.A. Schaaf. The Force Exerted by Surface Waves on Piles. *Journal of Petroleum Technology*, 2(05):149–154, 1950. ISSN 0149-2136. doi: 10.2118/950149-g.

[53] Iehisa Nezu and Michio Sanjou. Turburence structure and coherent motion in vegetated canopy open-channel flows. *Journal of Hydro-Environment Research*, 2(2):62–90, 2008. ISSN 1570-6443. doi: 10.1016/j.jher.2008.05.003. URL http://dx.doi.org/10.1016/j.jher.2008.05.003.

[54] Y. Ozeren, D. G. Wren, and Wei Cheng Wu. Experimental Investigation of Wave Attenuation through Model and Live Vegetation. *Journal of Waterway, Port, Coastal, and Ocean Engineering*, 140(5):04014019, 2014. ISSN 0733-950X. doi: 10.1061/(asce)ww.1943-5460.0000251.

[55] K. L. Phan, M. J.F. Stive, M. Zijlema, H. S. Truong, and S. G.J. Aarninkhof. The effects of wave non-linearity on wave attenuation by vegetation. *Coastal Engineering*, 147(July 2011):63–74, 2019. ISSN 03783839. doi: 10.1016/j.coastaleng.2019.01.004. URL https://doi.org/10.1016/j.coastaleng.2019.01.004.

[56] W.A. Price, K.W. Tomlinson, and J.N. Hunt. the Effect of Artificial Seaweed in Promoting the Build-Up of Beaches. *Coastal Engineering Proceedings*, 1(11):36, 1968. ISSN 0589-087X. doi: 10.9753/icce.v11.36.

[57] Johanna H. Rosman, Stephen G. Monismith, Mark W. Denny, and Jeffrey R. Koseff. Currents and turbulence within a kelp forest (Macrocystis pyrifera): Insights from a dynamically scaled laboratory model. *Limnology and Oceanography*, 55(3):1145–1158, 2010. ISSN 00243590. doi: 10.4319/lo.2010.55.3.1145.

[58] Johanna H. Rosman, Mark W. Denny, Robert B. Zeller, Stephen G. Monismith, and Jeffrey R. Koseff. Interaction of waves and currents with kelp forests (Macrocystis pyrifera): Insights from a dynamically scaled laboratory model. *Limnology and Oceanography*, 58(3):790–802, 2013. ISSN 00243590. doi: 10.4319/lo.2013.58.3.0790.

[59] Rijksdienst voor Ondernemend Nederland RVO. General information borssele wfz, 2021. URL https://offshorewind.rvo.nl/generalborssele.

[60] António José Espadinha Vieira Soares. Numerical simulation of vegetated flows using RANS equations coupled with a porous media approach in OpenFOAM. page 169, 2017.

[61] Harmen Stoppels and Alexis Montoison. Incompletelu: crout ilu for julia, 2021. URL https://github.com/haampie/IncompleteLU.jl.

[62] Tomohiro Suzuki, Marcel Zijlema, Bastiaan Burger, Martijn C. Meijer, and Siddharth Narayan. Wave dissipation by vegetation with layer schematization in SWAN. *Coastal Engineering*, 59(1):64–71, 2012. ISSN 03783839. doi: 10.1016/j.coastaleng.2011.07.006. URL http://dx.doi.org/10.1016/j.coastaleng.2011.07.006.

[63] Tomohiro Suzuki, Zhan Hu, Kenji Kumada, L. K. Phan, and Marcel Zijlema. Non-hydrostatic modeling of drag, inertia and porous effects in wave propagation over dense vegetation fields. *Coastal Engineering*, 149(135):49–64, 2019. ISSN 03783839. doi: 10.1016/j.coastaleng.2019.03.011. URL https://doi.org/10.1016/j.coastaleng.2019.03.011.

[64] Dastan Takhanov. Forchheimer Model for Non-Darcy Flow in Porous Media and Fractures. *Centre for Petroleum Studies*, Department(September):1–31, 2011.

[65] Jun Tang, Shaodong Shen, and Hui Wang. Numerical model for coastal wave propagation through mild slope zone in the presence of rigid vegetation. *Coastal Engineering*, 97:53–59, 2015. ISSN 03783839. doi: 10.1016/j.coastaleng.2014.12.006. URL http://dx.doi.org/10.1016/j.coastaleng.2014.12.006.

[66] Nils Tilton and Luca Cotelezzi. Linear stability analysis of pressure-driven flows in channels with porous walls. https://www.researchgate.net/publication/231926919_Linear_stability_analysis_of_pressure-driven_flows_in_channels_with_porous_walls, 06 2008.

[67] Maria Tsakiri and P. Prinos. Numerical simulation of convective currents in aquatic canopies using a porous media approach. In *Special Topics and Reviews in Porous Media*, volume 8, pages 91–108, 2017. doi: 10.1615/SpecialTopicsRevPorousMedia.2017019609. URL http://www.dl.begellhouse.com/journals/3d21681c18f5b5e7,0e5e7d7c2836d626,6a178de472008d0b.html.

[68] A. A. van Rooijen, R. T. McCall, J. S. M. van Thiel de Vries, A. R. van Dongeren, A. J. H. M. Reniers, and J. A. Roelvink. Modeling the effect of wave-vegetation interaction on wave setup. *Journal of Geophysical Research: Oceans*, 121(6):4341–4359, jun 2016. ISSN 21699275. doi: 10.1002/2015JC011392. URL http://doi.wiley.com/10.1002/2015JC011392.

[69] Arnold van Rooijen, Ryan J. Lowe, Dirk P. Rijnsdorp, Marco Ghisalberti, Niels G. Jacobsen, and Robert McCall. Wave-Driven Mean Flow Dynamics in Submerged Canopies. *Journal of Geophysical Research: Oceans*, 125(3):1–40, 2020. ISSN 21699291. doi: 10.1029/2019JC015935.

[70] Thomas J. van Veelen, Tom P. Fairchild, Dominic E. Reeve, and Harshinie Karunarathna. Experimental study on vegetation flexibility as control parameter for wave damping and velocity structure. *Coastal Engineering*, 157(January):103648, 2020. ISSN 03783839. doi: 10.1016/j.coastaleng.2020.103648. URL https://doi.org/10.1016/j.coastaleng.2020.103648.

[71] Thomas J. van Veelen, Harshinie Karunarathna, and Dominic E. Reeve. Modelling wave attenuation by quasi-flexible coastal vegetation. *Coastal Engineering*, 164(September 2019):103820, 2021. ISSN 03783839. doi: 10.1016/j.coastaleng.2020.103820. URL https://doi.org/10.1016/j.coastaleng.2020.103820.

[72] Mitchell Williams and Frej Gustafsson. Reshore - the living breakwater, 2022. URL https://www.reshore.blue/.

[73] Wei Cheng Wu and Daniel T. Cox. Effects of wave steepness and relative water depth on wave attenuation by emergent vegetation. *Estuarine, Coastal and Shelf Science*, 164(December):443–450, 2015. ISSN 02727714. doi: 10.1016/j.ecss.2015.08.009. URL http://dx.doi.org/10.1016/j.ecss.2015.08.009.

[74] Weiming Wu, Y. Ozeren, D. G. Wren, Qin Chen, Guoping Zhang, Marjorie Holland, Yan Ding, Soumendra Nath Kuiry, Mingliang Zhang, Ranjit Jadhave, James Chatagnier, Ying Chen, and Leili Gordji. Phase I Report for SERRI Project No. 80037: Investigation of surge and wave reduction by vegetation, 2011.

[75] Weiming Wu, Mingliang Zhang, Y. Ozeren, and Daniel Wren. Analysis of vegetation effect on waves using a vertical 2D RANS model. *Journal of Coastal Research*, 29(2):383–397, 2013. ISSN 07490208. doi: 10.2112/JCOASTRES-D-12-00023.1.

[76] Tze Yi Yang and I. Chi Chan. Drag force modeling of surface wave dissipation by a vegetation field. *Water (Switzerland)*, 12(9):1–15, 2020. ISSN 20734441. doi: 10.3390/w12092513.

[77] Zhiyong Yang, Jun Tang, and Yongming Shen. Numerical study for vegetation effects on coastal wave propagation by using nonlinear Boussinesq model. *Applied Ocean Research*, 70:32–40, 2018. ISSN 01411187. doi: 10.1016/j.apor.2017.09.001. URL https://doi.org/10.1016/j.apor.2017.09.001.

[78] K. Yazdchi and S. Luding. Towards unified drag laws for inertial flow through fibrous materials. *Chemical Engineering Journal*, 207-208:35–48, 2012. ISSN 13858947. doi: 10.1016/j.cej.2012.06.140. URL http://dx.doi.org/10.1016/j.cej.2012.06.140.

[79] Longhuan Zhu. Wave Attenuation Capacity of Suspended Aquaculture Structures with Sugar Kelp and Mussels. *Thesis*, 2020. URL https://digitalcommons.library.umaine.edu/etd/3222/.

[80] Longhuan Zhu and Qing Ping Zou. Three-Layer Analytical Solution for Wave Attenuation By Suspended and Nonsuspended Vegetation Canopy. *Coastal Engineering Proceedings*, (35):27, 2017. ISSN 0589-087X. doi: 10.9753/icce.v35.waves.27.

[81] Longhuan Zhu, Qing Ping Zou, Kimberly Huguenard, and David W. Fredriksson. Mechanisms for the Asymmetric Motion of Submerged Aquatic Vegetation in Waves: A Consistent-Mass Cable Model. *Journal of Geophysical Research: Oceans*, 125(2), 2020. ISSN 21699291. doi: 10.1029/2019JC015517.

[82] Longhuan Zhu, Jiarui Lei, Kimberly Huguenard, and David W. Fredriksson. Wave attenuation by suspended canopies with cultivated kelp (Saccharina latissima). *Coastal Engineering*, 168(April):103947, 2021. ISSN 03783839. doi: 10.1016/j.coastaleng.2021.103947. URL https://doi.org/10.1016/j.coastaleng.2021.103947.

[83] R.W. Zimmerman, A. Al-Yaarubi, C.C. Pain, and C.A. Grattoni. Non-linear regimes of fluid flow in rock fractures. *International Journal of Rock Mechanics and Mining Sciences*, 41(3):384, 2004. ISSN 13651609. doi: 10.1016/j.ijrmms.2003.12.045.

[84] Peggy Zinke. Flow resistance parameters for natural emergent vegetation derived from a porous media model. *River Flow 2010*, pages 461–468, 2010.

[85] Peggy Zinke. Application of a porous media approach for vegetation flow resistance. *River Flow 2012 - Proceedings of the International Conference on Fluvial Hydraulics*, 1:301–308, 2012.